

CYCLIC MODELING OF COLD-FORMED STEEL STRUCTURES
WITH SHEATHED SHEAR PANELS

by

Süha Kültür

B.S., Civil Engineering, Boğaziçi University, 2010

Submitted to the Institute for Graduate Studies in
Science and Engineering in partial fulfillment of
the requirements for the degree of
Master of Science

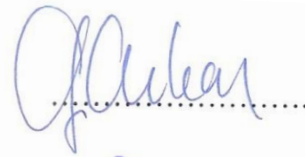
Graduate Program in Civil Engineering
Boğaziçi University

2013

CYCLIC MODELING OF COLD-FORMED STEEL STRUCTURES
WITH SHEATHED SHEAR PANELS

APPROVED BY:

Prof. Gülay Altay
(Thesis Supervisor)



Assist. Prof. Serdar Selamet



Assist. Prof. Cüneyt Vatansever



DATE OF APPROVAL: 23/08/2013

ACKNOWLEDGEMENTS

I would like to gratefully acknowledge my thesis supervisor, Prof. Gülay Altay, for her invaluable guidance, support, patience and encouragement throughout the preparation of the thesis. It would be impossible to complete this thesis without her great assistance and advices.

My thanks and appreciations also go to Assist. Prof. Serdar Selamet and Assist Prof. Cüneyt Vatansever for serving on my thesis committee with their positive and supportive attitudes to me.

I am grateful to my parents for their endless support, love and opportunities they have given me; with the special thanks to my sister, Sinem, who has never left me alone throughout my life and wish to present special thanks to my best friend, Alp for his endless support.

I would also like to acknowledge with appreciation the financial support that I have received from TUBİTAK. Their support has encouraged me to complete this thesis.

It is my loan to thank to the family of Ataçelik Yapı Üretim A.Ş. for their great support, understanding and tolerance throughout the preparation of the thesis.

ABSTRACT

CYCLIC MODELING OF COLD-FORMED STEEL STRUCTURES WITH SHEATHED SHEAR PANELS

The technology of cold-formed steel structures has been advanced and become one of the commonly used methods over time. However, the rate of application of the method has fallen short of the mark due to the designers have to deal with the different dimensioning principles and more failure mechanisms when the building constructed on a seismic region, such as in Turkey. Accordingly, in this study; design codes, specifications and manuals are investigated to form a general algorithm for the overall design of the shear wall as an assembly. Since the codes still need for experimental data; the previous major experimental researches are summarized. However, the tabulated design values of test results cannot be applied or extrapolated to wall assemblies in different configurations or construction details; it is tended towards to numerical methods instead of the experiments for the prediction of the lateral performance of the wall. Bouc-Wen-Baber-Noori (BWBN) model is selected for the simulation of the hysteretic behavior of the wall subjected to lateral in-plane load. It is assumed that the experimental force-displacement curve can be represented with a 4th degree polynomial. Then, the model is calibrated according to the experimental polynomial reasonably well. The model force-displacement backbone curves are interpreted with Equivalent Energy Elastic-Plastic (EEEP) method to obtain the design parameters such as, elastic limit, yield line, ductility, etc. The design limits are assigned to equivalent bracings with axial hinges which yields to similar results as the calibrated model for the single wall unit. Further, with some assumptions on the inter-story relations, nonlinear earthquake analysis of different wall configurations of multi-story structures is performed. It is observed that due to the insufficient test data provided about the selected experiment, experimental polynomial does not yield to the intended accuracy with the experiment itself. However, if more experimental studies with more data points are converted into BWBN model, the ranges for the parameters, each of which has different influence on the behavior, can be obtained for different wall configurations. Consequently, designers can perform FE analysis based on this introductory approach that needs for small number of elements to predict the lateral performance of the wall with minimized cost and time wasting of large-scale shear wall tests to be carried out for every new configuration where this construction technique is new to use such as Turkey.

ÖZET

TEKRARLI YÜKLER ALTINDA HAFİF ÇELİK YAPILARIN KAPLAMALI PANEL DUVARLAR İLE MODELLENMESİ

Hafif çelik yapı teknolojisi zaman içerisinde gelişmiş ve sık kullanılan yöntemlerden biri olmuştur. Ancak, Türkiye gibi deprem bölgelerinde, tasarımcıların daha farklı boyutlandırma kuralları ve yıkım mekanizmaları ile uğraşmak zorunda olmaları uygulama oranlarının nispeten düşük kalmasına neden olmuştur. Bu doğrultuda, bu çalışmada bir bütün olarak bir duvar panelinin tasarımı için genel bir algoritma geliştirmek adına tasarım standartları ve şartnameler incelenmiştir. Bu standartların hala test çalışmalarına ihtiyaç duyduğu gözlemlenmiş ve bugüne kadar yapılmış önemli test çalışmaları özetlenmiştir. Ancak, test sonuçlarına göre oluşturulmuş tasarım tablolarının farklı konfigürasyon ve konstrüktif detaylara sahip duvarlara uygulanamaması sebebiyle yatay performansın belirlenmesinde deneysel çalışmaların yerine geçebilecek sayısal çalışmalara yönelinmiştir. Bu doğrultuda, Bouc-Wen-Baber-Noori (BWBN) modeli, duvarın düzlemsel yatay yük altındaki histeretik davranışını yansıtmak için seçilmiştir. Deneysel kuvvet-deplasman eğrisinin 4. dereceden bir polinom ile ifade edilebileceği varsayılmış ve model, bu deney polinomuna göre kalibre edilmiştir. Model kuvvet-deplasman omurga eğrisi; elastik limit, akma çizgisi, süneklik gibi belirli tasarım parametrelerini elde etmek için Eşdeğer Enerji Elastik-Plastik (EEEP) yöntem ile yorumlanmıştır. Bu tasarım limitleri eksenel mafsallar ile eşdeğer çaprazlara atanmış ve model çalışmasıyla benzer sonuçlar elde edilmiştir. Katlar arasındaki ilişkilerdeki birkaç varsayımla, çok katlı yapılardaki farklı duvar yerleşimlerine göre doğrusal olmayan deprem analizi yapılmıştır. Seçilen deney verisinin yetersiz olmasından dolayı, deney polinomu istenilen kesinlik derecesine ulaşamamıştır. Ancak, eğer daha fazla veriye sahip daha fazla deney çalışması BWBN modeline dönüştürülebilirse, davranış üzerinde farklı etkileri olan her bir parametrenin farklı duvar tiplerine göre uygun değişim aralıkları belirlenebilecektir. Böylece tasarımcılar, az sayıda elemana ihtiyaç duyan bu giriş niteliğindeki yaklaşım ile sonlu elemanlar analizi yapabilir ve Türkiye gibi bu yapıım yönteminin yeni olduğu yerlerdeki her yeni konfigürasyon için yapılacak büyük çaplı deneylerin mali ve zaman kayıpları da en aza indirgenmiş olur.

TABLE OF CONTENTS

| | |
|---|-----------|
| ACKNOWLEDGEMENTS | iii |
| ABSTRACT..... | iv |
| ÖZET | v |
| LIST OF TABLES | x |
| LIST OF SYMBOLS | xi |
| LIST OF ACRONYMS/ABBREVIATIONS | xvi |
| 1. INTRODUCTION | 1 |
| 1.1. General Overview..... | 1 |
| 1.2. Problem Statement | 5 |
| 1.3. Objectives..... | 6 |
| 2. MEMBERS OF COLD-FORMED STEEL-FRAMED SHEATHED SHEAR WALLS .. | 7 |
| 2.1. Steel Wall Framing Members..... | 8 |
| 2.2. Sheathing Materials | 11 |
| 2.3. Connectors..... | 12 |
| 2.4. Base Shear Anchors and Hold-Down Devices..... | 14 |
| 3. LITERATURE REVIEW | 16 |
| 3.1. Design Codes Review | 16 |
| 3.1.1. General Remarks..... | 16 |
| 3.1.2. Design Flowchart for the Use of Current Design Codes | 18 |
| 3.1.2.1. Determination of Available Strength..... | 19 |
| 3.1.2.2. Design of Sheathing Braced Wall Stud. | 21 |
| 3.1.2.3. Design of Screw Connections..... | 26 |
| 3.1.2.4. Design of Anchorage Members and Hold-Downs..... | 28 |
| 3.1.2.5 Determination of the Deflection..... | 29 |

| | |
|---|-----|
| 3.2. Experimental Studies..... | 31 |
| 3.2.1. Major Experimental Studies since 1970's | 31 |
| 3.2.2. Selected Experimental Research..... | 45 |
| 3.3.1. Hysteresis Modeling | 48 |
| 4.1. The Bouc-Wen-Baber-Noori Model | 60 |
| 4.1.1. Background | 60 |
| 4.1.2. Equation of Motion and Constitutive Relations..... | 60 |
| 4.1.3. BWBN Parameters..... | 62 |
| 4.1.4. Summary of BWBN Model | 66 |
| 4.2. Solution Algorithm..... | 68 |
| 4.2.1 Quasi-Static BWBN Model | 70 |
| 4.2.2 Integration of the Stiff Set of ODEs | 73 |
| 4.2.3 Model and Experimental Polynomial Curves | 76 |
| 4.2.4 Error Minimization | 78 |
| 5. FINITE ELEMENT MODEL..... | 79 |
| 5.1. Interpretation of the Model Backbone Curve..... | 80 |
| 5.2. Finite Element Modeling - Equivalent Bracing Model..... | 87 |
| 5.3. Case Study..... | 89 |
| 6. CONCLUSION..... | 96 |
| APPENDIX A: SUMMARY OF EXPERIMENTAL STUDIES..... | 98 |
| APPENDIX B: MATLAB CODES FOR BWBN MODEL..... | 107 |
| MATLAB Code for Loading Protocol - Input Velocity..... | 107 |
| MATLAB Code for Quasi-Static Bouc-Wen-Baber-Noori Equations | 107 |
| MATLAB Code for the Model Polynomial Curve with the Minimized Error | 108 |
| MATLAB Code Add-on for the Calibration..... | 111 |
| REFERENCES | 113 |

LIST OF FIGURES

| | | |
|--------------|---|----|
| Figure 1.1. | Methods of Construction. | 2 |
| Figure 1.2. | Load Path for Seismic Force Acting on the Structure. | 4 |
| Figure 1.3. | Framework to Obtain the Global Response of the Structure..... | 5 |
| Figure 2.1. | Members of Cold-Formed Steel-Framed Sheathed Shear Walls. | 7 |
| Figure 2.2. | Methods of Forming. | 9 |
| Figure 2.3. | Cold-Formed Sections Used in Structural Framing. | 9 |
| Figure 2.4. | Sheathing Options for Cold-Formed Steel-Framed Shear Walls. | 11 |
| Figure 2.5. | Self-Tapping Screws and Total Thickness of the Connection. | 12 |
| Figure 2.6. | Screw Styles. | 13 |
| Figure 2.7. | Base Shear and Overturning. | 14 |
| Figure 2.8. | Anchors and Hold-Down Devices. | 15 |
| Figure 3.1. | Design Flowchart for the Use of Current Design Codes. | 18 |
| Figure 3.2. | Shear Wall Types. | 20 |
| Figure 3.3. | Buckling Modes of a Sheathed Stud. | 22 |
| Figure 3.4. | Failure Modes of Sheathing to Frame Connections under Shear Loading. | 26 |
| Figure 3.6. | Evaluation of Shear Capacity of Shear Walls with Openings. | 35 |
| Figure 3.7. | Shear Wall Configurations. | 37 |
| Figure 3.8. | Construction Stages of Steel-Framed House Subjected to Vibration Test. | 40 |
| Figure 3.9. | Hysteresis Test Data Enveloped by Backbone Curve. | 42 |
| Figure 3.10. | Energy Equivalent Elastic-Plastic (EEEP) Model. | 43 |
| Figure 3.11. | Special Detailing. | 44 |
| Figure 3.12. | Summary of all Sheathing Configurations of the Wall Specimens. | 45 |
| Figure 3.13. | Experimental Arrangement. | 46 |
| Figure 3.14. | Evaluation of the Conventional Elastic Limit. | 48 |
| Figure 3.15. | Deterioration in the Characteristics of the Hysteretic Behavior. | 49 |
| Figure 3.16. | SDOF Mechanical Model. | 50 |

| | | |
|--------------|--|----|
| Figure 3.17. | Plot of Resistance vs. Displacement that Covers Pinching, Stiffness Degradation and Load Deterioration. | 52 |
| Figure 3.18. | Individual Deterioration Modes Illustrated on a Peak-Oriented Model. | 53 |
| Figure 3.19. | Hysteresis Model. | 54 |
| Figure 3.20. | Skeleton-Part, E_{ps} , and Bauschinger-Part, E_{pb} | 55 |
| Figure 3.21. | Modeling with Idealized Equivalent Bracing. | 57 |
| Figure 3.22. | General Description of Steel Frame, Meshed Shell and Yield Pattern for the Shear Wall. | 58 |
| Figure 3.23. | A Sixteen-Node Equivalent Shell Element. | 59 |
| Figure 3.24. | Orthotropic Properties of Equivalent Shell Element. | 59 |
| Figure 4.1. | Schematic Model. | 61 |
| Figure 4.2. | Non-Damping restoring Force. | 61 |
| Figure 4.3. | Possible Hysteresis Shapes. | 63 |
| Figure 4.4. | Skeleton curves with varying n | 64 |
| Figure 4.5. | Parameters Control Degradation Rates. | 64 |
| Figure 4.6. | Baber and Noori's Pinching Function Effect. | 66 |
| Figure 4.7. | MATLAB Algorithm to Obtain the Model Force-Displacement Curve. | 69 |
| Figure 4.8. | Loading Protocol - Input Displacement. | 72 |
| Figure 4.9. | The Successive Hysteretic Cycles. | 75 |
| Figure 4.10. | Experimental and Model Polynomial Backbone Curves. | 77 |
| Figure 5.1. | MS Excel and SAP2000 Equivalent Bracing Flowchart. | 79 |
| Figure 5.2. | Method Developed to Determine the Equivalent Elasto-Plastic Model. | 80 |
| Figure 5.3. | Tri-Linear Idealized Hysteretic Model. | 81 |
| Figure 5.4. | Model and Experimental Force-Displacement Backbone Polynomial Curves. | 82 |
| Figure 5.5. | Tri-Linear Idealized Force-Displacement Curves. | 86 |
| Figure 5.6. | Proposed SDOF Single Unit Equivalent Braced Bar Model. | 87 |
| Figure 5.7. | Case Study: Three-Story Building. | 90 |
| Figure 5.8. | Spectrum Factor. | 92 |
| Figure 5.9. | Earthquake Forces Subjected to the Each Floor Level. | 93 |
| Figure 5.10. | Earthquake Forces Subjected to the Structure. | 94 |
| Figure 5.11. | Nonlinear Acceptance Criteria. | 95 |

LIST OF TABLES

| | | |
|------------|--|----|
| Table 2.1. | Mechanical Properties of Zinc Coated Galvanized Structural Steel. | 10 |
| Table 2.2. | Chemical Composition of Zinc Coated Galvanized Structural Steel. | 10 |
| Table 3.1. | Failure Mechanisms of the Cold-Formed Steel-Framed Sheathed Shear Walls. | 19 |
| Table 3.2. | Shear Resistance Adjustment Factor, C_0 | 21 |
| Table 3.2. | Sheathing Parameters. | 26 |
| Table 3.3. | Minimum Spacing, Edge and End Distances. | 27 |
| Table 3.4. | The Nominal Shear Strength per Screw, P_{ns} , Limited by Tilting and Bearing. | 28 |
| Table 3.5. | Design Coefficients and Factors for Light Framed Seismic Force- Resisting Systems. | 30 |
| Table 3.6. | Monotonic and Cyclic Test Results. | 47 |
| Table 4.1. | Summary of BWBN Hysteresis Model Parameters. | 67 |
| Table 4.2. | Final BWBN Parameters of the Calibrated Curves Related. | 74 |
| Table 4.3. | The 5 Coefficients of the Model and Experimental 4th Degree Polynomials. | 78 |
| Table 5.2. | The Comparison of the Calibrated Values Obtained from the Full-Scale Test and BWBN Model and Experimental Polynomials. | 84 |
| Table 5.3. | The Converted Axial Force-Displacement Curve Values for the Brace Members. | 89 |
| Table 5.5. | Distribution of Vertical Loads-I. | 91 |
| Table 5.6. | Distribution of Vertical Loads-II. | 91 |
| Table 5.7. | Earthquake Forces Subjected to each Floor Level. | 93 |
| Table 5.8. | Relative Joint Displacements Check. | 93 |

LIST OF SYMBOLS

| | |
|------------|---|
| A | Full unreduced cross-sectional area Parameter regulates the tangent stiffness and ultimate hysteretic strength |
| A_c | Gross cross-sectional area of chord member |
| A_e | Effective area at the stress F_n |
| A_0 | Total area of openings Effective ground acceleration coefficient |
| $A(T)$ | Spectral acceleration |
| b | Semi slip coefficient |
| B' | Tributary width of wall section to be subjected to seismic force |
| b | Width of the wall |
| C | Compressive force |
| c | Exponent defining the rate of deterioration Damping constant |
| C_D | Duration factor |
| C_d | Deflection amplification factor |
| C_0 | Shear resistance adjustment factor Initial column imperfection |
| C_1 | Term used to compute shear strain in wallboard |
| C_w | Warping constant of torsion of cross section |
| D | Depth of section Unthreaded shank diameter of the screw |
| D_{curv} | Displacement corresponding to F_y |
| D_{el} | Elastic limit displacement |
| D_i | Calculated value of the length of the diagonal at ith step |
| D_{max} | Displacement corresponding to F_{max} |
| D_{ult} | Ultimate displacement achieved during the tests |
| D_0 | Initial column imperfection |
| d | Nominal screw diameter |
| E | Modulus of elasticity |
| E_E | Cumulative elastic strain energy |

| | |
|--------------|--|
| E_H | Amount of energy consumed by the damping mechanism |
| E_i | Hysteretic energy dissipated in excursion i |
| E_P | Cumulative plastic strain energy |
| E_{ps} | Skeleton part of plastic strain energy |
| E_{pb} | Bauschinger part of plastic strain energy |
| E_T | Total amount of energy exerted by an earthquake |
| E_t | Tangent modulus |
| | Reference hysteretic energy dissipation capacity |
| E_0 | Initial column imperfection |
| E_1 | Term used to compute shear strain in wallboard |
| E' | Inelastic modulus of elasticity |
| e_1, e_2 | Edge distances |
| | Error functions |
| F | Strength ratio of a shear wall w/ openings to the one w/o openings |
| F_{corner} | Load subjected to the upper-left corner of the wall |
| F_e | Elastic buckling stress |
| F_{el} | Elastic Limit Force |
| F_k | Linear restoring force component |
| F_h | Hysteretic (non-linear) restoring force component |
| F_{max} | Maximum load achieved during the tests |
| F_n | Nominal buckling stress |
| F_s | Dowel bearing strength of the wood-based sheathing |
| F_u | Tensile strength |
| F_{ult} | Force level corresponding to D_{ult} |
| F_y | Yield point |
| G | Shear modulus of steel |
| g_i | Total dead load on the i th story |
| H, h | Wall height |
| h_i | Height of i th floor |
| h_n | Step size |
| $h(z)$ | Pinching function |
| J | St. Venant torsion constant of cross section |
| K | Effective length factor |

| | |
|--------------------------|---|
| K_a | Secant stiffness |
| K_D | Factor based on the unthreaded shank diameter |
| K_i | Initial stiffness of the shear wall |
| K_t | Effective length factor for torsion |
| K_x, K_y | Effective length factor for bending about principal axes |
| k_e | The ratio of elastic rigidity |
| k_p | Plastic area rigidity |
| k_1, \dots, k_4 | Stages of Bogacki–Shampine method |
| L | Laterally unbraced length of the member |
| L_i | Length of full height shear wall segment |
| L'_i | New coordinate of the upper-right corner at i th step |
| L_t | Unbraced length of compression member for torsion |
| L_x, L_y | Unbraced length of compression member for bending about principle axes |
| m | Mass |
| N, \bar{N}, M, \bar{M} | Unit step function derived from signum function |
| n | Live load participation factor |
| \bar{Q}_0 | Sheathing parameter |
| q | Distributed seismic load |
| | Load increment |
| q_i | Total live load on the i th story |
| p_1, p_2 | Screw spacing |
| p_1, \dots, p_5 | Coefficients of 4th degree polynomial |
| P_n | Nominal axial strength |
| P_{ns} | Nominal shear strength per screw |
| $P(t)$ | Non-dimensional applied force |
| \bar{P}_0 | Amplitude of the applied force |
| R | Response modification factor |
| r | Sheathing area ratio |
| r | Radius of gyration of full unreduced cross section about axis of buckling |
| r_0 | Polar radius of gyration of cross section about shear center |
| r_x, r_y | Radii of gyration of cross section about centroid principal axes |
| R_{nom} | Nominal unit strength of wall panel |
| $S(T)$ | Spectrum factor |

| | |
|------------------------|--|
| S_u | Maximum wall resistance |
| s | Center-to-center distance between fasteners |
| T | Tensile force |
| | Natural period of the structure |
| T_A, T_B | Spectrum characteristic periods |
| T_1 | First modal period of the structure |
| t | Thickness |
| $t_{\text{sheathing}}$ | Nominal panel thickness |
| t_{stud} | Nominal framing thickness |
| V | Shear force |
| V_{all} | Allowable shear strength of wall panel |
| V_{req} | Required shear strength of wall panel |
| V_t | Total base shear |
| v | Strength degradation function |
| W | Total weight of the structure |
| w_i | Weight of i th story |
| Z_u | Ultimate hysteretic strength |
| α | Rigidity ratio (weighting constant) |
| | Stiffness ratio |
| α_s | Stiffness hardening ratio |
| β | An adjustment factor to determine the deflection |
| β, γ, n | Hysteresis shape parameters |
| β_i | Cyclic deterioration in excursion i |
| γ | Actual shear strain in the sheathing |
| | Shear deformation angle |
| | Hysteretic energy dissipation capacity |
| | Plastic rigidity ratio |
| $\bar{\gamma}$ | Permissible shear stain of sheathing |
| $\varepsilon(t)$ | Dissipated hysteretic energy |
| λ | Stiffness degradation factor |
| | Pinching parameter |
| λ_c | Column slenderness parameter |

| | |
|--|---|
| λ_k | Stiffness degradation factor |
| λ_l | Load deterioration factor |
| λ_p | Strength ratio |
| ρ | An adjustment factor to determine the deflection |
| μ | Friction coefficient |
| | Ductility |
| Θ_i | Angle between the top chord and the diagonal at ith step |
| σ_{CR} | Critical buckling stress |
| σ_t | Torsional buckling stress |
| Φ_k | Stiffness degradation coefficient |
| Φ_l | Load deterioration coefficient |
| ω_0 | Pre-yield natural frequency of the system |
| Ω | Factor of safety |
| Δ_{el} | Conventional elastic limit displacement |
| Δ_i | Relative story displacement |
| ΔL_i | Displacement value at the upper-right corner at ith step |
| η | Stiffness degradation functions |
| δ_b | Bauschinger deformation |
| δ_s | Initial gap |
| δ_p | Pinched complementary yield displacement |
| δ_v | Vertical elongation at the overturning restraint |
| | Strength degradation parameter |
| δ_y | Elastic limit deformation |
| | Elastic strain energy at yielding |
| δ_1 | Deflection due to cantilever bending |
| δ_2 | Deflection due to shear deformation in the plane of the sheathing |
| δ_3 | Inelastic deflection of sheathing fasteners |
| δ_4 | Deflection due to overturning anchorage deformation |
| δ_η | Stiffness degradation parameter |
| $\zeta_1(\varepsilon), \zeta_2(\varepsilon)$ | Pinching functions control the progress of the pinching |
| ζ_0 | Linear damping ratio |
| $\zeta_s, p, q, \psi_0, \delta_\psi$ | Pinching parameters |

LIST OF ACRONYMS/ABBREVIATIONS

| | |
|--------|---|
| AISI | American Iron and Steel Institute |
| APA | American Plywood Association |
| ASCE | American Society of Civil Engineers |
| ASD | Allowable Stress Design |
| ASTM | American Society for Testing Materials |
| BWBN | Bouc-Wen-Baber-Noori |
| CEN | European Committee on Standardization |
| CFSEI | Cold-Formed Steel Engineers Institute |
| COFS | Committee on Framing Standards |
| CP | Collapse Prevention |
| CTICM | Centre Technique Industrial Construction Metallic |
| TDY-07 | Turkish Earthquake Resistant Design Code |
| ECCS | European Convention for Constructional Steelwork |
| EEEP | Energy Equivalent Elastic-Plastic |
| FEM | Finite Elements Method |
| FH | Fiber Hinge |
| FSAL | First Same as Last |
| GSB | Gypsum Sheathing Board |
| GWB | Gypsum Wall Board |
| HSLAS | High-Strength Low-Alloy Steel |
| IBC | International Building Code |
| IO | Immediate Occupancy |
| LS | Life Safety |
| NAHB | National Association of Home Builders |
| NBCC | National Building Code of Canada |
| ODE | Ordinary Differential Equation |
| OSB | Oriented Strand Board |
| PHM | Polygonal Hysteresis Model |
| PLY | Plywood |
| SCI | Steel Construction Institute |

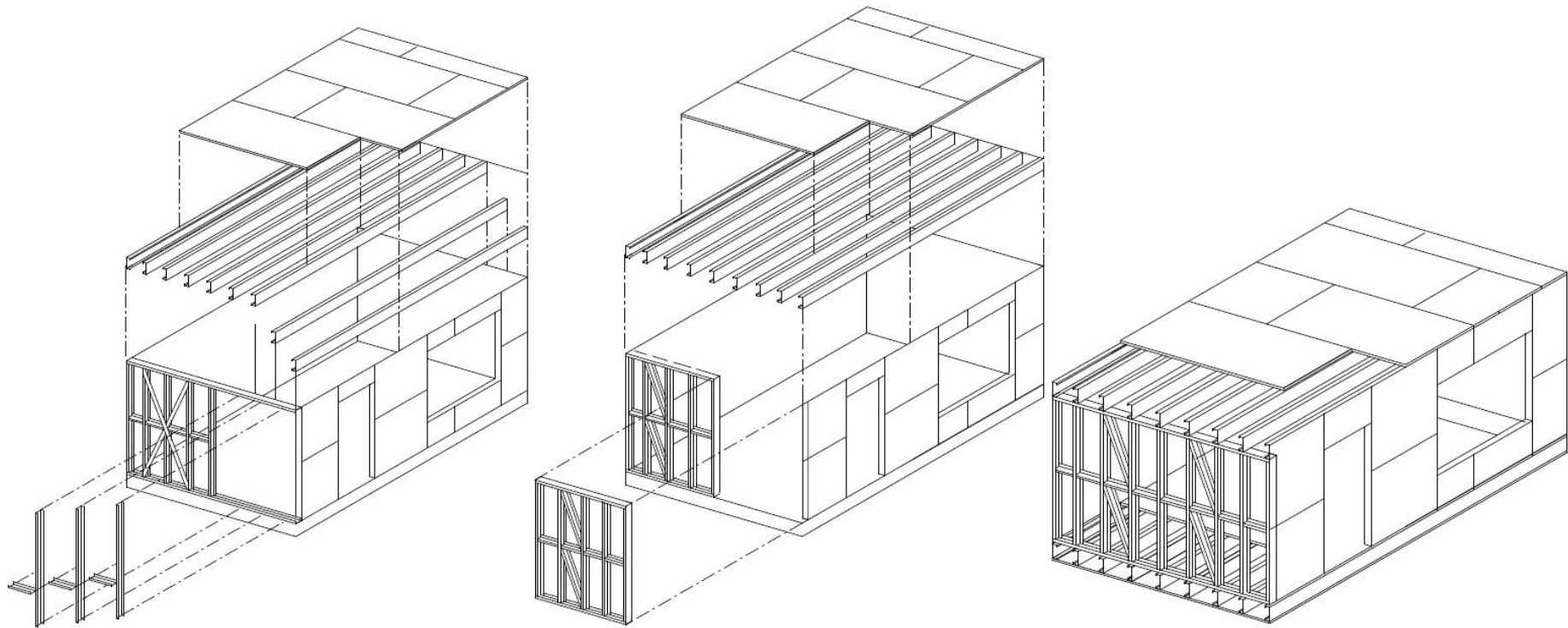
| | |
|------|---------------------------------|
| SDOF | Single-Degree-of-Freedom |
| SFA | Steel Framing Alliance |
| SHM | Smooth Hysteresis Model |
| SS | Steel Sheet |
| SSS | Steel Sheet Sheathed |
| TSE | Turkish Standards Institute |
| UBC | Uniform Building Code |
| USS | United States Steel Corporation |

1. INTRODUCTION

1.1. General Overview

Cold-formed steel-framed structures are constructed with basically cold-formed steel sections which can be prefabricated into panels or modules, or assembled on site using various methods of connection. The different forms of construction are demonstrated in Figure 1.1. In the stick-built construction (Figure 1.1a), discrete members are assembled on site to form columns, walls, rafters, beams and bracing to which cladding, internal lining and other elements are attached. The elements are generally delivered cut to length, with pre-punched holes, but connections are made on site using self-drilling self-tapping screws, bolts, or other appropriate site techniques. For panel construction, wall panels, floor cassettes and roof trusses may be prefabricated in a factory and later assembled on site, as in Figure 1.1b. Some of the finishing materials may be applied in the factory, to speed on-site construction. Panels can comprise the steel elements alone or the facing materials and insulation can be applied in the factory. The panels are connected on site using conventional techniques (bolts or self-drilling screws). In modular construction, units are completely prefabricated in the factory and may be delivered to site with all internal finishes, fixtures and fittings in place, as illustrated Figure 1.1c. Units may be stacked side by side, or one above the other, to form the stable finished structure (SCI P301, 2009).

However, until quite recently, modern technology has played a minor role in the design and construction of light-frame buildings (particularly those made from timber) and the construction techniques have been developed over long periods of time, based mainly on tradition and experience (Paevere, 2002). Furthermore, light-frame buildings made from cold-formed steel is a newer and more complex construction method and less knowledge of construction detailing about it has been accumulated so far, when it is compared to the wooden structures. Since there is not so much knowledge about the global response of such a complex structural system under environmental loadings (especially for lateral loads) to which it is subjected during its lifetime, gross simplifying assumptions are made in structural design that may lead uneconomical or unsafe structures.



a) Stick-Build Construction

b) Panel Construction

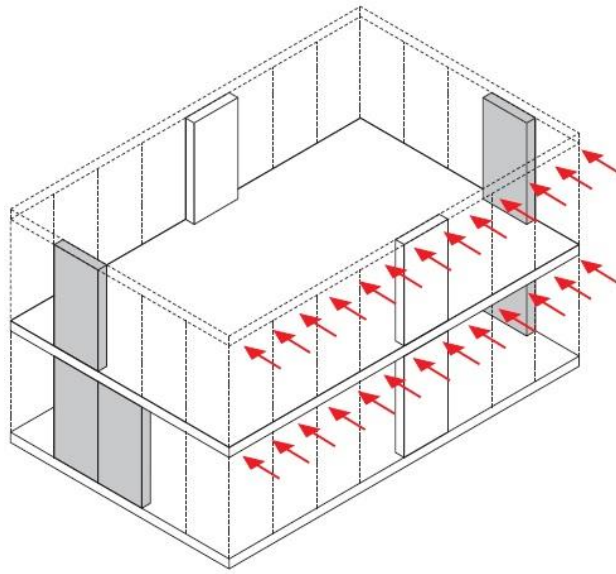
c) Modular Construction

Figure 1.1. Methods of Construction (adapted from SCI P301, 2009).

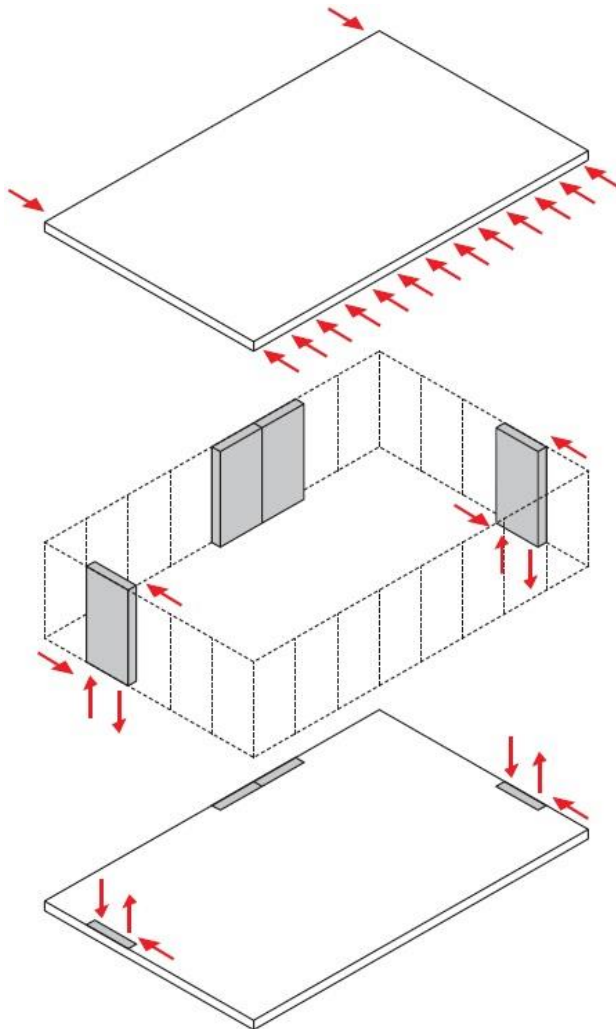
Accordingly, to obtain optimum design of cold-formed steel-framed structures; whichever the construction method preferred, the global response of the structure based on the load path and load share and distribution mechanism should be investigated well. These structures should be designed to withstand vertical and horizontal loads providing that all major building elements and every connection between each element resist the loads and transfer them from one element to the next until they reach the ground. When the subject is the load path, design for the vertical loads due to the weight of the building itself (dead load), the operational load (live load) and snow load is relatively less complicated. Vertical load is transferred from horizontal elements such as roof and floors of the structure to the load bearing walls below, then to the foundation and finally to the ground. However, the particular effects of lateral loads generated from wind and seismic forces based on their load paths should be understood well. Since the issue of the thesis is seismic design, the terms for lateral force or lateral design are used for seismic force and seismic design, respectively hereinafter regardless of the design for wind forces.

Seismic forces are generated by the shaking of the building during an earthquake. The shaking motion causes a force to develop within the structure in locations where the structure's mass is the largest. This is at the roof, floor and wall lines parallel to the earthquake forces. The load is transferred through the roof diaphragm and from the diaphragm by fasteners or framing anchors into the top of walls that run parallel to the direction of the load. This force then added to the force generated within the parallel wall and transferred down through the shear walls. This process is repeated through successive floors until the loads are transferred into the foundation and from there into the ground (APA, 1999). The load path scheme is illustrated in Figure 1.2.

Although the primary advantage of light-framed structures is their lightweight that results in less force due to inertia during an earthquake, thus less damage on the structure; seismic design of such buildings are still very crucial especially for the multi-story structures in earthquake zones like almost all regions in Turkey. So, it is mandatory to understand how seismic forces affect the structure and to obtain the knowledge of construction detailing and connections affect the ultimate performance of the structure.



a) Seismic Force acting on the Structure in one Direction



b) Load Path for Each Story

Figure 1.2. Load Path for Seismic Force Acting on the Structure (Stahl D560, 2002).

A cold-formed steel-framed structure is an assemblage of several components or sub-assemblies with repetitive members such as walls, floors, roof systems (as for panel construction) with inter-component connection elements between them. The elements of a light-frame structure that enable it to resist earthquake are its shear walls. So if the individual load-deflection performance of a single shear wall is known, then the global response of the structure can be obtained in an inductive framework demonstrated in Figure 1.3.

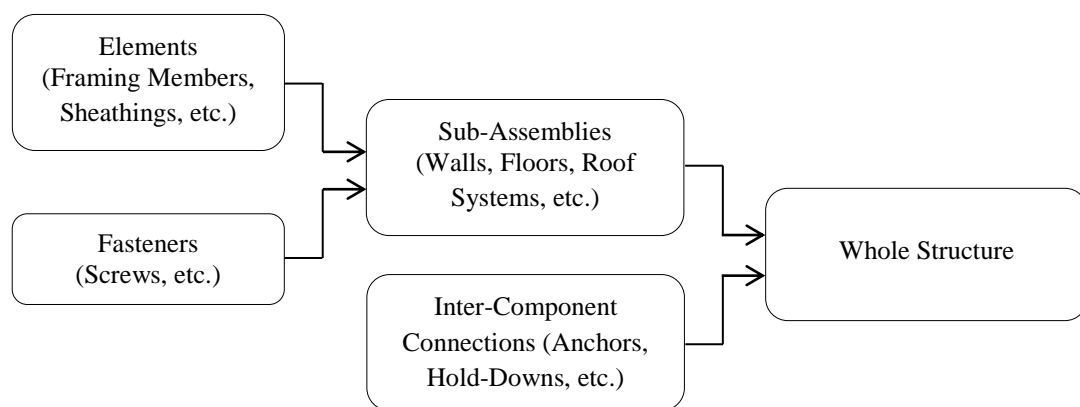


Figure 1.3. Framework to Obtain the Global Response of the Structure.

1.2. Problem Statement

The behavior of cold-formed steel-framed shear walls, the primary lateral load resisting elements, is dependent on several variables such as loading protocol and conditions, wall dimensions and aspect ratio, stud geometry and spacing, sheathing type and orientation, presence of blocking members, fastener types and schedule, anchor types and spacing, presence of hold-down devices, non-structural architectural details, etc. Interaction among all these variables determines the lateral strength of the wall instead of the each individual performance of the component. Due to the complex nature of this interaction and the lack of applicable analytical methods, lateral strengths of wall assemblies are obtained from experimental investigations.

From late 1970's, different experiments have been carried out on various wall assemblies subjected to in-plane shear load, thus an extensive database of experimental results is obtained and published in several design standards and guidelines. However, the

tabulated design values cannot be applied or extrapolated to wall assemblies in different configurations or construction details, so the application of the design tables are limited by the variation of the wall configuration tested so far. When it is taken into account that construction materials differ among different cultures, it becomes obligatory to conduct similar experiments with the available local materials where this construction technique is new to use, such as Turkey. A reliable numerical model that estimates the lateral strength and deflection with covering individual influence of each parameter listed above may reduce the cost and time wasting of research by minimizing the number of large-scale shear wall tests to be carried out for every new configuration.

If different force-displacement curves obtained from the experiments are managed to be represented by a numerical model which is sensible to the change in parameters such as stud spacing, fastener schedule, etc. and generalized for all configurations, it could be readily converted to equivalent finite elements model that could be used by a vast majority of designers. Consequently, it would allow for designers to accurately predict the behavior of a shear wall and provide for flexibility in terms of choices for wall configurations. Through the use of the equivalent model, multi-story structures could be designed against seismic forces in earthquake prone zones like almost all regions in Turkey.

1.3. Objectives

In order to fulfill the needs mentioned in Section 1.2, the objectives of this thesis are; to provide an overview of the seismic design requirements of design standards for sheathing braced design and a design flowchart with the use of current design codes; to provide an extensive literature review of previous cold-formed steel shear wall experimental programs and numerical methods for the simulation of the behavior of the walls under in-plane lateral loads, to apply an efficient analytical hysteresis model based on a mechanics approach to estimate the shear wall strength and deflection and calibrate it in accordance with a selected wall configuration, to represent the behavior of the wall with an equivalent bracing system for finite elements model, and to solve different wall configurations with the defined model to check the applicability of the model.

2. MEMBERS OF COLD-FORMED STEEL-FRAMED SHEATHED SHEAR WALLS

Components of a cold-formed steel-framed sheathed shear wall are demonstrated in Figure 2.1. Different from the steel bracing option, the skeleton of the structure is usually sheathed with plain or corrugated metal sheets and wood or gypsum based panels. When it is considered that the lateral force, from the roof or an upper floor, is applied to the wall at the upper corner, it will create mainly tension and compression at the boundaries (Figure 2.1) and internal forces at the fasteners. If the sheathing has adequate strength and stiffness and it is effectively connected with the skeleton, then the interaction between profiles, sheathings and sheathing fasteners can be advantageously taken into account in the structural analysis (Fiorino *et al.*, 2007). Thus, each member can structurally contribute the overall performance of the wall and the wall will act as a diaphragm.

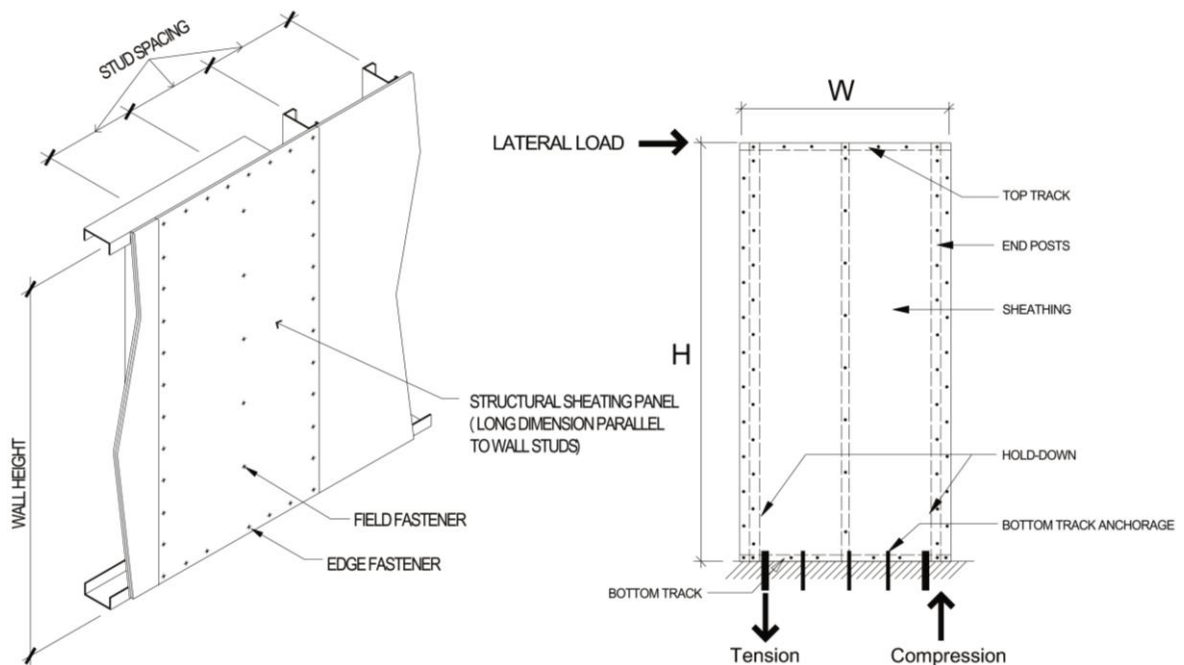


Figure 2.1. Members of Cold-Formed Steel-Framed Sheathed Shear Walls
(Prescriptive Method, 1997 and Ellis, 2012).

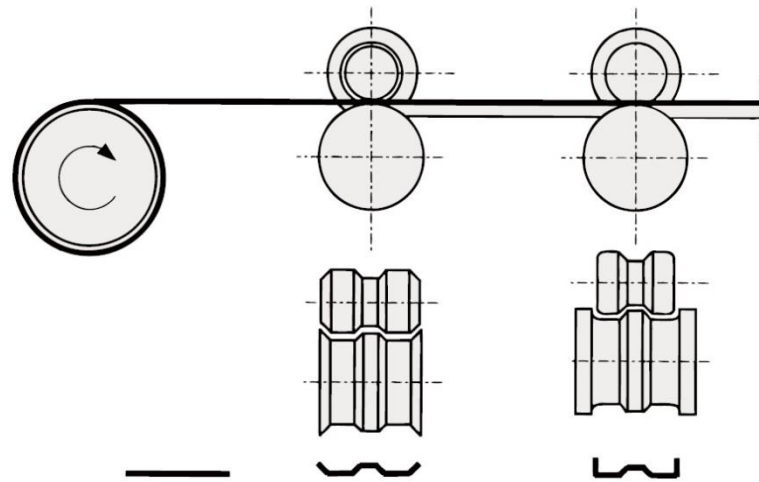
2.1. Steel Wall Framing Members

Cold-formed shapes usually imply relatively small, thin sections made by bending sheet or strip steel in roll-forming machines, press brakes, or bending brakes as illustrated in Figure 2.2. Because of the relative ease and simplicity of the bending operation and the comparatively low cost of forming rolls and dies, the cold-forming process lends itself well to the manufacture of unique shapes for special purposes and makes it possible to use thin material shaped for maximum stiffness (Wolford and Yu, 2000).

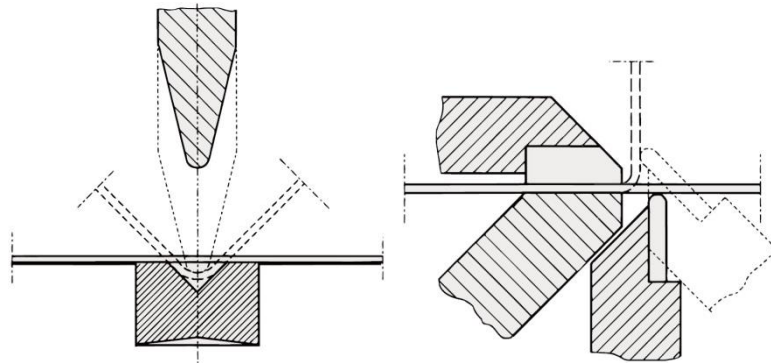
The cross section of a cold-formed member is achieved by a bending operation at room temperature, rather than the hot rolling process used for the heavier structural steel shapes. The dominant cold forming process is known as roll-forming (Figure 2.2a). In this process, a coil of steel is fed through a series of rolls, each of which bends the sheet progressively until the final shape is reached at the last roll stand. The number of roll stands may vary from 6 to 20, depending upon the complexity of the shape. Because the steel is fed in coil form, the process can achieve speeds up to about 90m/min. and is well suited for quantity production. Small quantities may be produced with a press-brake or bending brake operation (Figure 2.2b and 2.2c, respectively), particularly if the shape is simple, such as an angle or channel cross section (Brockenbrough and Merritt, 1999).

The thickness of steel sheet or strip generally used in cold-formed steel structural members ranges from 0.38 mm to about 6.35 mm. Steel plates and bars as thick as 25.4 mm can be cold formed successfully into structural shapes. In general, the depth of cold-formed individual framing members ranges from 50.8 to 305 mm, and the thickness of material ranges from 1.22 to about 6.35 mm (Yu and LaBoube, 2010).

The main structural components of wall frames are studs, vertical structural elements that support vertical loads and/or transfer lateral loads, and tracks, horizontal structural elements that are used for applications such as top and bottom plate for walls. Among all sections illustrated in Figure 2.3, shapes in (a) and (b) are the most common ones for, tracks and studs, respectively.



a) Cold-Roll Forming



b) Press Brake Operation

c) Bending Brake Operation

Figure 2.2. Methods of Forming (Stahl - Merkblatt480).

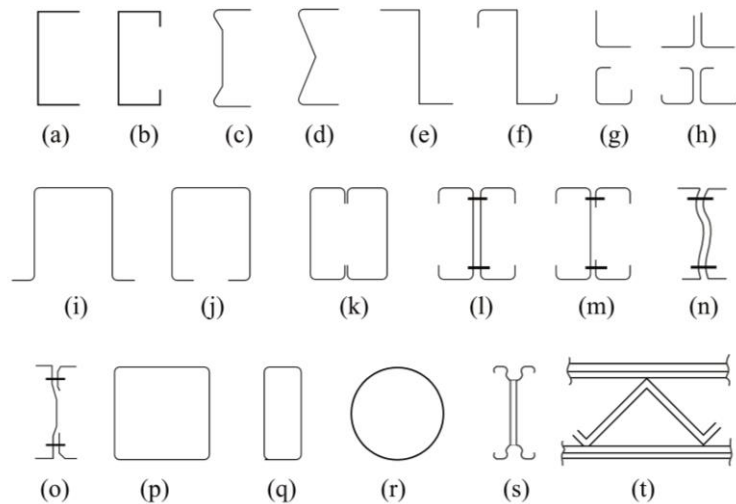


Figure 2.3. Cold-Formed Sections Used in Structural Framing (Yu and LaBoube, 2010).

Various material grades suitable for cold-forming are explained AISI S100-07 (2007) and EN.1993.1.3 (2006). From a wide range of different grades, galvanized cold-formed sections are usually formed with steel sheets manufactured in Turkish market in grades illustrated in Table 2.1. The sheets are manufactured according to TS EN 10346 (2010) which is adopted from DIN norms and defines technical delivery conditions of the continuously hot-dip coated steel flat products. “+Z” means zinc coated besides the available coating options such as “ZA” and “AZ” for continuously hot-dipped zinc-aluminum and aluminum-zinc coated steel sheets, respectively. The American Society for Testing and Materials (ASTM) terms such as SS shall designate sheet material whereas HSLAS shall designate high-strength low-alloy steel. Table 2.2 also demonstrates the chemical composition of zinc coated galvanized structural steel in accordance with TS EN 10346 (2010).

Table 2.1. Mechanical Properties of Zinc Coated Galvanized Structural Steel in Accordance with TS EN 10346 (2010) (Erdemir, 2013).

| Explanation | Manufacturing Standard | | Equivalent ASTM Grade | Mechanical Properties | | |
|---|------------------------|----------|--------------------------------|----------------------------------|------------------------------------|---|
| | Standard | Quality | | Yield Strength (MPa) <i>min.</i> | Tensile Strength (MPa) <i>min.</i> | Fracture Elongation (%) $L_0=80$ mm <i>min.</i> |
| Continuous hot-dip zinc coated structural steel | TS EN 10346:2009 | S220GD+Z | ASTM A653 SS Gr.230 | 220 | 300 | 20 |
| | | S250GD+Z | ASTM A653 SS Gr.255 | 250 | 330 | 19 |
| | | S280GD+Z | ASTM A653 SS Gr.275 | 280 | 360 | 18 |
| | | S320GD+Z | ASTM A653 HSLAS Gr.340 | 320 | 390 | 17 |
| | | S350GD+Z | ASTM A653 HSLAS Gr.380 Class 2 | 350 | 420 | 16 |

Table 2.2. Chemical Composition of Zinc Coated Galvanized Structural Steel in Accordance with TS EN 10346 (2010) (Erdemir, 2013).

| Explanation | Manufacturing Standard | Percentage by Mass % | | | | |
|---|------------------------|----------------------|----------------|----------------|---------------|---------------|
| | | C <i>max.</i> | Si <i>max.</i> | Mn <i>max.</i> | P <i>max.</i> | S <i>max.</i> |
| Continuous hot-dip zinc coated structural steel | TS EN 10346:2010 | 0.20 | 0.60 | 1.70 | 0.10 | 0.045 |

2.2. Sheathing Materials

The most widely used types of sheathings may be classified as wood-based panels, gypsum-based boards and steel sheathings as illustrated in Figure 2.4 (Fiorino *et al.*, 2007).



a) Plywood (PLY)

b) Oriented Strand Board (OSB)

c) Gypsum Wall Board (GWB)

Figure 2.4. Sheathing Options for Cold-Formed Steel-Framed Shear Walls

(APA, 2011 and Gypsum Association, 2013).

The main types of structural wood-based panels are veneer panels and particleboard panels (Faherty and Williamson, 1999). The most common example for veneer panels is plywood, PLY, (Figure 2.4a) which is composed of thin sheets of veneer, or plies, arranged in layers to form a panel. PLY may have an even number of plies, but it always has an odd number of layers, each layer consisting of one or more plies, or veneers. On the other hand, the most popular particleboard panel is oriented strand board, OSB, (Figure 2.4b) which is composed of compressed strands arranged in layers (usually three to five) oriented at right angles to one another. Wood is strongest along its grain and shrinks and swells most across the grain. Thus, by altering the grain direction between adjacent layers, strength and stiffness in both directions are maximized and shrinkage and swelling are minimized in each direction of the plywood whereas the nature of the cross-lamination of OSB distributes the wood's natural strength in both directions of the panel (APA, 2011).

Gypsum wall boards (GWB) differ from other panel-type building products, because they consist of a noncombustible core, composed primarily of gypsum, and a paper surfacing on the face, back and long edges (Figure 2.4c). When joints and fastener heads are covered with a joint compound system, GWB creates a continuous surface suitable for most types of interior decoration (Gypsum Association, 2013).

2.3. Connectors

There are two connection types in cold-formed steel-framed shear walls: steel-to-steel (framing members such as studs and tracks, steel sheathings, steel braces, and gusset plates, etc.) and rigid material-to-steel (wood or gypsum based sheathings) connections. Screws, welds, bolts, pins, nails, cold rivets and other special devices such as adhesives are generally used in such connections. However, the most common fastener for steel framing is the self-tapping screw (Fiorino *et al.*, 2007).

Self-tapping screws are externally threaded fasteners with the ability to form, or tap, their own internal mating threads when installed. Cold-formed steel construction utilizes two specific types of tapping screws: self-drilling and self-piercing tapping screws as illustrated in Figure 2.5, respectively (ASTM C1513, 2004).

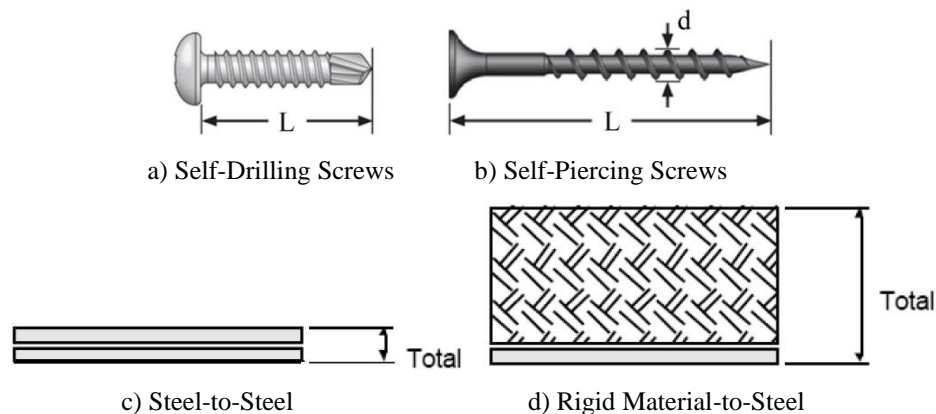


Figure 2.5. Self-Tapping Screws (Simpson Strong-Tie, 2011) and Total Thickness of the Connection (CFSEI TN F102, 2011).

Self-drilling screws are externally threaded fasteners with the ability to drill their own hole and form, or tap, their own internal threads without deforming their own thread and without fracturing during assembly. These screws are high-strength, one-piece installation fasteners and are used if the connection is multiple thicknesses of 0.8 mm steel or thicker. Self-piercing screws are externally threaded fasteners with the ability to self-pierce metallic material, form a sleeve by extruding steel sheet and form, or tap, their own mating threads when driven. Self-piercing screws are high-strength, one-piece one-side

installation fasteners with sharp point angles and are used to attach rigid sheathing materials to 0.8 mm steel (one thickness) or thinner (CFSEI TN F102, 2011).

To assure the proper performance of the connections, it is important to select proper fastener from a wide range of screws in different length and diameter having various head, thread or point styles (Figure 2.6) based on the material types to be joined, total thickness of the material in the connection and the corrosive environment. A body diameter is specified by a nominal screw size whereas the length of the fastener is measured from the bearing surface of the fastener to the end of the point as shown in Figure 2.5. Also, when specifying the screw length based on the total thickness in the connection (Figure 2.5) steel connections require three threads to be exposed beyond the grip length for a good connection as stipulated by AISI S200-07, 2007 (CFSEI TN F102, 2011).

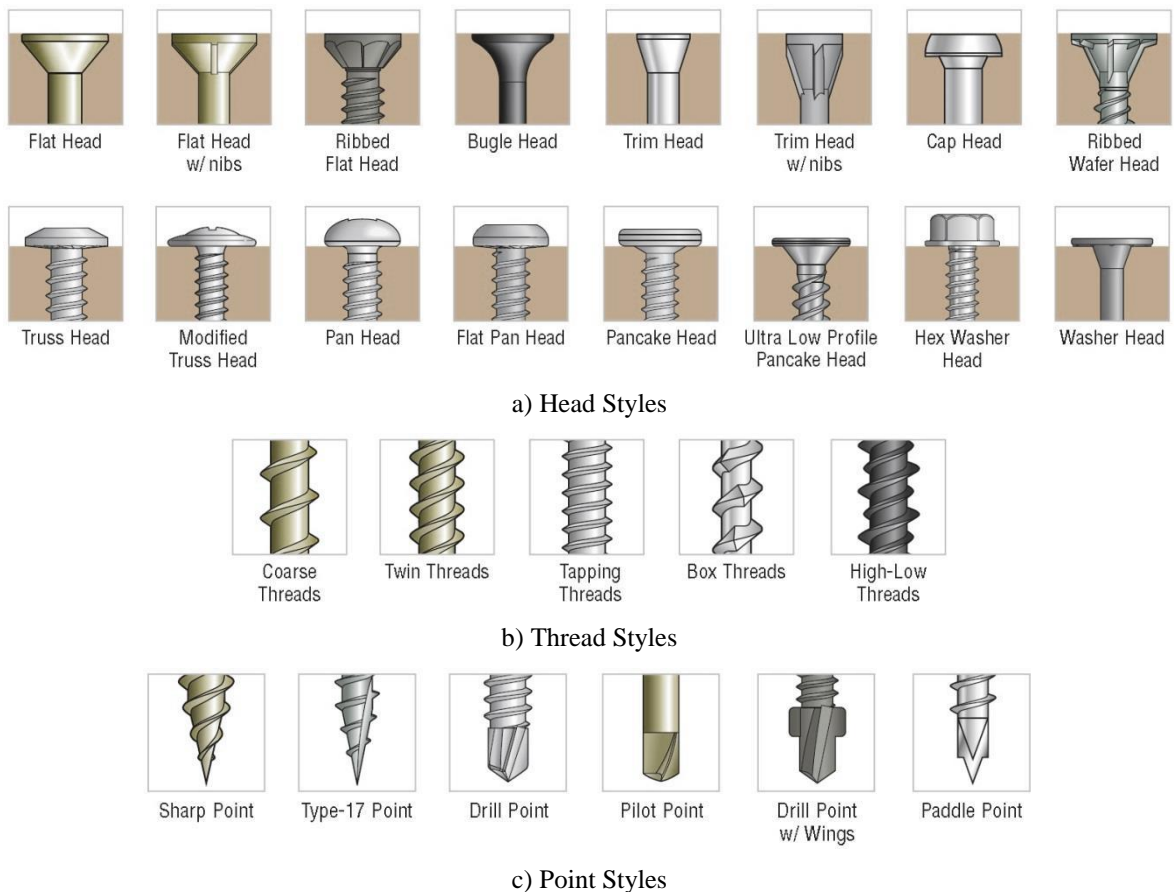


Figure 2.6. Screw Styles (Simpson Strong-Tie, 2011).

The head style is determined to meet specific application requirements. For example, a steel-to-steel connection requires a fastener head with some bearing surface on the top of

the material being connected, such as a hex or pan head whereas a steel-to-wood-based-sheathing requires a fastener head to be flush with the plywood or oriented strand board, such as a flat or wafer head style. Furthermore, self-piercing and self-drilling screws intended for cold-formed steel applications generally have a coarse thread. Drill screws that have fine threads are used for drilling thicker steel and the screw may easily strip if used in thinner cold-formed steel applications. Based on the total thickness of the connection, the point type is chosen in accordance with the recommended thickness provided by the manufacturers (CFSEI TN F102, 2011).

2.4. Base Shear Anchors and Hold-Down Devices

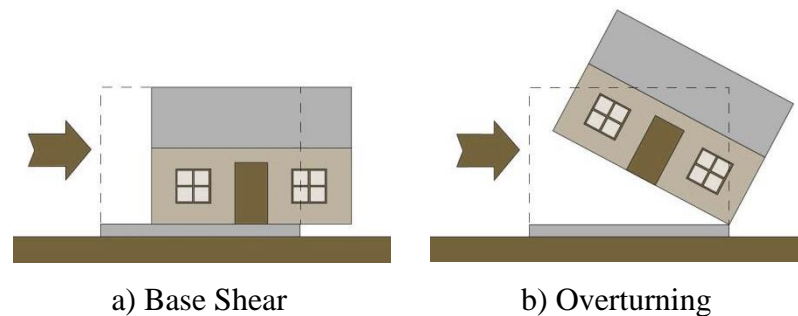


Figure 2.7. Base Shear and Overturning (APA, 1999).

Base shear (Figure 2.7a) is the force acting at the base of the structure in a direction parallel to the axis of the shear wall. The base shear connection keeps the building from sliding off its foundation. The purpose of a shear wall is to transfer the lateral load acting on the wall from above down through the floor below and into the foundation. The sheathing on the wall provides the rigidity and strength to accomplish this task. When transferring shear between the second and first floor shear walls; the sheathing, if constructed so that all panel edges occur over and are attached to common framing, will provide this shear transfer connection. At the foundation, where the sheathing from above is fastened to the plate below, the base shear transfer is accomplished by bolting the plate down to the foundation (Figure 2.8a) (APA, 1999).

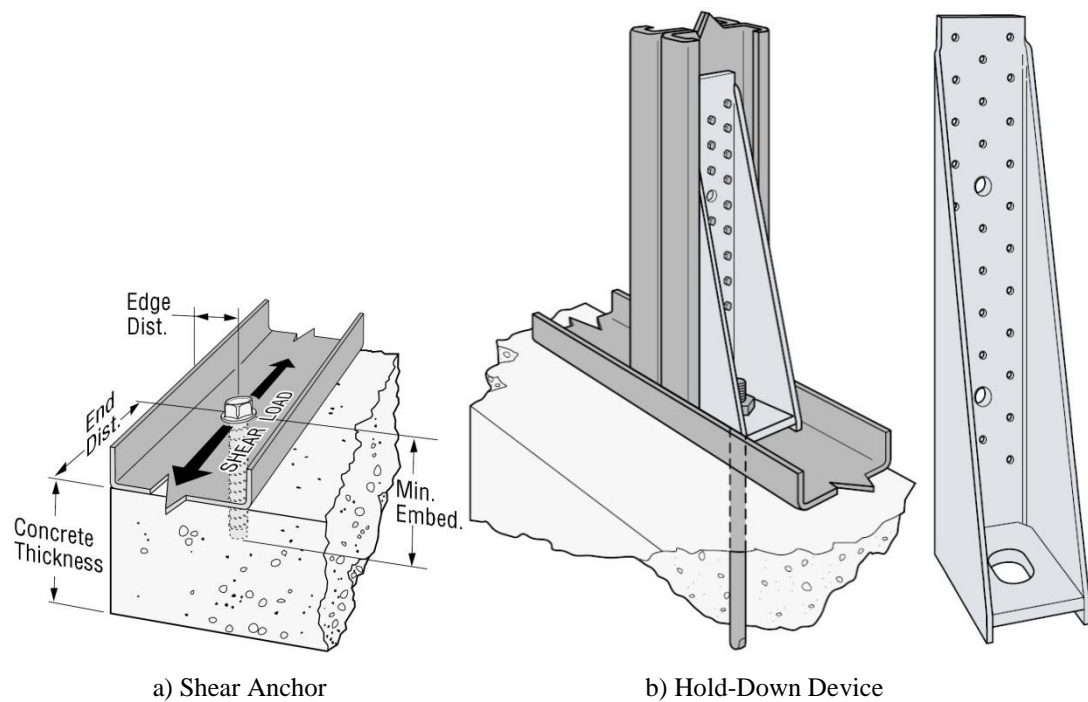


Figure 2.8. Anchors and Hold-Down Devices (Simpson Strong-Tie, 2010).

Once the shear wall is bolted soundly to the foundation with the base shear anchors (Figure 2.8a) and thus, prevented from sliding, the force acting on the shear wall at the roof level and the second floor level, if any, acts in a such way as to overturn the shear wall. The taller the structure, the greater the force is. Overturning (Figure 2.7b) is prevented by anchoring the double studs at each end of shear wall segment down to the foundation with a tension tie. These ties are called hold-downs (Figure 2.8b). The tension ties in shear walls located in floor above the ground floor must be continuous through the lower floor walls and must be ultimately tied into the foundation. The base shear anchors are placed to prevent sliding only, and will not hold down the shear wall against overturning. If used for this purpose, the sheathing on the shear wall will unzip from the bottom plate (APA, 1999)

3. LITERATURE REVIEW

3.1. Design Codes Review

3.1.1. General Remarks

The technology of cold-formed steel structures was advanced and especially, in the United States became one of the commonly used methods over time. This development proceeded among European countries as well as Turkey; however, the rate of application of the method fell short of the mark due to the conservative designers with traditional design habits had to deal with the different dimensioning principles and more failure mechanisms (Uzgider and Arda, 1989).

It is noteworthy that during the last three decades, research and development in cold-formed steel has been actively conducted at many institutions and individual companies in Australia and New Zealand, Austria, Canada, the Czech Republic, Finland, France, India, Japan, the Netherlands, the People's Republic of China, the Republic of South Africa, Sweden, Romania, the United Kingdom, Germany, and Russia some of which use their own national design codes and others use the dimensioning principles according to the American Iron and Steel Institute (AISI) design manuals has previously been translated into their own languages. Most of them also use EN.1993.1.3 (2006) published by the European Committee for Standardization (CEN) in collaboration with a working group of the European Convention for Constructional Steelwork (ECCS), for cold-formed, thin-gage members and sheeting (Yu and LaBoube, 2010).

On the other hand, the only and valid Turkish Code TS 11372 (1994) was created based on the 1968 edition of the "Specification for the Design of Cold-Formed Steel Structural Members" of AISI and the 1978 edition of the "Regles de Calclus des Constructions en Elements a Parois Minces an Acier" of CTICM and the newest reference it referred to is 1986 dated. However; today, cold-formed steel structures are becoming more popular than ever before, so it is inevitable to renew the long standing Turkish Code

with in the considerations of the recent developments in the world and consistent with the local design rules.

Since the 1946 edition of the Specification, ten subsequent versions of AISI standards were issued and in 1999, the AISI formed a new committee, the Committee on Framing Standards (COFS), to provide special provisions for the more narrow requirements and to develop standards specific to steel framing used in light-frame building construction. Provisions for the design of the sheathed cold-formed steel-framed shear walls as lateral load-resisting systems were first appeared in UBC1997 (1997) and in IBC2003 (2003), segmented (Type I) and perforated (Type II) shear wall types were introduced (Figure 3.2) whereas IBC2006 (2006) referenced AISI Lateral (2004) with shear wall deflection equations. The intent of AISI Lateral (2004) was to pull the requirements those were scattered among various building code provisions, design guides, technical notes and research reports together into one document that was recognized by the codes (Allen, 2006 and Ellis, 2012). The requirements for Type I walls in AISI Lateral (2004) were based on the studies conducted by Serrette *et al.* (1996, 1997 and 2002) at the University of Santa Clara whereas the requirements for Type II walls were based on the recognized provisions for wood systems, that was proven to be valid for steel-framed systems as for all wood systems (LaBoube and Larson, 2006). The code also provided a semi empirical calculation method that covered the bending, overturning, shear and inelastic deformation based on experimental data provided by Serrette and Chau (2003).

The most recent North American codes, specifications and manuals are more comprehensive than the European norms for the overall design of a shear wall as an assembly. Supportively, IBC 2012 Section 2211 states that wall studs shall be designed in accordance with either AISI S100-07 (2007) or AISI S211-07 (2007) whereas light frame shear walls, diagonal strap bracing that is part of a structural wall and diaphragms used to resist wind, seismic and other in-plane lateral loads shall be designed in accordance with AISI S213-07-S1-09 (2009). Since the EN 1993-1-3 (2006) does not provide an assembly design rules, so the emphasis is given especially on North American specifications in the following sections.

3.1.2. Design Flowchart for the Use of Current Design Codes

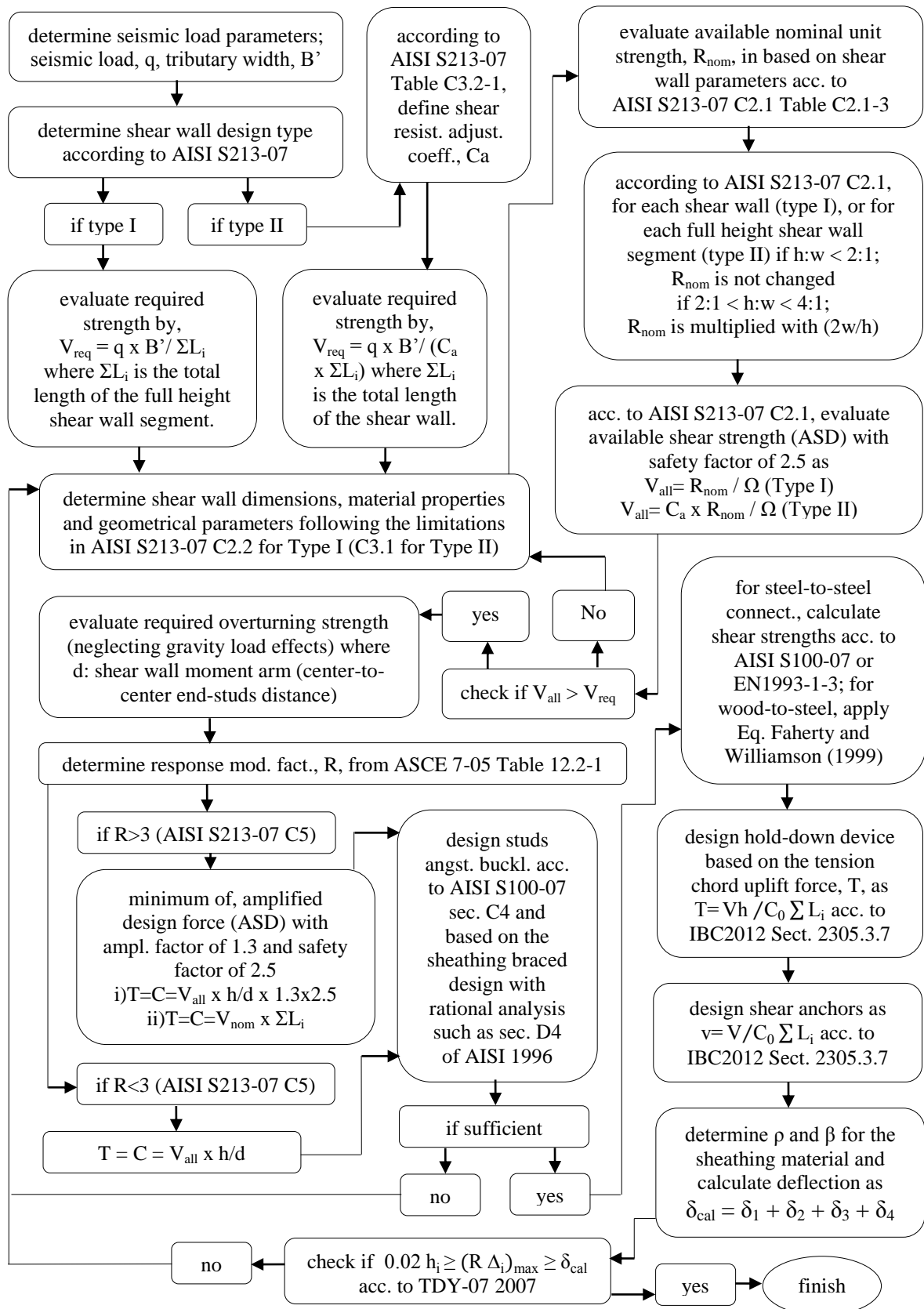


Figure 3.1. Design Flowchart for the Use of Current Design Codes.

There are different failure mechanisms related to the components that govern the ultimate strength and stiffness of the wall as an assembly are listed in Table 3.1. The components are briefly introduced in Chapter 2 and design of them for corresponding failure mode summarized throughout Section 3.1.2.

Table 3.1. Failure Mechanisms of the Cold-Formed Steel-Framed Sheathed Shear Walls
(adapted from Fiorino, 2003).

| Component | Failure Modes |
|--------------------------------|--|
| Sheathings | For wood-based sheathings, neglected; For steel sheathings, bearing in the steel sheathing, buckling of steel sheathing |
| Sheathing-to-frame connections | Bearing in the steel frame; Tilting of the screw; Screw shear Bearing in the wood-based panel |
| Frame members | Stud buckling |
| Hold-down devices | Shear in hold-down-to frame connection Tension in hold-down to foundation connection |
| Anchors | Anchor-to-frame connection Anchor-to-foundation connection |

3.1.2.1. Determination of Available Strength. There are two design methods for the evaluation of in-plane lateral load capacity of shear walls defined for wooden structures in IBC2003 (2003): Type I and Type II shear walls. Since the cold-formed steel-framed sheathed shear walls have similar lateral behavioral characteristics with light-frame wooden structures, AISI S213-07-S1-09 (2009) (The most recent version), also adopted by IBC2012 (2012), discusses the walls under these two types. Type I, or segmented, shear wall method is a traditional approach that takes into account the strength contribution of only full-height sheathed shear wall segments and each segment is anchored with a pair of hold-down devices as shown in above part of Figure 3.2. On the other hand, type II, or perforated, shear wall method is an empirical approach that treats a shear wall with openings as a single wall segment has an in-plane shear capacity reduced by a shear resistance adjustment factor, C_0 , given in Table 3.2. As it is illustrated in the below part of Figure 3.2, type II shear wall method requires only two hold-down devices, one at each end of the entire wall. In order to satisfy the strength demand, the use of higher grade or thicker framing members or sheathings, or denser fastener schedules and anchors due to the

negligence of strength contribution of the sheathed parts above and/or below openings; and increased number of hold-down devices besides their difficulty in the installation make type I less preferable when it is compared to type II.

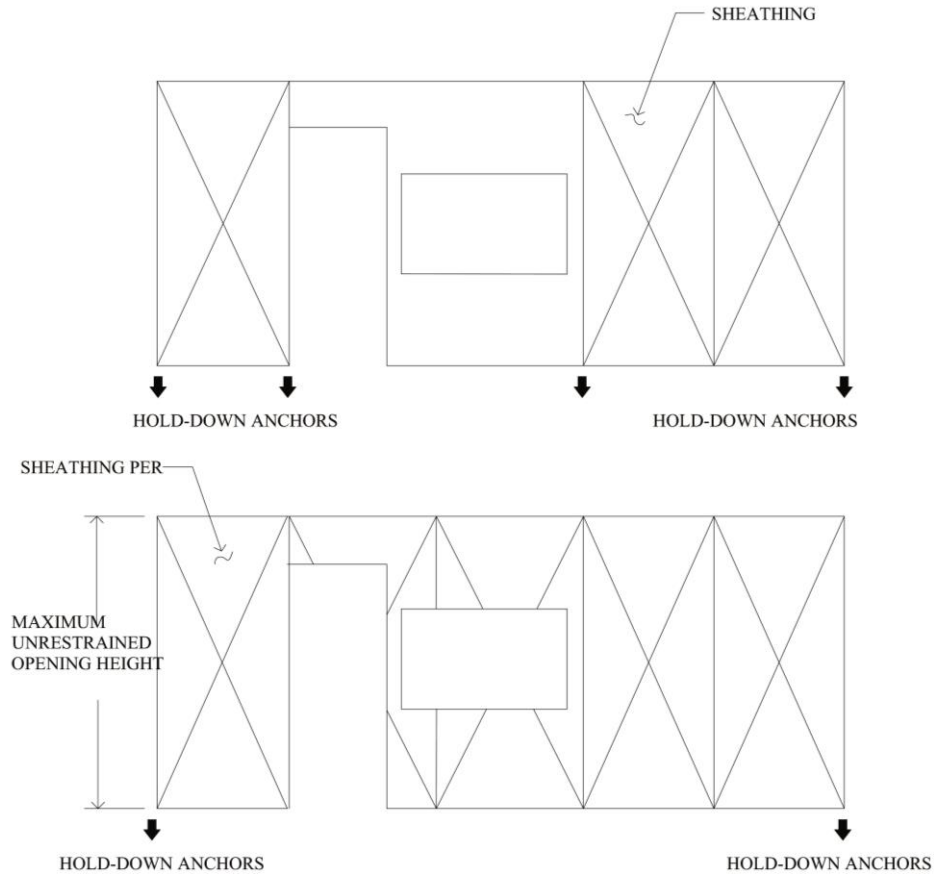


Figure 3.2. Shear Wall Types (Ellis, 2008).

Based on sections C3.2.1, C3.2.2 and Table C3.2-1 (Table 3.2) of AISI S213-07-S1-09 (2009), the resistance of a perforated shear wall shall be calculated based on shear resistance adjustment factor, C_0 , obtained with the percentage of full-height sheathing as the sum of the widths of perforated shear wall segments divided by the total width of the perforated shear wall, including openings and the maximum opening height as the maximum opening clear height. If areas above and below an opening remain unsheathed, the height of the opening shall be defined as the height of the wall (AISI S213-07-S1-09, 2009). It should be also noted that the perforated shear wall can be applicable when the some limitations on the geometry and elevations of the wall, layout of the openings, etc. set forth by C3.1 of AISI S213-07-S1-09 (2009) are satisfied.

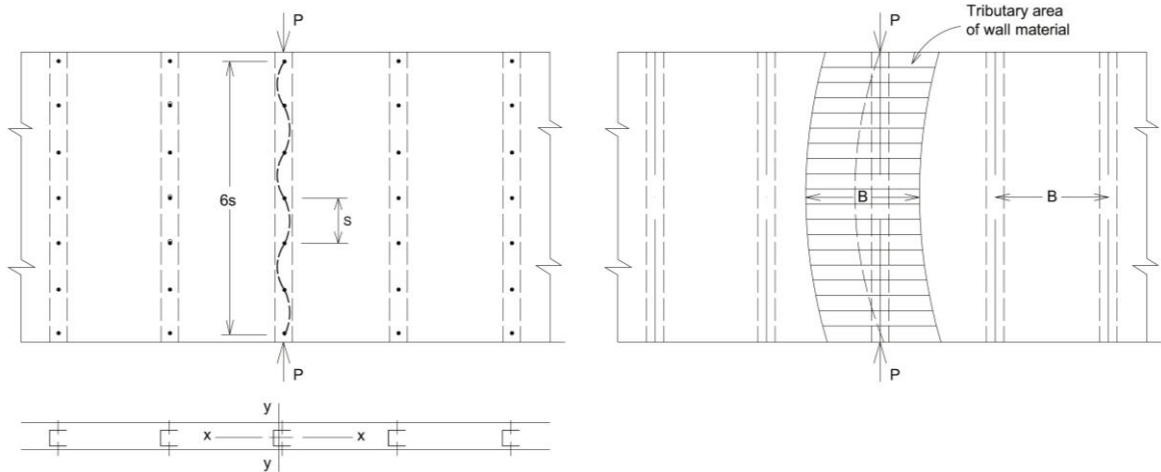
Table 3.2. Shear Resistance Adjustment Factor, C_0
(Table C3.2-1 - AISI S213-07-S1-09, 2009).

| Wall Height, H | Maximum Opening Height | | | | |
|-------------------------------------|---|---------|---------|---------|---------|
| | H/3 | H/2 | 2H/3 | 5H/6 | H |
| 2440 mm | 810 mm | 1220 mm | 1630 mm | 2030 mm | 2440 mm |
| 3050 mm | 1020 mm | 1530 mm | 2030 mm | 2540 mm | 3050 mm |
| Percentage of Full-Height Sheathing | Shear Resistance Adjustment Factor, C_0 | | | | |
| 10% | 1.00 | 0.69 | 0.53 | 0.43 | 0.36 |
| 20% | 1.00 | 0.71 | 0.56 | 0.45 | 0.38 |
| 30% | 1.00 | 0.74 | 0.59 | 0.49 | 0.42 |
| 40% | 1.00 | 0.77 | 0.63 | 0.53 | 0.45 |
| 50% | 1.00 | 0.80 | 0.67 | 0.57 | 0.50 |
| 60% | 1.00 | 0.83 | 0.71 | 0.63 | 0.56 |
| 70% | 1.00 | 0.87 | 0.77 | 0.69 | 0.63 |
| 80% | 1.00 | 0.91 | 0.83 | 0.77 | 0.71 |
| 90% | 1.00 | 0.95 | 0.91 | 0.87 | 0.83 |
| 100% | 1.00 | 1.00 | 1.00 | 1.00 | 1.00 |

3.1.2.2. Design of Sheathing Braced Wall Stud. Since the shear diaphragm action of wall material can increase the load carrying capacity of wall studs significantly, the effect of sheathing material on the design of wall studs were considered in Section D4 of the AISI provisions from 1980 to 2004 based on the comprehensive studies by Simaan and Peköz (Yu and LaBoube, 2010). AISI S100-07 (2007) Section D4 states that the wall studs shall be designed in accordance with AISI S211-07 (2007) which defines two methodologies for the design: all-steel design and sheathing braced design. In all steel design, structural contribution of attached sheathings is neglected and the studs are regarded as unsheathed and designed to comply with the requirements of Chapter C of AISI S100-07 (2007). On the other hand, AISI S211-07 (2007) provides a rational design method for sheathing braced shear wall stud. The assumptions and general requirements of the rational design provided by AISI S211-07 (2007) Chapter B and its Commentary.

When the stud buckles between fasteners, as shown in Figure 3.3, the failure mode may be flexural buckling, torsional buckling, or torsional–flexural buckling, depending on

the geometric configuration of the cross section and the spacing of fasteners. For these types of column buckling, the critical loads are based on the stud itself, without any interaction with the wall material. Therefore the design formulas given in Section C4 of AISI S100-07 (2007) can be applicable to these cases (Yu and LaBoube, 2010).



a) Buckling of Studs between Fully Effective Fasteners

b) Overall Column Buckling of Studs

Figure 3.3. Buckling Modes of a Sheathed Stud (AISI 1996 Specification, 1996).

AISI S211-07 (2007) permits sheathing braced design in accordance with an appropriate theory, tests, or rational engineering analysis. The following excerpts are adapted from Section D4 of AISI 1996 Specification (1996) for the design of wall studs, which can be considered an appropriate theory for design, besides Section C4 of AISI S100-07 (2007) for the Allowable Stress Design (ASD) method: Wall studs in compression in which the resultant of all loads acting on the member is an axial load passing through the centroid of the effective area, A_e , calculated at the stress level, F_n , are designed according to nominal axial strength defined in AISI S100-07 (2007) C4.1 as

$$P_n = \frac{A_e F_n}{\Omega} \quad (3.1)$$

where the safety factor, Ω , used to determine the allowable axial strength shall be equal to 1.8 and F_n shall be calculated as follows

$$F_n = (0.658^{\lambda_c^2}) F_y \quad \text{for } \lambda_c \leq 1.5 \quad (3.2)$$

$$F_n = (0.877/\lambda_c^2)F_y \quad \text{for } \lambda_c > 1.5 \quad (3.3)$$

where $\lambda_c = (F_y/F_e)^{1/2}$ and F_e is the minimum theoretical elastic buckling stress calculated for each of the following three conditions to lead the minimum value of F_n (noting that the following excerpts are based on the singly-symmetric C-sections):

- (i) To prevent column buckling between fasteners in the plane of the wall, $(F_n)_1$ shall be calculated in accordance with AISI S100-07 (2007) Section C4 with KL equal to two times the distance between fasteners. The minimum of following two cases is the governing buckling stress. The first one, the elastic flexural buckling stress, is calculated based on the effective length KL equals to two times the distance between fasteners as

$$KL/r = 2s/r_y \quad (3.4)$$

$$F_e = \frac{\pi^2 E}{(KL/r)^2} = \frac{\pi^2 E}{(2s/r_y)^2} \quad (3.5)$$

where E is the modulus of elasticity of steel, K is the effective length factor, L is the laterally unbraced length of the member, s is the center-to-center distance between fasteners and r is the radius of gyration of full unreduced cross section about axis of buckling. The other one, when the member subject to torsional or flexural-torsional buckling, F_e shall be calculated as

$$F_e = \frac{1}{2\beta} \left[(\sigma_{ex} + \sigma_t) - \sqrt{(\sigma_{ex} + \sigma_t)^2 - 4\beta\sigma_{ex}\sigma_t} \right] \quad (3.6)$$

where $\beta = 1 - (x_0/r_0)^2$, $r_0 = (r_x^2 + r_y^2 + x_0^2)^{1/2}$ is the polar radius of gyration of cross-section about shear center where x_0 is the distance from shear center to centroid along principal x -axis, and r_x and r_y are the radii of gyration of cross section about centroid principal axes,

$$\sigma_{ex} = \frac{\pi^2 E}{(K_x L_x / r_x)^2} \quad (3.7)$$

where K_x is the effective length factor for bending about x-axis and L_x is the unbraced length of member for bending about x-axis.

$$\sigma_t = \frac{1}{Ar_0^2} \left[GJ + \frac{\pi^2 EC_w}{(K_t L_t)^2} \right] \quad (3.8)$$

where A is the area of full unreduced cross section, G is the shear modulus, J is the Saint-Venant torsion constant of cross-section, C_w is the torsional warping constant of cross-section, K_t is the effective length factor for twisting and L_t is the unbraced length of member for twisting.

- (ii) To prevent flexural and/or torsional overall column buckling, $(F_n)_2$ shall be calculated in accordance with AISI S100-07 Section C4 and AISI 1996 Section D4 with F_e taken as the smaller of two theoretical elastic buckling stress under concentric loading, σ_{CR} , values as

$$\sigma_{CR} = \sigma_{CR} + \bar{Q}_a \quad (3.9)$$

$$\sigma_{CR} = \frac{1}{2\beta} \left[(\sigma_{ex} + \sigma_{tQ}) - \sqrt{(\sigma_{ex} + \sigma_{tQ})^2 - 4\beta\sigma_{ex}\sigma_{tQ}} \right] \quad (3.10)$$

where σ_{ey} , σ_{ex} and σ_t calculated as the above equations based on the value of KL equals to L , and

$$\sigma_{tQ} = \sigma_t + \bar{Q}_t \quad (3.11)$$

$$\bar{Q} = \bar{Q}_0 (2 - s/s') \quad (3.12)$$

$$\bar{Q}_a = \bar{Q}/A \quad (3.13)$$

$$\bar{Q}_t = (\bar{Q}d^2) / (4Ar_0^2) \quad (3.14)$$

where s is the fastener spacing (mm), $s' = 305$ mm and \bar{Q}_0 is obtained from the table and d is the depth of the section.

- (iii) To prevent shear failure of sheathing, a value of $(F_n)_3$ shall be used in the following equation, based on the AISI 1996 Specification (1996) Section D4, so that the shear strain of sheathing, γ , does not exceed the permissible strain, $\bar{\gamma}$. The shear strain, γ , shall be determined as follows

$$\gamma = \left(\frac{\pi}{L}\right) \left[C_1 + E_1 \frac{d}{2} \right] \quad (3.15)$$

where C_1 and E_1 are the absolute values of C_1 and E_1 specified below

$$C_1 = \frac{F_n C_0}{\sigma_{ey} - F_n + \bar{Q}_a} \quad (3.16)$$

$$E_1 = \frac{F_n [(\sigma_{ex} - F_n) (r_0^2 E_0 - x_0 D_0) - F_n x_0 (D_0 - x_0 E_0)]}{(\sigma_{ey} - F_n) r_0^2 (\sigma_{tQ} - F_n) - (F_n x_0)^2} \quad (3.17)$$

where C_0 , D_0 and E_0 are initial column imperfections which shall be assumed to be at least

$$C_0 = L/350 \text{ (in a direction parallel to the wall)} \quad (3.18)$$

$$D_0 = L/700 \text{ (in a direction perpendicular to the wall)} \quad (3.19)$$

$$D_0 = L/(d \times 10.000), \text{ rad., (a measure of the initial twist of the stud from the initial, ideal, unbuckled shape)} \quad (3.20)$$

If $F_n > 0.5 F_y$, then in the definitions for σ_{ey} , σ_{ex} and σ_{tQ} , the parameters E and G shall be replaced by E' and G' , respectively as defined below

$$E' = 4EF_n \frac{(F_y - F_n)}{F_y^2} \quad (3.21)$$

$$G' = G \left(\frac{E'}{E} \right) \quad (3.22)$$

Sheathing parameters \bar{Q}_0 and $\bar{\gamma}$, defined by AISI 1996 Specification (1996) Section D4, shall be permitted to be determined from representative full-scale tests, conducted and evaluated as described by published documented methods, or from the small scale test values given in Table 3.2 (AISI 1996 Specification (1996) Table D4). Table 3.2 is applicable with the limitations (i) all values are for sheathing on both sides of the assembly; (ii) all fasteners are no.6, type S-12 self-drilling drywall screws with pan or bugle head or equivalent; and (iii) all sheathing is 12.7 mm thick except as noted.

Table 3.2. Sheathing Parameters (AISI 1996 Specification (1996) Table D4).

| Sheathing | \bar{Q}_0 (kN) | $\bar{\gamma}$ (length/length) |
|-------------------------------------|------------------|--------------------------------|
| 9.5 mm to 15.9 mm thick gypsum | 107.0 | 0.008 |
| Lignocellulosic board | 53.4 | 0.009 |
| Fiberboard (regular or impregnated) | 32.0 | 0.007 |
| Fiberboard (heavy impregnated) | 64.1 | 0.010 |

3.1.2.3. Design of Screw Connections. There are four possible failure modes for screw connections when the shear wall is subjected to in-plane lateral load. . Therefore, the shear strength of screw connections is equal to the minimum of shear strengths associated to each failure modes listed as (illustrated in Figure 3.4):

- (i) bearing failure in the steel frame (including steel sheathings),
- (ii) tilting failure of the screw,
- (iii) screw shear failure, and
- (iv) bearing failure of the rigid sheathing material (wood or gypsum based sheathings)

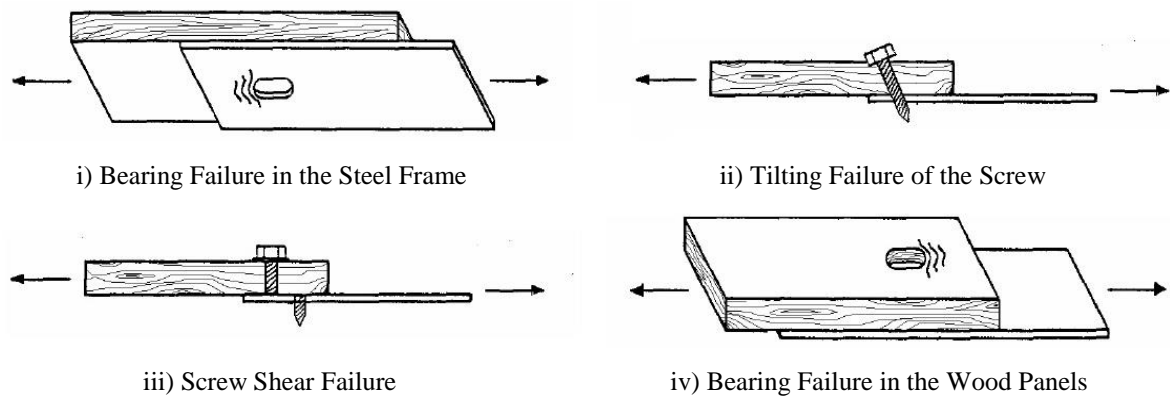


Figure 3.4. Failure Modes of Sheathing to Frame Connections under Shear Loading, Fiorino (2003).

AISI S100-07 (2007) and EN 1993-1-3 (2006) provide the requirements of self-tapping screw connections with the limitations on the fastener schedule as stated in Figure 3.5 and Table 3.3. Different from the EN 1993-1-3 (2006), if the end distance is parallel to the force on the fastener, the nominal shear strength per screw, P_{ns} , shall be limited by AISI S100-07 (2007) as

$$P_{ns} = t e F_u \quad (3.23)$$

where t is the thickness of part in which end distance is measured, e is the distance measured in line of force from center of a standard hole to nearest end of connected part, and F_u is the tensile strength of part in which end distance is measured.

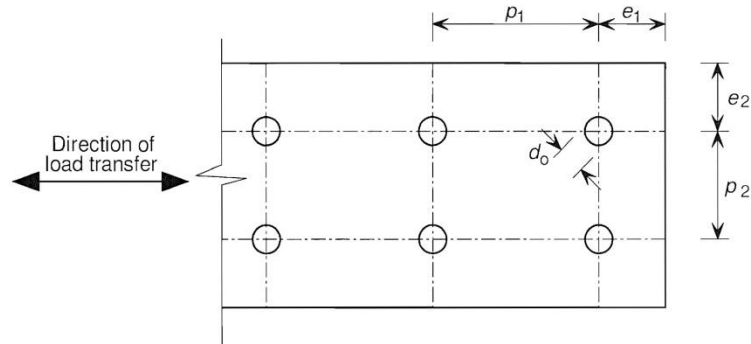


Figure 3.5. Minimum Spacing, Edge and End Distances (EN 1993-1-3, 2006).

Table 3.3. Minimum Spacing, Edge and End Distances.

| Code | Nom. Screw Diameter | Minimum Spacing and Edge Distances | | | |
|---------------------|---|------------------------------------|---------------|-----------------|---------------|
| | | see Eq.3.23 | $p_1 \geq 3d$ | $e_2 \geq 1.5d$ | $p_2 \geq 3d$ |
| AISI S100-07 (2007) | $2.03 \text{ mm} \leq d \leq 6.35 \text{ mm}$ | | $p_1 \geq 3d$ | $e_2 \geq 1.5d$ | $p_2 \geq 3d$ |
| EN 1993-1-3 (2006) | $3.00 \text{ mm} \leq d \leq 8.00 \text{ mm}$ | $e_1 \geq 3d$ | $p_1 \geq 3d$ | $e_2 \geq 1.5d$ | $p_2 \geq 3d$ |

The nominal shear strength per screw, P_{ns} , limited by tilting and bearing for steel members is determined as Table 3.4 where d is the nominal screw diameter, t_1 is the thickness of member in contact with screw head or washer whereas t_2 is the thickness of member not in contact with screw head or washer and F_{u1} and F_{u2} are the tensile strengths of these members, respectively. When allowable strength design method is concerned; safety factor, Ω , equals to 3.00. Moreover, if the nominal strength is obtained from laboratory testing or reported by manufacturers, the safety factor shall be taken as $1.25\Omega \leq 3.00$ (AISI S100-07, 2007).

The bearing strength of the screws for wood based sheathings is determined by the following equation (Faherty and Williamson, 1999)

$$P_{ns} = \Omega C_D \frac{t_s D F_s}{K_D} \quad (3.24)$$

where C_D is the duration factor equals to 1.6 for seismic loads, t_s is the thickness of the wood-based sheathing, D is the unthreaded shank diameter of the screw, F_S is the dowel bearing strength of the wood-based sheathing and K_D is the factor based on the unthreaded shank diameter equals to 2.2 (for $D \leq 4.3$ mm), $10 D+0.5$ (for $4.3 \text{ mm} < D < 6.4$ mm), or 3.0 (for $D > 6.4$ mm)

Table 3.4. The Nominal Shear Strength per Screw, P_{ns} , Limited by Tilting and Bearing.

| Code | Thickness Ratio | | | |
|---------------------|--|--------------------------------|---|---|
| | $t_2/t_1 \leq 1$ | $1 < t_2/t_1 < 2.5$ | $t_2/t_1 \geq 2.5$ $t_1 < 1 \text{ mm}$ | $t_2/t_1 \geq 2.5$ $t_1 \geq 1 \text{ mm}$ |
| AISI S100-07 (2007) | <i>smallest of</i> $4.2 (t_2^3 d)^{1/2} F_{u2}$ $2.7 t_1 d F_{u1}$ $2.7 t_2 d F_{u2}$ | <i>by linear interpolation</i> | <i>smaller of</i> $2.7 t_1 d F_{u1}$ $2.7 t_2 d F_{u2}$ | |
| EN 1993-1-3 (2006) | $3.2 (t_2^3 d)^{1/2} F_{u2}$ and $t_2/d \leq 0.43$ | <i>by linear interpolation</i> | $3.2 (t_1^3 d)^{1/2} F_{u1}$ and $t_1/d \leq 0.43$ | <i>smaller of</i> $2.1 t_1 d F_{u1}$ $2.1 t_2 d F_{u2}$ |

3.1.2.4. Design of Anchorage Members and Hold-Downs. Where the dead load stabilizing moment is not sufficient to prevent uplift due to overturning moments on the wall, an anchoring device shall be provided to work as an overturning restraint. Anchoring devices shall maintain a continuous load path to the foundation. Anchorage for uplift forces due to overturning shall be provided at each end of the perforated shear wall. The uplift anchorage shall conform to the requirements of IBC2012 (2012) Section 2305.3.7, except that for each story the minimum tension chord uplift force, T , shall be calculated in accordance with the following:

$$T = \frac{V h}{C_0 \sum L_i} \quad (3.25)$$

where T is the tension chord uplift force, V is the shear force in perforated shear wall, h is the perforated shear wall height, C_0 is the shear resistance adjustment factor obtained from Table 3.1 and $\sum L_i$ is the sum of widths of perforated shear wall segments.

The unit shear force, v , transmitted into the top of a perforated shear wall, out of the base of the perforated shear wall at full height sheathing and into collectors connecting shear wall segments shall be calculated in accordance with the following:

$$v = \frac{V}{C_0 \sum L_i} \quad (3.26)$$

where v is the unit shear force in N/mm. In addition, perforated shear wall bottom plates at full-height sheathing shall be anchored for a uniform uplift force, t , equal to the unit shear force, v , determined above.

3.1.2.5 Determination of the Deflection. According to the Turkish Earthquake Resistant Design Code (TDY-07, 2007), maximum value of relative story drift, $(\delta_i)_{\max}$ of the i th floor of the structure in each direction is calculated as,

$$\delta_i = R \Delta_i \quad (3.27)$$

$$\frac{(\delta_i)_{\max}}{h_i} \leq 0.02 \quad (3.28)$$

where Δ_i is the relative reduced story drift at the i th floor, R is the response modification factor and h_i is the story height of the i th floor. ASCE 7-05 (2006) Table 12.2-1 states the design coefficients and factors for seismic force-resisting light-framed structures as in Table 3.5. Therefore, maximum value of relative story drift can be obtained with using the response modification coefficients in Table 3.5, thus the seismic drift limit which shall satisfy Equation 3.29.

$$(\delta_i)_{\max} \geq \delta_{\text{cal}} \quad (3.29)$$

AISI S213-07 (2007) Equation C2.1-1 provides a semi-empirical calculation method for the overall deflection of the shear wall, δ_{cal} , based on the study of Serrette and Chau (2003) which takes into account the contributions of (i) deflection due to cantilever bending, δ_1 ; (ii) deflection due to shear deformation in the plane of the sheathing, δ_2 ; (iii) inelastic deflection of sheathing fasteners, δ_3 ; and (iv) deflection due to overturning anchorage deformation, δ_4 , as in Equation 3.30.

$$\delta_{cal} = \delta_1 + \delta_2 + \delta_3 + \delta_4 \quad (3.30)$$

$$\delta_{cal} = \frac{vh^3}{3E_s A_c b} + \omega_1 \omega_2 \frac{vh}{\rho G t_{sheathing}} + \omega_1^{5/4} \omega_2 \omega_3 \omega_4 \left(\frac{v}{\beta}\right)^2 + \frac{h}{b} \delta_v \quad (3.31)$$

$$\omega_1 = \left(\frac{s}{152}\right) \quad \omega_2 = \left(\frac{0.838}{t_{stud}}\right) \quad \omega_3 = \sqrt{\frac{h/b}{2}} \quad (3.32)$$

$$\omega_4 = 1 \text{ for wood structural panels, } \sqrt{\frac{228}{F_y}} \text{ for sheet steel} \quad (3.33)$$

$$\rho = 1.85 \text{ for plywood, } 1.05 \text{ for OSB, and } 0.075 \sqrt{\frac{t_{sheathing}}{0.457}} \text{ for sheet steel} \quad (3.34)$$

$$\beta = 810 \text{ for plywood, } 660 \text{ for OSB, and } 500 \sqrt{\frac{t_{sheathing}}{0.457}} \text{ for sheet steel} \quad (3.35)$$

where V is the lateral load applied to the wall, v is the shear demand ($=V/b$), b is the width of the wall, A_c is the gross cross-sectional area of chord member, E_s is the modulus of elasticity of steel, h is the height of the wall, β and ρ are an adjustment factors, G is the shear modulus of the sheathing material, $t_{sheathing}$ is the nominal panel thickness, s is the fastener spacing at panel edges, t_{stud} is the nominal framing thickness and δ_v is the vertical elongation at the overturning restraint (or hold-down device). All units are in N, mm, mm² and MPa.

Table 3.5. Design Coefficients and Factors for Light Framed Seismic Force-Resisting Systems (ASCE 7-05, 2006).

| Seismic Force-Resisting System | Response Modification Coefficient, R | System Over-strength Factor, Ω_0 | Deflection Amplification Factor, C_d |
|--|--------------------------------------|---|--|
| Light-framed walls sheathed with wood structural panels rated for shear resistance or steel sheets | 6.5 | 3 | 4 |
| Light-framed walls with shear panels of other materials | 2 | 2.5 | 2 |
| Light-framed wall systems using flat strap bracing | 4 | 2 | 3.5 |

3.2. Experimental Studies

3.2.1. Major Experimental Studies since 1970's

Research activities about the evaluation of seismic performance of cold-formed steel-framed sheathed shear wall systems have been started in late 1970's and accelerated in 1990's majorly in North America. Since 2000, there are different research teams on earth have been carrying out experimental studies to obtain the in-plane lateral behavior, thus, to develop design procedures for such shear wall systems. Such research programs are in progress, particularly, at the Santa Clara University, the McGill University, the University of North Texas, the Politehnica University of Timisoara, the University of Naples, the University of Queensland, etc. and by research teams sponsored by the American Iron and Steel Institute (AISI) or European Communities. The major studies held by the researchers are explained in this section whereas details of these experimental programs such as loading protocol; wall geometry; sheathing, frame, fastener and anchorage features, etc. are provided in Appendix A.

Due to the lack of design provisions in building codes to use steel studs in shear walls, to withstand the lateral forces, as for the wooden studs reflected in the main building codes; AISI and the United States Steel (USS) Corporation sponsored several experimental research projects, carried out at Vanderbilt University, by Thomas S. Tarpy, Jr. with other researchers to be mentioned below, in late 1970's to determine the in-plane shear resistance and deflections of full-scale sheathed steel stud wall assemblies commonly encountered in practice (Klippstein and Tarpy, 1992).

Within the context of these projects, McCreless and Tarpy (1978) observed different failure modes for different aspect ratios. For shorter specimens, where flexural deformation controlled the behavior (i.e. the final failure occurred due to the excessive rotation) such that bottom track around the clip angle deformed first, then the screws in the tension corner rotated through the gypsum wallboard and separation of the wallboard cracked at the end. For longer specimens, where shear deformation controlled the behavior (i.e. the final failure due to the shearing of the frame) such that the edge screws rotated through the gypsum wallboard first, then the stud framing sheared through the top of the wallboard at

the end. It was concluded that the various aspect ratios had no significant influence on the shear strength, however, shear stiffness decreased as the aspect ratio increased (i.e. the shorter height and longer walls had more shear stiffness.). It was recorded that the displacements caused the first remarkable damage were higher for large aspect ratios (i.e. longer height and shorter walls) whereas the expected improvement effect of the additional horizontal stiffener in the shear strength was not observed through the experiments.

Tarpy and Hauenstein (1978) performed an experimental program led to the conclusions that (i) if the adequate attachment was provided between the bottom track and the floor framing system, the uplift failure would be avoided; (ii) the reduction of the fastener spacing around the wall perimeter could provide higher shear strength; and (iii) a safety factor of 2.0 was recommended for design purposes to ensure that the design load level does not exceed the damage threshold level.

Tarpy (1980) found that (i) the use of cement plaster over the surface of the wall resulted in an increase of the shear strength and stiffness; (ii) the use of two layers of GWB increased the shear capacity, while decreasing the shear stiffness, in comparison with single layer; (iii) the reduction of the fastener spacing increased the shear strength and stiffness; (iv) cyclic load decreased shear strength and damage threshold level; (v) the corner anchorage influenced the shear stiffness and threshold load level dramatically, which was seen by the significant decrease in the shear strength when corner angles (hold-down device) were replaced with bolt and washer anchors; (vi) Densely spaced powder actuated fasteners (connected to a supporting concrete beam) provided similar restraint to the hold-down; (vii) the shear resistance did not vary extensively when using different types of interior shear anchorage; (viii) The use of a diagonal brace placed at the bottom corner between the chord members and the adjacent stud had little effect on the shear capacity; and (ix) cyclic load weakened the wall panels by decreasing the damage threshold load level and the ultimate shear strength.

Tarpy and Girard (1982) stated that the shear strength to the in-plane loading is a function of the behavior of the connection between the sheathing and the steel stud frame and the type of the anchorage used to fix the wall panel, to the foundation, floor or roof assembly. The results showed that all wall specimens experienced same basic failure mode.

The bottom track deformed around the anchorage device (either clip angle, powder actuated fastener, or washers) at the tension or uplift corner of the wall and as the increasing load, the gypsum wallboard cracked from the corner fasteners to the edge of the panel. This process continued with increased track deformation and increased tearing of the wallboard until the wall panel was no longer able to carry additional load. The authors concluded that the use of the clip angles in addition to the bolt and washer anchorage details increased the shear capacity whereas the use of closely spaced powder actuated fasteners increased the shear capacity for a negligible amount compared to the effect of the clip angles. It was suggested a rigid connection between the wall panel and foundation (or floor, roof frame etc.) thus, the use of clip angles since the wall, when anchored through floor joists, exhibited lower shear resistance and stiffness than when connected directly to the test frame. It was noted that welding the studs to the track was as effective as using self-drilling screws and resulted in similar shear performance. The use of plywood increased the shear strength whereas the use of gypsum sheathing board decreased it when they were used instead of gypsum wallboard at one specimen each. Furthermore, decreasing the stud spacing increased shear strength not significantly, but slightly. Finally, for design purposes, a minimum factor of safety of 2.0 was recommended to determine the design shear strength from the ultimate shear strength for steel-stud framed wall panels investigated in the study.

Tissel (1993) conducted tests, for the American Plywood Association (APA), on wall specimens that were sheathed with either oriented strand board (OSB) or plywood (PLY) and that had various frame thicknesses, to investigate the influence of the fastener size and spacing and stud frame thickness on the shear wall strength. The author reported that failure due to buckling of single end studs or tearing of bottom track around the anchor bolts yielded to a premature collapses prevented the wall panel to achieve its full shear capacity. Thus, the study could not recommend itself as a true indicator of the capacity of the steel stud shear walls but additional tests to be fulfilled to obtain the design shear values for these walls.

In late 1990's, experimental studies investigating the lateral in-plane behavior of the wall panel systems was accelerated majorly by a research group under the guidance of Reynaud Serrette, as the project director, and the sponsorship of AISI at Santa Clara

University, California. The research team carried out experiments on numerous wall specimens and published their research reports most of which are still in use in Steel Framing Alliance (SFA) publication list.

Serrette *et al.* (1996) concluded that: (i) perpendicular orientation of the boards yielded higher capacity than the parallel orientation; (ii) maximum strength of the OSB tested found to be less than of the PLY had the similar thickness; (iii) tighter fastener schedules produced significant increase in the shear capacity (could be increased for 50%); (iv) attachment of GWB on the other side of the framing did not contribute significant increase to the shear capacity.

Serrette and Ogunfunmi (1996) revealed that (i) the individual contribution of studs to the lateral resistance is relatively small for every case even if the top and bottom of them were assumed to be fixed; (ii) 97% percent of the capacity was provided by flat straps for the X-bracing case; (iii) for the case including the sheathing, board and the bracing, straps did not enhance the stiffness of the wall, however the permanent deflection of the wall was reduced and load capacity was increased approximately 20% with the presence of the straps; and (iv) when the gypsum panels were applied to the bare wall frame, there was a 130% increase in shear load capacity over the X-bracing case. They concluded that (i) the gypsum board was shown to have significant shear strength, but under seismic loading, the static values should be reduced to compensate for opening of holes around the screw shank; and (ii) Although flat strap tension bracing possessed high shear strength, the use of straps plus wall panels (e.g., gypsum board) was found not to be much practical.

Serrette *et al.* (1997) showed that (i) the capacity of PLY and OSB walls could be enhanced with denser edge screws providing that chord studs were designed to exceed the shear capacity of the sheathing; (ii) for heavily loaded walls, framing members should be checked against a failure as result of the eccentricity of the shear load at the connection due to the combined bending and axial load; (iii) using thicker steel sheathing provided higher design capacities whereas the failure mode moved from rupture at the edge of the sheathing to screw pullout from the framing; and (iv) higher aspect ratio walls were capable of resisting higher loads at relatively larger displacements, however, after large

events, the wall had low to zero stiffness; and recommended that designers should consider designing chord studs and tracks for 150% of the yield strength of the X-braced flat strap.

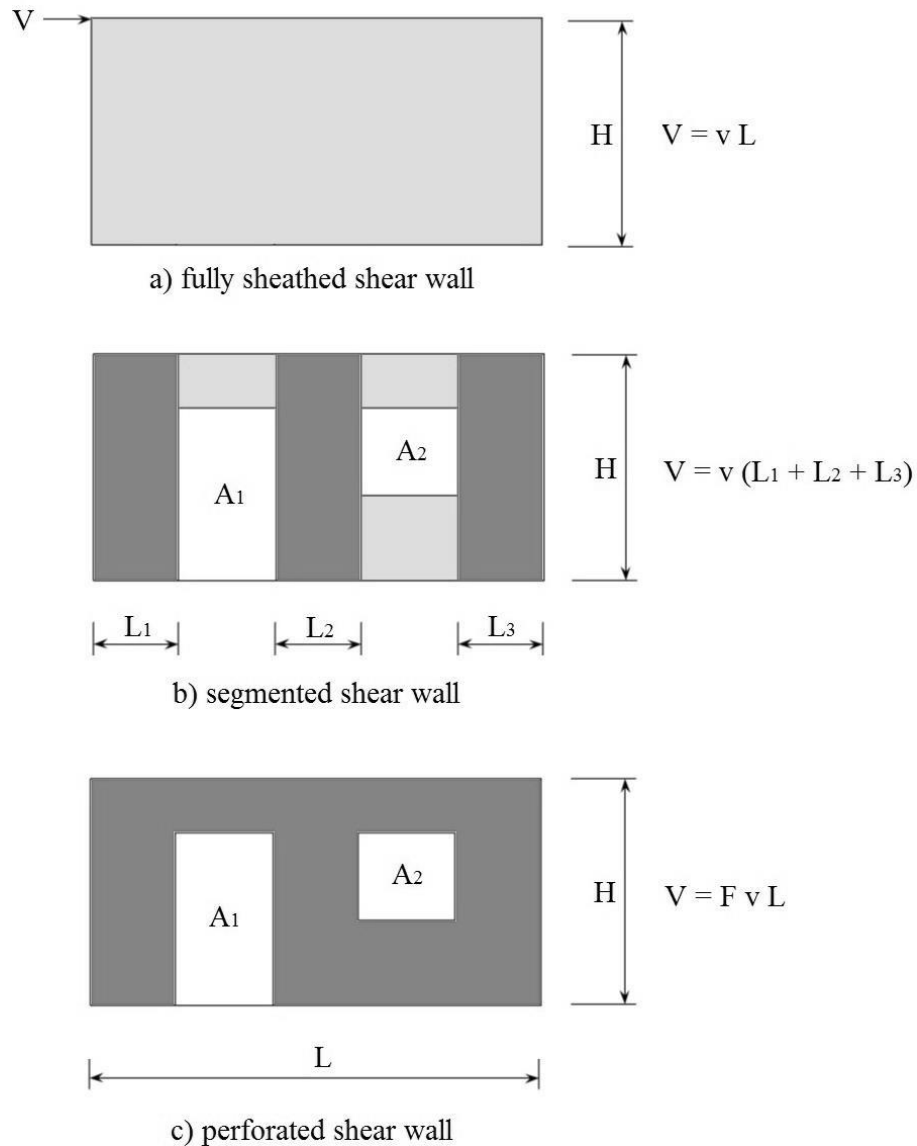


Figure 3.6. Evaluation of Shear Capacity of Shear Walls with Openings.

The shear capacity of shear walls as influenced by the presence of openings is another phenomena studied by several researchers. There are two main design methods for the evaluation of the shear capacity of sheathed shear walls with openings demonstrated in Figure 3.6, as segmented shear wall method and perforated shear wall method. Segmented shear wall method is a simple approach that evaluates the contribution of only full-height portions of wall segment and neglects the wall portions above or below the openings. Therefore, the shear resistance of these members is severely underestimated, thus, number

of the required fasteners and hold-downs are increased on the full-height portions to resist the same lateral load. Instead, Yasumura and Sugiyama (1984) determined an empirical equation to relate shear capacity and sheathing area ratio,

$$F = r / (3 - 2r) \quad (3.36)$$

where F is the ratio of the strength of a shear wall with openings to the strength of a shear wall without openings, based on the sheathing area ratio, r , defined by Sugiyama (1981),

$$r = \frac{1}{1 + \frac{A_0}{H \sum L_i}} \quad (3.37)$$

where A_0 is the total area of openings, h is the height of the wall and L_i is the length of the full height wall segment. Later, Sugiyama and Matsumoto (1994) published two more equations based on tests of longer wall models:

$$F = 3 r / (8 - 5r) \quad (3.38)$$

for the shear deformation angle $\gamma = 1/300$ radian, and

$$F = r / (2 - r) \quad (3.39)$$

for $\gamma = 1/100$ and $1/60$ radian with two limitations: (i) the depth-to-width ratio in the wall space above and/or below an opening is not less than $1/8$, and (ii) the sheathing area ratio is not less than 30%.

Regardless the empirical sheathing area ratio, segmented and perforated shear wall methods are compared in Figure 3.1, however for both shear wall capacity of a fully sheathed shear wall without openings is required. In order to obtain the influence of the presence of openings on capacity of the fully sheathed shear walls, National Association of Home Builders (NAHB) Research Center and Virginia Polytechnic Institute and State University were leading the major role in experimental studies in late 1990's.

In order to determine the capacity of full scale steel-framed shear walls as influenced by the presence of openings and check the validity of Equation 3.15, NAHB Research Center (1997) carried out an experimental research containing monotonic tests of four 12190 mm-length walls with different opening configurations as illustrated in Figure 3.7. Recorded data was compared to the shear capacity calculated using the empirical equation as well as the effect of reduced anchoring constraints (hold-down brackets) was investigated. The results showed that the empirical formulas generally valid in the calculation of ultimate capacity, however actual behavior more closely followed Equation 3.18. Also, influence of the hold-downs was stated that they reduced uplift and increased the ultimate capacity by allowing a greater number of sheathing fasteners to actively participate in resisting shear.

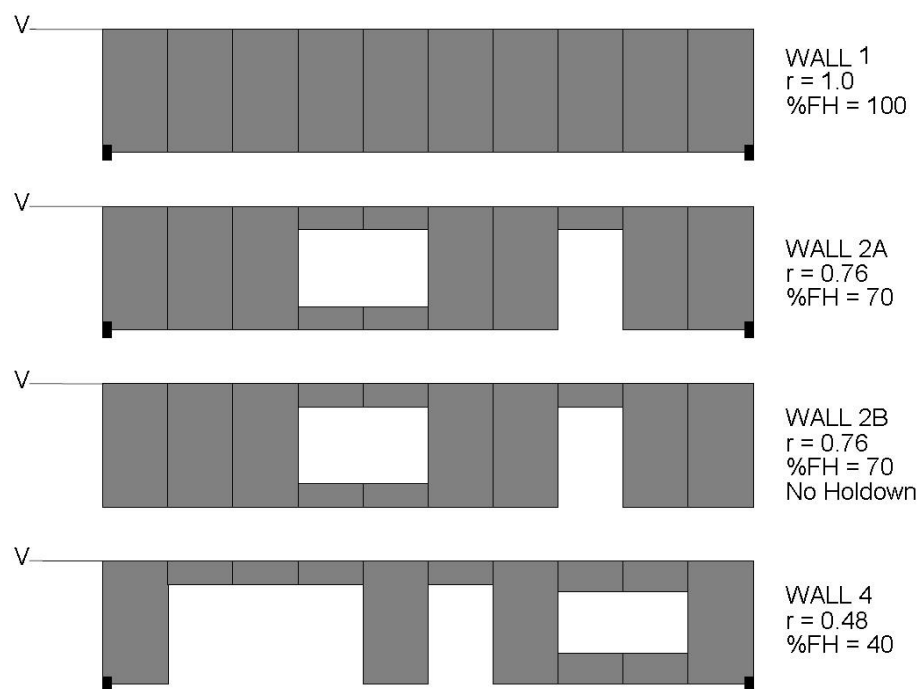


Figure 3.7. Shear Wall Configurations, NAHB Research Center (1997).

Salenikovich *et al.* (1999) submitted a report to AISI with the conclusions as (i) Sugiyama's equations were found to be conservative at all levels of monotonic and cyclic loading; especially, Equation 3.39 produced the closest estimates in the elastic range whereas the use of Equation 3.36 was found to be more conservative and able to provide acceptable prediction of shear wall strength for both monotonic and cyclic loading in cold-formed steel shear walls; (ii) Long, fully-sheathed walls were significantly stiffer and

stronger but less ductile than walls with openings, as result of the increased rocking of wall sections in the middle of the wall specimen that were not restrained against overturning; (iii) cyclic loading did not affect elastic performance of the walls but reduced their deformation capacity; and (iv) gypsum sheathing added 30% to stiffness and strength of fully sheathed walls in monotonic tests, however contribution of gypsum wallboard in other loading circumstances remained questionable.

As a follow up, Dolan *et al.* (2000) submitted another report to AISI with the conclusions as (i) the first two conclusions drawn by Salenikovich, *et al.* (1999) mentioned above were similarly achieved (ii) strength of fully-sheathed walls was affected by cyclic loading to a greater extent than walls with openings; (iii) the steel-frame walls degraded in abrupt, stepwise manner due to bending of framing elements and pulling heads of sheathing screws through sheathing arbitrarily along the studs or top and bottom tracks. Sometimes, sheathing screws tore through panel edges. Rare cases of fatigue of mechanical connections were observed at the corners of the walls. The randomness of failure locations indicated that the sheathing fasteners share the load uniformly; (iv) based on one specimen, orienting the sheathing horizontally with OSB and gypsum sheathing provided 90% of the strength of a wall with OSB sheathing and overturning anchors for the fully sheathed condition. The orientation with the staggered joints prevented any shear plane occurring in the height of the wall; (v) changing the sheathing orientation from vertical to horizontal did not provide sufficient capacity to equal the performance of fully anchored walls. (vi) the use of screws instead of shear bolts to transmit shear to the foundation reduced the capacity of the wall by 21% - 29%; (vii) the use of mechanical tie-down anchors at the ends of the walls increased the capacity of the walls by almost 15% when compared to use of bolts resisting shear in the bottom track only; (viii) Ttests revealed that the drywall gypsum sheathing does not contribute significantly to the strength of the wall under cyclic loading similar observations were made by Salenikovich, *et al.* (1999); (ix) the stiffness and strength of the walls would be increased if the tear through of the sheathing material and the pull through of the screw head were eliminated or reduced. Improved performance can be achieved by changing the screw head type, or adding reinforcement to the sheathing along the edges; (x) stiffness of the perforated shear walls would be increased if the track bending stiffness were increased.

Kawai *et al.* (1999) stated that damping ratios of steel-framed houses vary in a wide range based on the interior and exterior finishes used. To obtain the seismic behavior of such buildings, thus, design them more properly and economically, vibration characteristics of a typical steel-framed house in each construction stage, as illustrated in Figure 3.8, were investigated and the effects of interior and exterior finishes were quantified. The steel-framed house was examined in three stages. At the first stage, plywood was installed in the load-bearing walls, floors and roofing. At the second stage, gypsum board (excluding ceilings and some walls) was installed in the roofing and some eastern and western external walls and at the third stage, gypsum board (including ceilings) and exterior walls were installed, and interior finish was completed. The steel-framed house was tested by three methods: microtremor¹ test, sweep test and free vibration test with small, medium and large levels of exciting force are set at different velocities.

When the results of three test methods were examined, it was stated that the damping ratio ranged from about 2.5 to 7.0%, and the natural frequency ranged from about 6.4 to 7.8 Hz. The damping ratio and the natural frequency were found to increase with the progress of construction. This is because the installation interior and exterior finishes increased the stiffness and damping effects of the house. Increasing exciting force increased the damping ratio and decreased the natural frequency. This was probably because the increase in the exciting force damaged the sheathings, finishes, and their connections at a micro level. The damping ratio obtained at the large exciting force level in the completed stage is about 5.5 to 7.0% and was considerably large. It was obvious that the damping ratio of the steel-framed house was strongly influenced by the presence of interior and exterior finishes and the level of exciting force, and was considered to assume a relatively large value. In the consideration of the above findings it was decided to set the damping ratio at 6% in the seismic response analysis.

Serrette *et al.* (2002) showed that (i) for the double-sided walls, the demand on the low-steels-graded stud exceeded the capacity, thus stud failure occurred whereas with high-steel-graded stud screws attaching the hold-down to the chord failed prematurely, prevented to reach the wall capacity, (ii) high demand on screw caused the panel to unzip

¹ Microtremor is a low amplitude ambient vibration of the ground caused by man-made or atmospheric disturbances

along the joint before the SSS could develop its full strength, (iii) GWB was failed due to the breaking of the wallboard at the fasteners along and screw pull-through. It was also recommended that if chord buckling and hold-down failure were prevented, the capacity of the double-sided wall would be closer to double the capacity of the single-sided wall.

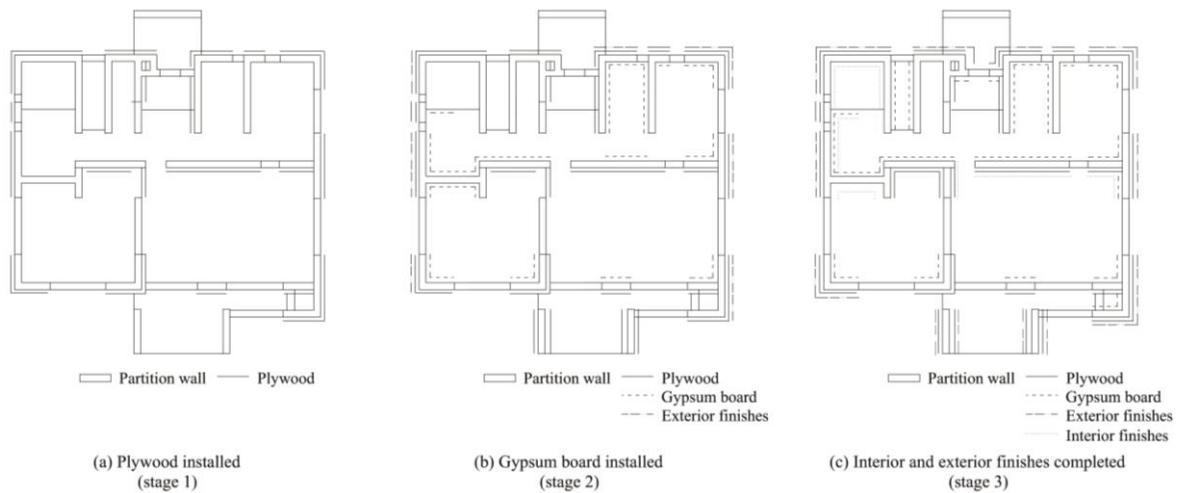


Figure 3.8. Construction Stages of Steel-Framed House Subjected to Vibration Test
(Kawai *et al.*, 1999).

In the early 2000's, a research team was made at McGill University, with the objective to develop and publish specific guidelines for the seismic design of cold-formed shear wall systems composed of cold-formed steel frame and wood sheathing by means of experimental and theoretical studies.

At the onset of the research program, Zhao (2002) provided an extensive literature review of previous cold-formed steel shear wall test programs conducted in North America as well as an overview of the seismic requirements for a number of different design standards. It was aimed to derive a feasible numerical method for the estimation of shear strength of steel stud walls. Accordingly, a theoretical method for the prediction of shear capacity based on the first possible failure mode, following the American wood design procedure, was presented and the results from the method were compared with peak loads obtained from existing tests.

It was shown that the predicted shear capacity generally was consistent with the experimental peak load results. The usage of cold-formed steel stud walls without

consideration of their possible load carrying capacity with significant inelastic deformations was pointed out; since an R value (force modification factor) was not defined in the National Building Code of Canada (NBCC, 1995). Thus, the previous test data was used to evaluate various lateral force design methods and to determine a preliminary ductility based force modification factor for use in seismic design suggested for use with the NBCC. Based on the investigation, a preliminary ductility related R value of 2.0 recommended for the NBCC was suitable for the seismic design of cold-formed steel stud shear walls sheathed with wood panels. In the rest of the study, a possible procedure to obtain ductility factors from quasi-static tests was explained, parameter studies were carried out and, the test frame was designed for the proposed future tests of cold-formed steel shear walls to be conducted to verify the findings described in the study.

In order to assemble a bank of data for various experimental wall configurations constructed in accordance with the design of Zhao (2002), numerous tests were carried out by Branston (2004), Chen (2004) and Boudreault (2006).

Branston (2004) pointed out that implementing a suitable data interpretation model that closely represents the actual performance of the shear wall is as important as the loading protocol to obtain the realistic design values. Thus, he made an extensive research on existing fourteen data interpretation techniques to obtain the most suitable one for the evaluation of specific design properties such as yield force, stiffness, ductility, energy dissipation capacity, etc., besides the experiments of wood panel sheathed steel-framed shear wall specimens carried out. He suggested the equivalent energy elastic-plastic (EEEP) model as the most suitable model which is based on the equivalency of the energy dissipated by the wall specimen to the energy represented by bi-linear model curve. With the use of bi-linear curve with simplicity, the curve depicts linear elastic behavior of the system until the yield point and perfectly plastic behavior until failure with the simplicity of identification of key design parameters may be derived from the test data. The EEEP model was utilized on the experimental data carried out by the author.

Once the backbone curve was constructed for each reversed cyclic test (for both positive and negative displacement cycles demonstrated on Figure 3.10), the EEEP curve was created based on the equivalent energy approach by first determining three main

parameters from the monotonic corrected test curve or the backbone curve for the reversed cyclic tests. These parameters include the maximum wall resistance attained (S_u), and the two points on the test curve corresponding to $0.4S_u$ and $0.8S_u$ (post-peak), and corresponding displacements $\Delta_{net,u}$, $\Delta_{net,0.4u}$, and $\Delta_{net,0.8u}$, respectively.

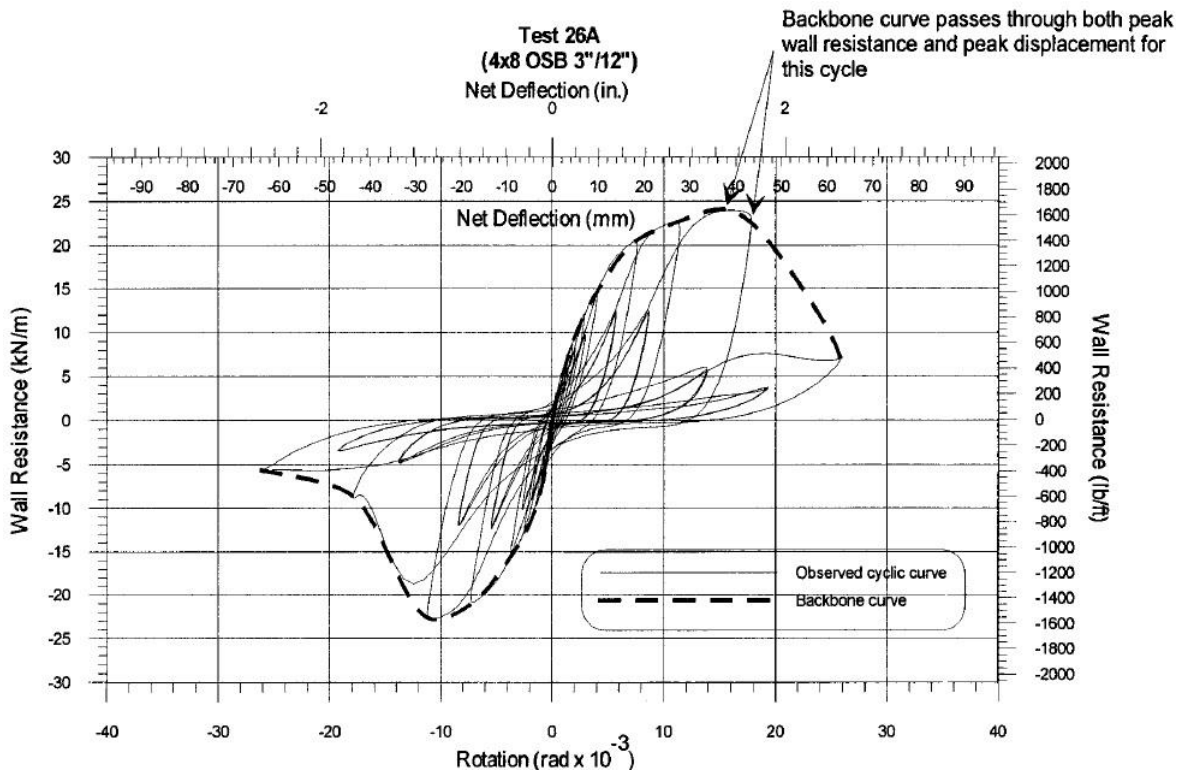


Figure 3.9. Hysteresis Test Data Enveloped by Backbone Curve (Branston, 2004).

In the case of the reversed cyclic tests, because only a limited number of data points formed the backbone curve, a polynomial trend line (known function) was used to replicate the backbone curve and give a more accurate result when step-by-step integration was used to calculate the area under the curve (a third order, fourth order, fifth order, or sixth order polynomial was used depending on fit). A straight line passing through the origin and $(0.4S_u, \Delta_{net,0.4u})$ defines the elastic portion of the bi-linear EEEP curve. A reasonable estimate of the maximum service load level is commonly chosen to be 40 % of the ultimate resistance. This elastic portion has a slope equal to the unit elastic stiffness, k_e , on the wall resistance (force per unit length) vs. deflection response plot (Figure 3.11) or the elastic stiffness, K_e , on the wall resistance (force) vs. deflection response plot. The horizontal line depicting the plastic portion of the EEEP curve is positioned so that the area bounded by the EEEP curve, the x-axis, and the limiting displacement $\Delta_{net,0.8u}$ is equal to the area

below the observed test curve (A) (calculated by step-by-step integration). This amounts to equating the two oppositely hatched areas ($A_1 = A_2$) shown in Figure 3.10.

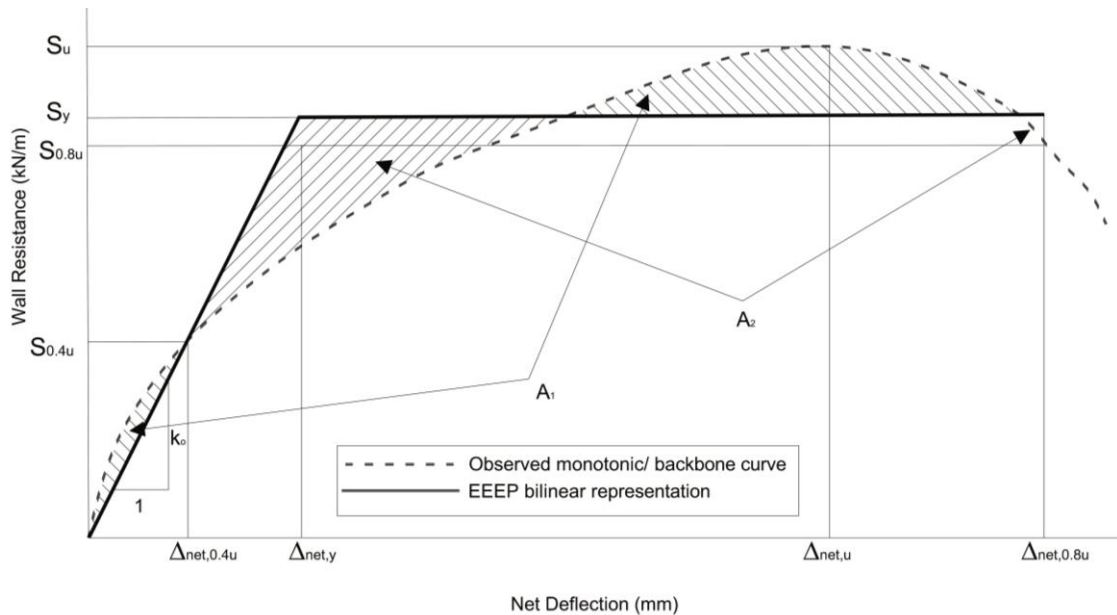


Figure 3.10. Energy Equivalent Elastic-Plastic (EEEEP) Model (Branston, 2004).

AISI Lateral (2004) had provided limited range of nominal shear strength for seismic loads for sheet steel sheathed (SSS) shear walls, based on the research conducted by Serrette *et al.* (1997, 2002) which covered limited steel sheet thickness options, 0.457 mm and 0.686 mm, for limited wall aspect ratios, 2:1 and 4:1, respectively. Due to the limited research on the cold-formed steel-framed SSS shear walls, thus to address a wider range of options for SSS, Yu (2007) conducted series of monotonic and cyclic experiments to obtain additional data with alternative sheathing configurations such as 0.686 mm, 0.762 mm and 0.838 mm steel sheets for different aspect ratios and different fastener schedule following similar test procedure and loading protocol with Serrette. Additional experimental data was obtained with the study for SSS shear walls with the discovery of the use of thicker framing members would improve the shear strength of this type of shear walls, significantly. The findings and recommendations of the research were published as AISI Research Report RP07-3 (2007).

As a follow up, Yu and Chen (2009) continued the research as phase 2 with the necessity to provide additional data and verify the discrepancy in the results of the study of

Yu (2007), regarded as phase 1, when compared to previous work by other researchers. The phase 2 had two main objectives. First one was to verify and propose revised shear strength values in AISI S213-07-S1-09 (2007) for 0.457 mm and 0.686 mm steel sheets with different fastener schedule and wall aspect ratios. The existing experimental studies of cold-formed steel shear walls (Serrette 1996, 1997, 2002; Yu 2007) have been focused on wall aspect ratios 2:1 and 4:1, in which one sheet of sheathing was usually installed, and one or no interior stud was used. However in the actual application, shear walls with a larger aspect ratio less than 2:1 are frequently used. For those wider shear walls, multiple sheets of sheathing will be installed and more than one interior studs will be used to support the gravity loads and other demands. Therefore, the second objective of the research was to determine seismic detailing requirements to assure satisfactory performance of a 1830 mm-wide shear wall with a 610 mm and a 1220 mm-wide steel sheathing. The test results indicated that the special detailing would increase the nominal strength as well as improve the ductility of the shear wall. Special detailing comprised adding strapping and blocking members and using staggered screw patterns at the ends and joints on studs as demonstrated in Figure 3.12. It was concluded that the special seismic detailing shall be installed for 0.838 mm or 1.092 mm framed shear walls with steel sheathing thickness equal to or less than 0.838 mm. The findings and recommendations of the research were published as AISI Research Report RP09-2 (2009).

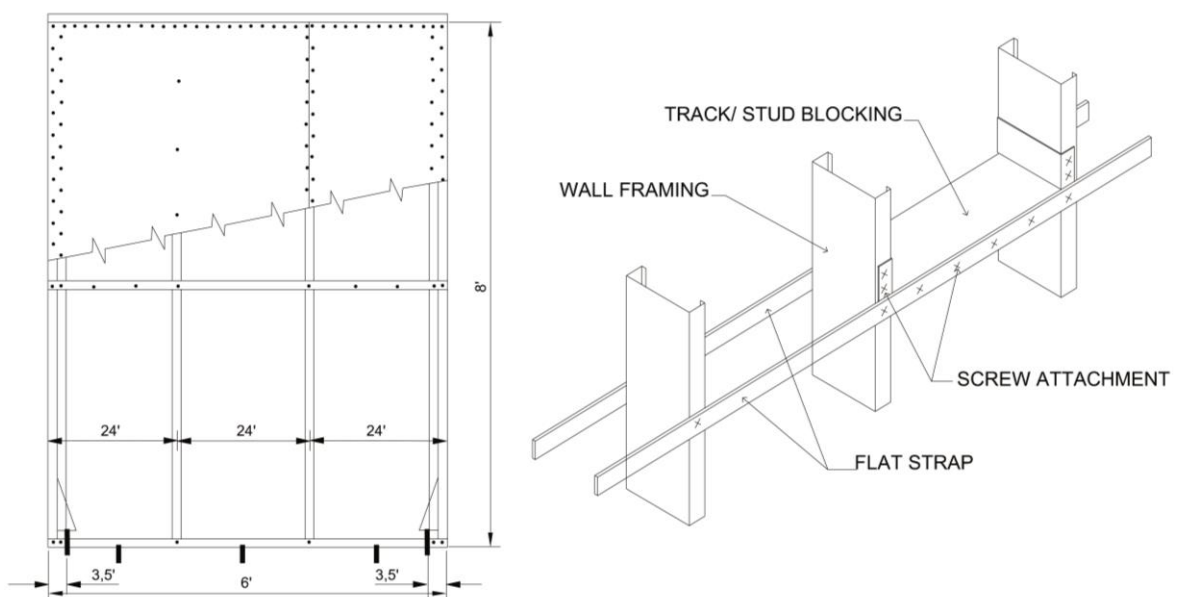


Figure 3.11. Special Detailing (adapted from Yu and Chen, 2009).

3.2.2. Selected Experimental Research

To investigate the shear behavior of some of the most commonly used wall panel types among the light-weight steel structures; an experimental program was carried out at the University of Timisoara, Department of Steel Structures and Structural Mechanics (Fülöp and Dubina, 2004a). The program was based on the statically, both monotonic and cyclic, testing of the six series of full-scale wall panels with different sheathing features. It was aimed to make comparisons between monotonic and cyclic behaviors of wall panels with different cladding materials and cross bracings, to assess the effect of openings and to provide experimental information for the calibration of numerical analysis methods. This program is chosen to numerically model among other experimental studies mentioned in Chapter 3, because the sheathing configurations used in the experiment are very similar to those commonly preferred in Turkey. There are six types of shear wall investigated in the study by the authors and three of which are preferred to be explained in detail and referred as Wall Type I, Wall Type II and Wall Type III instead of original notations, OSB I, Series I and Series II, respectively, herein after.

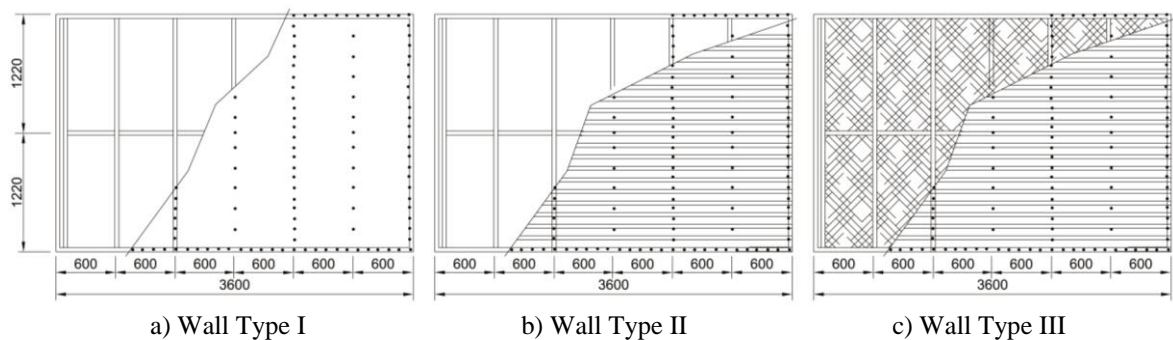


Figure 3.12. Summary of all Sheathing Configurations of the Wall Specimens (Fülöp and Dubina, 2004a).

The main frame of the 3600 mm x 2440 mm (length x height) wall panels was identical for each series and made of cold-formed steel members as illustrated in Figure 3.13. Top and bottom tracks were 600 T 225-62, while studs were 600 S 175-62 at 600 mm on center, fixed at each end to tracks with two pairs of SL4-F-4.8x16 (SFS, 2006) self-drilling self-taping screws. Double studs (back-to-back) were used at the ends of the walls and around openings. The test series for the OSB sheathed wall specimens, ‘Wall Type I’ (Figure 3.13a), 10 mm thick oriented strand board, OSB, (1200 mm × 2440 mm) was used

as the external cladding, placed vertically and fixed to the frame at 250 mm intervals on each vertical stud using bugle head self-drilling screws of 4.2 mm diameter spaced at 250 mm in the field and at 105 mm at the perimeter of the frame. In ‘Wall Type II’ (Figure 3.13b), steel corrugated sheet was used as the external cladding material where the 0.5 mm-thick sheets were placed in a horizontal position with a useful width of 1035 mm and one corrugation overlapping and tightened each other with seam fasteners SL2-T-A14-4.4x20 (SFS, 2006) at 200 mm intervals through the corrugation. The corrugated sheet was fixed to the wall frame using SD3-T15-4.8x22 (SFS, 2006) self-taping screws, on end studs at every corrugation, spaced at 115 mm, while on intermediate studs at every second corrugation, spaced at 230 mm. Steel corrugated sheet was used in ‘Wall Type III’ (Figure 3.13c), as the external cladding similar to that used in the ‘Wall Type II’ and the 12.5 mm thick gypsum wall boards, GWB, (1200 × 2440 mm) were used additionally on the interior side of the specimen. They were placed vertically and fixed to the frame at 250 mm intervals on each vertical stud.

Experiments were conducted as displacement controlled with the measurement of the corresponding load with a load cell (LC) for each displacement value. The experimental arrangement is summarized in Figure 3.14.

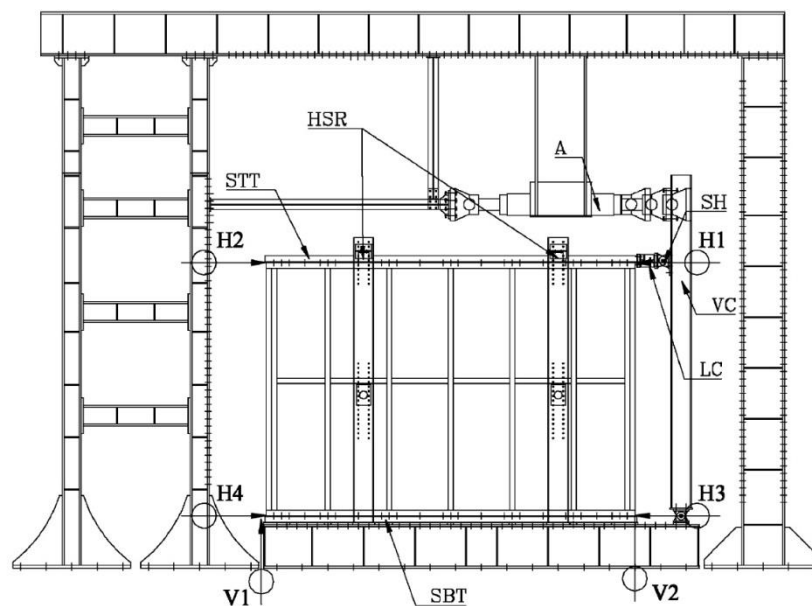


Figure 3.13. Experimental Arrangement (Fülöp and Dubina, 2004a).

Table 3.6. Monotonic and Cyclic Test Results (Fülöp and Dubina, 2004a) Based on the Method Proposed by Kawai *et al.*,1999.

| Sheathing Type | Initial Rigid. | Duct. | Elastic Limit | | Yield Limit | | Max Limit | | | Ultimate Limit | |
|----------------|----------------|-----------------------|---------------|------|-------------|-------|-----------------------|--------|-------|----------------|-------|
| | K0 | μ | Fel | Del | Fy | Dcurv | $\frac{2}{3} F_{max}$ | Fmax | Dmax | Fult | Dult |
| | kN/mm | $\frac{D_{max}}{Del}$ | kN | mm | kN | mm | kN | kN | mm | kN | mm |
| WALL TYPE I | 4.406 | 4.07 | 30.159 | 6.84 | 55.142 | 21.32 | 49.810 | 74.716 | | 55.142 | |
| | | 3.73 | | | 49.369 | 16.68 | | | | 49.369 | |
| | 3.988 | 3.68 | 27.726 | 6.95 | 54.088 | 21.44 | 43.315 | 64.972 | | 54.088 | |
| | | 3.61 | | | 48.521 | 18.30 | | | | 48.521 | |
| | 4.197 | 3.67 | 28.942 | 6.90 | 48.945 | 17.49 | 46.563 | 69.844 | 25.32 | 48.945 | 42.85 |
| WALL TYPE II | 3.670 | 6.57 | 25.273 | 6.89 | 41.489 | 24.69 | 31.391 | 47.087 | | 41.489 | |
| | | 4.59 | | | 32.128 | 12.65 | | | | 32.128 | |
| | 3.555 | 4.46 | 24.772 | 6.97 | 38.685 | 20.93 | 44.061 | 66.092 | | 38.685 | |
| | | 4.18 | | | 34.887 | 15.95 | | | | 34.887 | |
| | 3.387 | 5.34 | 23.805 | 7.03 | 40.313 | 23.90 | 47.360 | 71.040 | | 40.313 | |
| | | 4.36 | | | 34.589 | 16.92 | | | | 34.589 | |
| | 3.175 | 4.15 | 22.496 | 7.09 | 38.300 | 20.55 | 44.077 | 66.116 | | 38.300 | |
| | | 4.35 | | | 32.638 | 14.27 | | | | 32.638 | |
| | 3.447 | 4.37 | 24.086 | 6.99 | 33.560 | 14.95 | 41.722 | 62.584 | 30.54 | 33.560 | 42.61 |
| WALL TYPE III | 3.766 | 5.22 | 26.873 | 7.14 | 49.186 | 30.66 | 38.531 | 57.796 | | 49.186 | |
| | | 5,73 | | | 38.868 | 16.07 | | | | 38.868 | |
| | 4.024 | 5.11 | 27.238 | 6.77 | 48.126 | 29.42 | 36.713 | 55.070 | | 48.126 | |
| | | 5.68 | | | 38.751 | 14.75 | | | | 38.751 | |
| | 3.936 | 5.20 | 27.340 | 6.95 | 50.986 | 30.15 | 40.023 | 60.034 | | 50.986 | |
| | | 5.62 | | | 41.921 | 16.02 | | | | 41.921 | |
| | 3.676 | 4.65 | 24.812 | 6.75 | 47.821 | 27.81 | 37.880 | 56.821 | | 47.821 | |
| | | 5.14 | | | 39.734 | 15.48 | | | | 39.734 | |
| | 3.851 | 5.54 | 26.566 | 6.90 | 39.819 | 15.58 | 38.287 | 57.430 | 38.24 | 39.819 | 57.29 |

First, a preliminary classical monotonic displacement increase test and then cyclic tests with the displacement amplitudes obtained from the monotonic test were performed on different wall specimens in according to ECCS-No: 45 (1986). A monotonic test using a loading velocity of 1cm/min was performed for each type of wall panel. Based on the recorded force-displacement curve, the conventional elastic limit is obtained based on method recommended by ECCS-No: 45 (1986). The Recommendation states that first, the tangent at the origin of the F-d curve is evaluated, which gives a tangent modulus, $E_t = \tan \alpha_t$; then the tangent has a slope of $0.1 \times E_t$ is located on the curve and the intersection of the two tangents defines the level of conventional elastic limit force, $F_{\Delta el}$, whereas the

corresponding displacement becomes the conventional elastic limit displacement, Δ_{el} as illustrated in the Figure 3.15. Furthermore, Table 3.6 summarizes the monotonic and cyclic test results obtained from the positive and negative envelopes for both un-stabilized and stabilized backbone curves for all types of wall specimens (Fülöp and Dubina, 2004a).

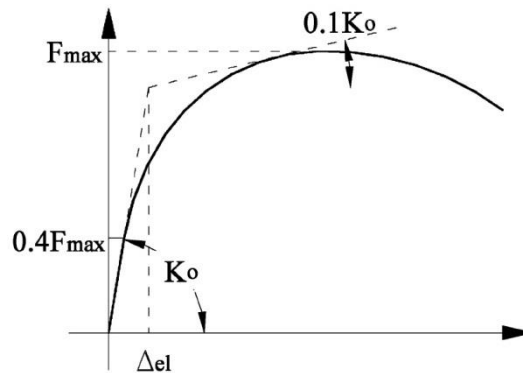


Figure 3.14. Evaluation of the Conventional Elastic Limit (Fülöp and Dubina, 2004a).

3.3. Numerical Studies

3.3.1. Hysteresis Modeling

Shear walls, the earthquake force resisting members of cold-formed steel-framed structures, are designed to dissipate seismic energy by an inelastic material behavior. Compared to the monotonic loading; in the case of cyclic loading, a reduction of strength of about 10% can be identified (Dubina, 2008). So, to avoid strength overestimation and to simulate the nature of earthquake excitation reasonably well, cyclic loading is mostly preferred. However, under repeated cyclic deformation, there is perpetually deterioration in the characteristics of the hysteretic behavior as illustrated in Figure 3.16. Such deterioration must be taken into account in the modeling and design of the seismic-resistant structural systems (Sivaselvan and Reinhorn, 2000).

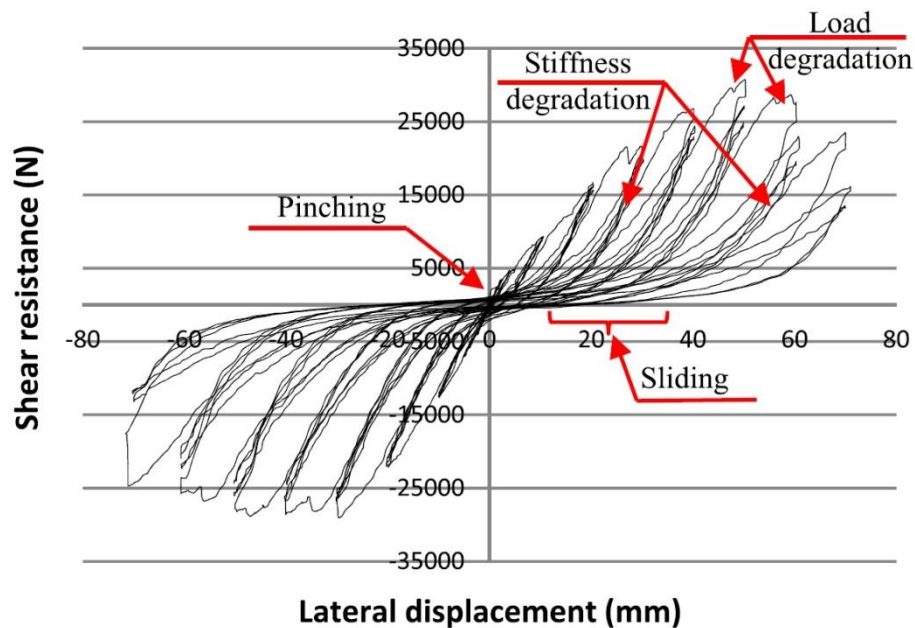


Figure 3.15. Deterioration in the Characteristics of the Hysteretic Behavior (Zeynalian *et al.*, 2012).

The basic requirement to perform such an inelastic analysis is the availability of accurate constitutive models capable of representing different structural phenomena, such as pinching, stiffness degradation, load deterioration, and sliding. Pinching (or slip) occurs as a result of crack closure or bolt slip and refers to the hysteretic cycles passing closer to the horizontal axis when the direction of the load is reversed, as shown in Figure 3.15. In other words, pinched hysteretic loops are narrower in the middle and wider at the ends. Cold-formed steel structures exhibit a gradual loss of lateral stiffness when subjected to reversed cyclic loading, even those that are detailed sensibly; this is usually referred to as stiffness degradation. This behavior can be seen in the hysteretic loops by a progressive reduction of slope in each loading cycle, as shown in Figure 3.15. Load (strength) deterioration is another common phenomenon, as depicted in Figure 3.15 denoting degradation of strength when the structure is cyclically loaded to the same displacement level. In other words, it is the reduction of the capacity in the backbone curve. Sliding, which affects the amount of energy dissipated by the structure, occurs as a result of cracking, tearing, and plastic deformation of connections in some load-bearing structural elements. The greater is the sliding in each cycle; the smaller would be the enclosed area in the hysteretic curves, which is equivalent to lower energy dissipation by the structure. This sliding is visible in

the beginning of the cyclic loops by the generation of the almost horizontal part of the hysteretic loops, as shown in Figure 3.15 (Zeynalian *et al.*, 2012).

Several hysteretic models have been developed to simulate the structural phenomena briefly mentioned above and can be broadly classified as (i) polygonal hysteretic model (PHM) and (ii) smooth hysteretic model (SHM).

Models based on piecewise linear behavior are PHMs which are also referred as multi-linear models. Such models are most often motivated by actual behavioral stages of an element or structure, such as initial or elastic, cracking, yielding, stiffness and strength degrading stages, and crack and gap closures, etc. The model parameters can represent and therefore governed by rules that fix distinct points and dictate the transition between various stages or branches that occur during the branches (Sivaselvan and Reinhorn, 2000). Various characteristics of different PHMs are presented on the basis of studies carried out by Mostaghel (1999), Ibarra *et al.* (2005) and Aoki and Ikeda (2006) below.

A well-known analytical description of the structural multi-linear hysteretic model based on a single-degree-of-freedom (SDOF) mechanical system, consisting of a combination of springs and mass, was proposed by Mostaghel (1999). The model that covers pinching, stiffness degradation and load deterioration, is including a mass, m , four springs, and a viscous damper with a damping constant, c , as it demonstrated in Figure 3.16.

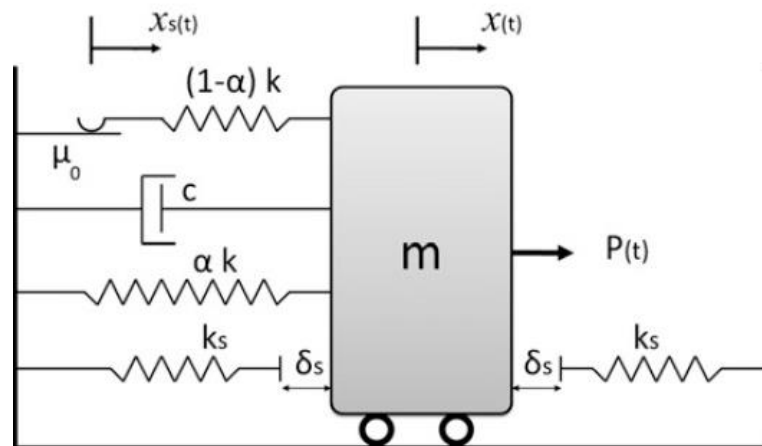


Figure 3.16. SDOF Mechanical Model Proposed by Zeynalian *et al.*, 2012.

The spring of stiffness, αk , is directly connected to the mass. The deformation of this spring is represented by x . The other spring has a stiffness, $(1-\alpha)k$, and is connected to the mass by means of a slider with friction coefficient μ . The deformation of this spring is represented by u . k denotes the total stiffness of the two springs, and $0 \leq \alpha \leq 1$ is the stiffness ratio. The equilibrium equation of motion of non-pinched and non-degraded model is formed as follows:

$$m\ddot{x} + c\dot{x} + \alpha kx + (1-\alpha)ku = \bar{P}_0 p(t) \quad (3.40)$$

where the applied force is denoted by $\bar{P}_0 p(t)$, where \bar{P}_0 is the amplitude and $p(t)$ is a non-dimensional function of time. Then the response of a bilinear hysteretic system that includes strength pinching, stiffness degradation and load deterioration is represented after some numerical manipulations and assumptions by the non-dimensional dynamic equation as follows

$$\ddot{y}(\tau) + 2\xi\dot{y} + \alpha y(\tau) + \alpha_s(|y| - \gamma_s) \text{sgn}(y) \bar{N}(|y| - \gamma_s) + (1-\alpha)z = P_0 p(\tau) \quad (3.41)$$

where N , \bar{N} , M , and \bar{M} are unit step function derived from signum function, $\xi = c/2m\omega$, α is the stiffness ratio, α_s is the stiffness hardening ratio, δ_s is the initial gap, δ_p is the pinched complementary yield displacement, $\gamma_s = \delta_s/\delta$ and $\gamma_p = \delta_p/\delta$, λ_p is the strength ratio and Φ_k and Φ_l are stiffness degradation and load deterioration coefficients, respectively, defined as

$$\Phi_k = 1/[1 + \lambda_k h(t)] \quad (3.42)$$

$$\Phi_l = 1/[1 + \lambda_l h(t)] \quad (3.43)$$

where $h(t)$ is the total non-dimensional hysteretic energy absorbed by the friction force of the slider; and the parameters $\lambda_k \geq 0$ and $\lambda_l \geq 0$ are the stiffness degradation and load deterioration factors, respectively. The final equilibrium equation that covers pinching, stiffness degradation and load deterioration phenomena is

$$\dot{z} = \dot{y} \Phi_k \left\{ \begin{array}{l} \bar{N}(\dot{y}) \left[\bar{M}(z - \lambda_p \Phi_l) \bar{M}(y) + \bar{M}(z - \Phi_l) \bar{N}(y) \right] \\ + M(\dot{y}) \left[N(z + \lambda_p \Phi_l) N(y) + N(z + \Phi_l) M(y) \right] \end{array} \right\} \quad (3.44)$$

Also, the rate of absorption of the total non-dimensional hysteretic energy, $\dot{h}(t)$, is given as

$$\dot{h} = \Phi_1(1-\alpha) \left[\begin{array}{l} N(\dot{y})N(y-\gamma_p) + M(\dot{y})M(y+\gamma_p) \\ + \lambda_p \bar{N}(\dot{y})M(y) + \lambda_p M(\dot{y})N(y) \end{array} \right] |\dot{y}-\dot{z}| \quad (3.45)$$

When the unknowns y , z and h are solved simultaneously, the plot of resistance versus displacement is obtained as Figure 3.17.

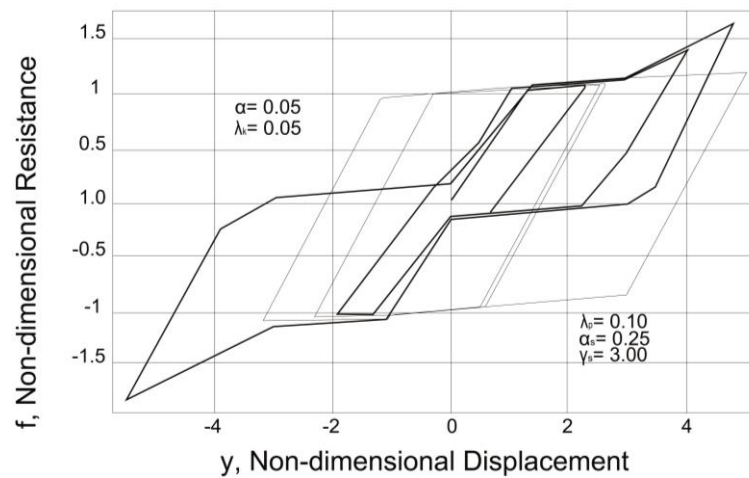


Figure 3.17. Plot of Resistance vs. Displacement that Covers Pinching, Stiffness Degradation and Load Deterioration (Mostaghel, 1999).

Ibarra *et al.* (2005) stated four different cyclic deterioration modes: basic strength, post-capping strength, unloading stiffness, and reloading stiffness deterioration. The cyclic deterioration rates are controlled by the rule based on the hysteretic energy dissipated when the component is subjected to cyclic loading. It is assumed that every component possesses a reference inherent hysteretic energy dissipation capacity, regardless of the loading history applied to the component.

The cyclic deterioration in excursion i , is defined by parameter β_i , which is given by the following expression:

$$\beta_i = \left(\frac{E_i}{E_t - \sum_{j=1}^i E_j} \right)^c \quad (3.46)$$

where E_i is the hysteretic energy dissipated in excursion i , $\sum E_j$ is the hysteretic energy dissipated in all previous excursions through loading in both positive and negative directions, E_t is the reference hysteretic energy dissipation capacity, $E_t = \gamma F_y \delta_y$. The parameter γ expresses the hysteretic energy dissipation capacity as a function of twice the elastic strain energy at yielding ($F_y \delta_y$), it is calibrated from experimental results and can be different for each deterioration mode. Finally, c is the exponent defining the rate of deterioration. Rahnama and Krawinkler (1993) suggest that a reasonable range for c is between 1.0 and 2.0. If the displacement history consists of constant amplitude cycles, a unit value for c implies an almost constant rate of deterioration. For the same displacement history, a value $c=2$ slows down the rate of deterioration in early cycles and accelerates the rate of deterioration in later cycles.

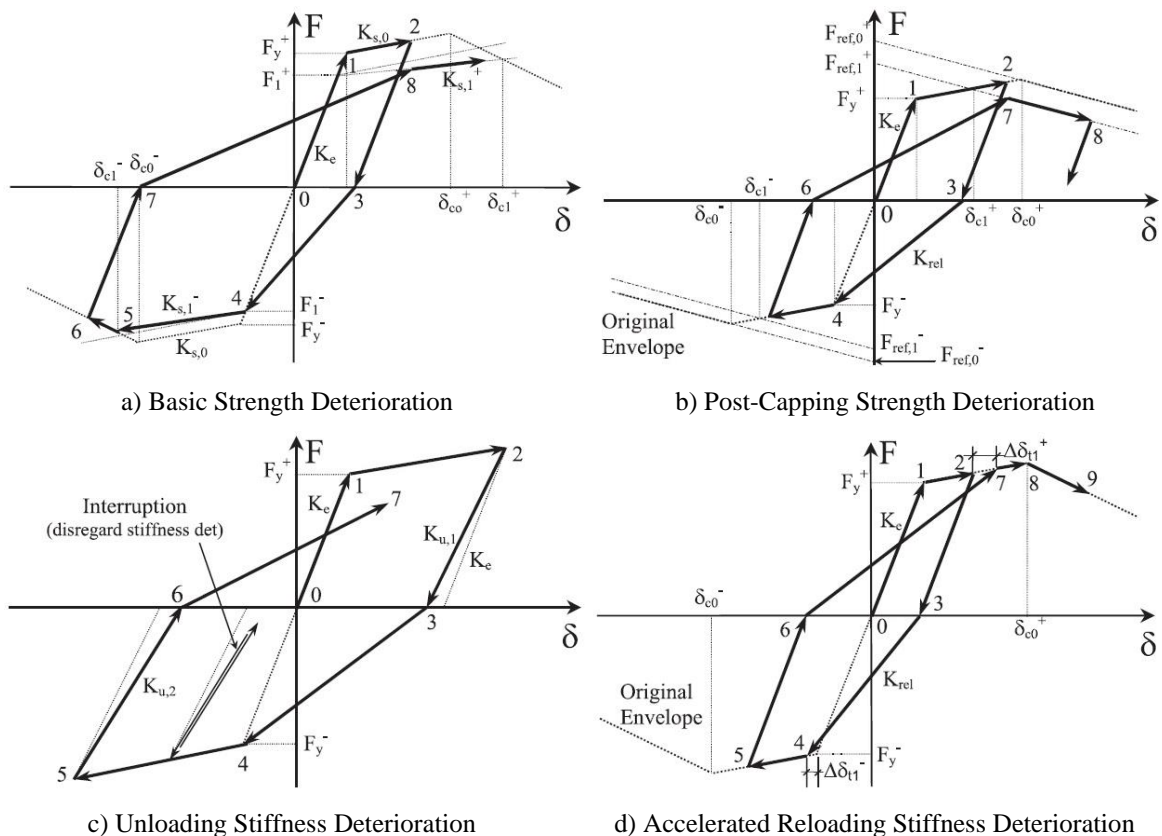


Figure 3.18. Individual Deterioration Modes Illustrated on a Peak-Oriented Model

(adopted from Ibarra *et al.*, 2005).

Throughout the loading history, β_i must be within the limits $0 < \beta_i \leq 1$, otherwise the hysteretic energy capacity is exhausted and collapse is assumed to take place. The individual modes of deterioration such as basic strength deterioration, post-capping strength deterioration, unloading stiffness deterioration, and accelerated reloading stiffness deterioration are demonstrated in Figure 3.18 and described in detail as well as the calibration of the model in the study of Ibarra (2005).

Aoki and Ikeda (2006) converted the low-rise steel frame buildings into single degree of freedom systems and modeled them with a proposed semi-slip model. They stated that a non-buckling steel frame structure including tension embrace has a slip-type hysteresis model (Figure 3.19a) whereas a moment frame structure has normal-bilinear-type hysteresis model (Figure 3.19b). In slip-type hysteresis model, the displacement advances without resistance in the slip area, but in some structures, this slip area can have consumption of energy for structural reasons. For example, this behavior appears on steel housing structure in which steel-frame components are fastened to wooden panel with tapping screws. For that reason, they expressed the level of this slip area by using a “semi-slip coefficient”, b , and with its use, “semi-slip type model” (Figure 3.19c). Then the hysteresis model is classified as slip-type when $b = 0.0$, and becomes normal-bilinear-type when b approaches 1.0.

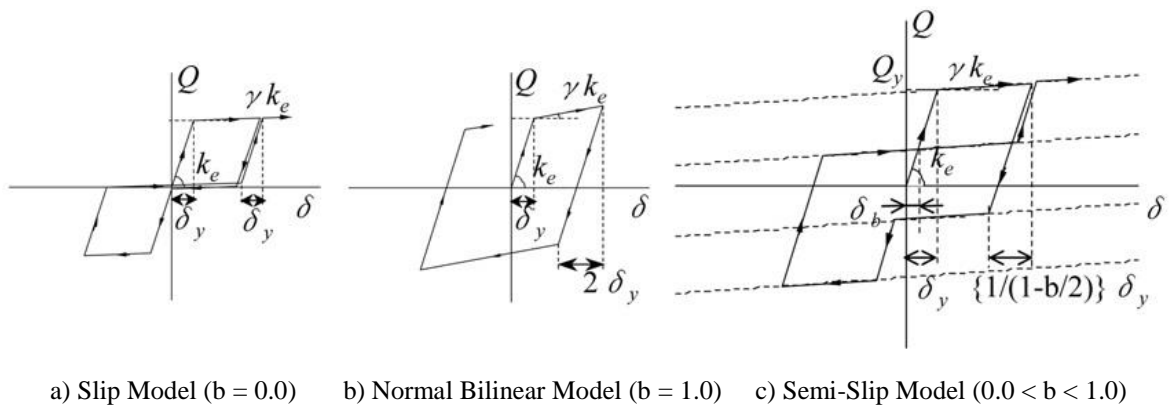


Figure 3.19. Hysteresis Model Proposed by Aoki and Ikeda (2006).

The ratio of elastic rigidity, k_e , to plastic area rigidity, k_p , was introduced as the plastic rigidity ratio, γ , and fixed to 0.15 for normal bilinear type and 0.015 for slip-type. The value for γ is determined by making a linear approach as

$$\gamma = 0.135b + 0.015 \quad (3.47)$$

$$b = 2\delta_b / (\delta_b + \delta_y) \quad (3.48)$$

where δ_y is the elastic limit deformation whereas δ_b is the Bauschinger² deformation.

The total amount of energy exerted by an earthquake, E_T , is equated to the energy consumed by the system as follows

$$E_T = E_P + E_E + E_H \quad (3.49)$$

where E_P expresses the cumulative plastic strain energy, E_E expresses the cumulative elastic strain energy and E_H expresses the amount of energy consumed by the damping mechanism. E_P is also divided into two parts, skeleton part of plastic strain energy, E_{ps} , and Bauschinger part of plastic strain energy, E_{pb} ,

$$E_P = E_{pb} + E_{ps} \quad (3.50)$$

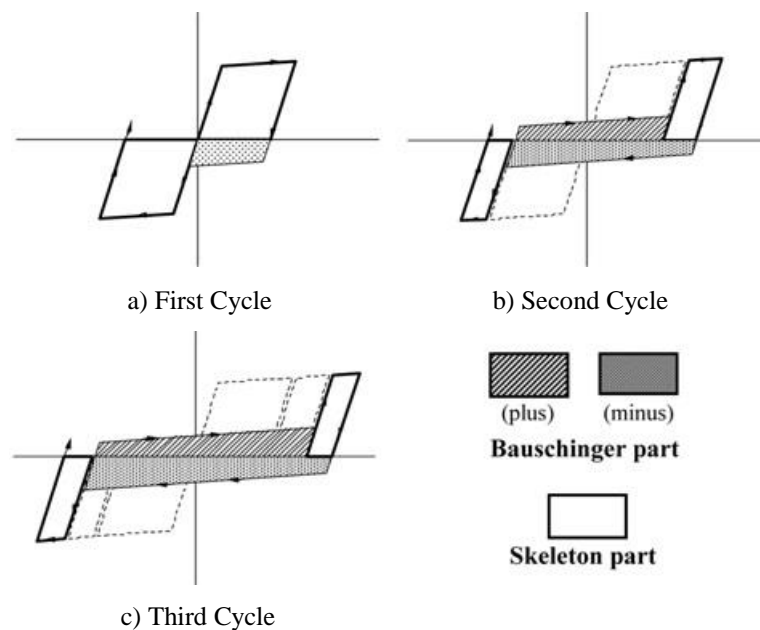


Figure 3.20. Skeleton-Part, E_{ps} , and Bauschinger-Part, E_{pb} (Aoki and Ikeda, 2006).

² The Bauschinger effect is named after the German engineer Johann Bauschinger and refers to a property of materials where the material's stress/strain characteristics change as a result of the microscopic stress distribution of the material.

When the inexperienced displacement of the hysteresis cycle is defined as skeleton-part, and the experienced range displacement as Bauschinger-part (Figure 3.20), the skeleton-part contributes directly to the damage of the building, whereas the Bauschinger-part is related to the low cycle fatigue damage. This relationship can be shown by using the hysteresis model as given in Figure 3.20.

On the other hand, Smooth hysteretic models have continuous change of stiffness due to yielding but sharp changes due to unloading and deteriorating behavior (Sivaselvan and Reinhorn, 1999). The most famous SHM is the model was first suggested by Bouc (1967) as a versatile, smoothly varying hysteresis model for a single degree of freedom (SDOF) mechanical system under forced vibration. This model modified by several researchers and took its final form as the Bouc-Wen-Baber-Noori (BWBN) model which is used in this paper for the hysteretic behavior simulation and explained in detail in Chapter 4.

3.3.2 Finite Element Modeling

In order to model the lateral in-plane behavior of the cold-formed framed sheathed shear walls, there are several finite elements based methods developed depending on the number of elements. The wall can be simulated by either a conventional finite element analysis where framing members are modeled as beam-column elements while the structural sheathing used in the wall is simulated by meshes of shell elements; or a single equivalent shell element have the orthotropic mechanical and geometric properties; or an equivalent bracing system. All these methods can be classified as semi analytical, since they required for experimental data for the nonlinear analysis. There are different types finite elements based methods utilized for modeling is summarized below, for the numerical analysis in this paper, an equivalent bracing model similar to the one proposed by Fülöp and Dubina (2004b) is preferred.

Fülöp and Dubina (2004b) used tri-linear hysteretic model based on a Drain-3DX (1994) computer code to take into account the three main characteristics of panel behavior, (i) pinching, (ii) over-strength as difference between allowable elastic design limit and actual capacity and (iii) plastic deformation capacity. A single degree of freedom system

(SDOF) with a fiber-hinge accommodating the desired hysteretic behavior was constructed and calibrated using the results of full scale testing program carried out by Fülöp and Dubina (2004a). According to this approach the shear panel can be replaced with an equivalent bar model consisting of pinned rectangular frame with dissipative diagonals as demonstrated in Figure 3.21. As all column ends are hinged the frame itself is a mechanism and it does not contribute to load bearing capacity. Braces are modeled as ‘TYPE 8’ fiber hinge (FH) beam-column elements with FH to accommodate the hysteretic behavior.

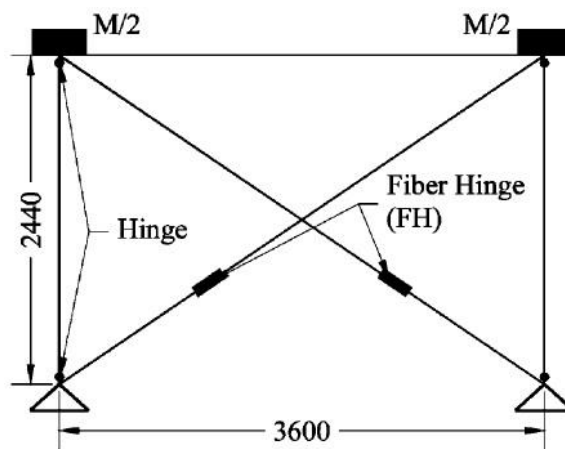


Figure 3.21. Modeling with Idealized Equivalent Bracing (Fülöp and Dubina, 2004b).

Uygar (2006) used an analytical computational model on SAP2000 (2010) consisting of frame members and shell elements meshed according to fastener schedule following two methods (Figure 3.22). The first method was called as constraint defined model. Constraints were defined at each joint and a lateral load was applied at the upper left corner of the wall. Then resultant force obtained at each screw was compared with the shear strength of the screw calculated based on the experimental results. If the resultant force was less than the strength, applied force was increased until the first joint reached the capacity. The second method was nonlinear analysis called as nonlinear link defined model. Screw connections were modeled as nonlinear link elements to simulate behavior of perfectly elastic to the yield level and perfectly plastic beyond the yield level.

Two methods for different fastener schedules yielded to similar results with 3% percent difference found reasonable. Yield pattern obtained from the nonlinear analysis (Figure 3.22), was found consistent with the observations of related experiments. To obtain the nominal shear capacity of the wall, nonlinear link defined model was utilized with an

incremental load until the wall deflection limit defined as $L/240$ in IBC2003 (2003). When the wall reached its deflection limit, corresponding load was assumed as the nominal shear capacity of the wall. Findings of the study showed that both methods were consistent with the nominal shear values for seismic forces as given in the code.

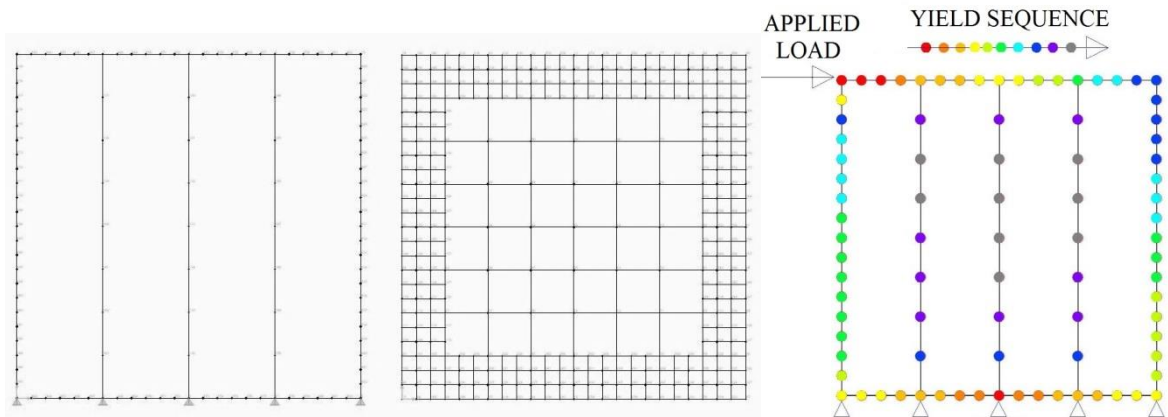


Figure 3.22. General Description of Steel Frame, Meshed Shell and Yield Pattern for the Shear Wall (adapted from Uygar, 2006).

Martinez and Xu (2011) proposed a simplified approach to model the shear wall with equivalent shell elements (Figure 3.23). By taking the advantage of in-line framing, studs and sheathing plates can be modeled as orthotropic shell elements using the equivalent rigidity of orthotropic ribbed plates in bending theory. Equivalent thickness and elastic moduli in x and y direction besides the shear modulus are determined with equating the axial and flexural rigidities of stud-sheathing system and equivalent shell element (Figure 3.24). When the shear wall panels are transformed into flat shells, it is aimed to lessen the burden of the use of finite element analysis in which all framing members are modeled as beam-column elements and structural sheathings simulated by meshes of shell elements which can be time consuming process. Nonlinear behavior of shear wall panels is simulated by a stiffness degradation factor, $\lambda(q)$, intended to be used for the nonlinear static pushover analysis, used to revise the initial stiffness of the shear wall, K_i , with the secant stiffness, K_a , corresponding to the load increment, q using the formulation below

$$K_a^{(q)} = \lambda^{(q)} K_i \quad (3.51)$$

$$\lambda^{(q)} = 1 - \left(\frac{P_a^{(q)}}{P_R} \right)^\beta \quad (3.52)$$

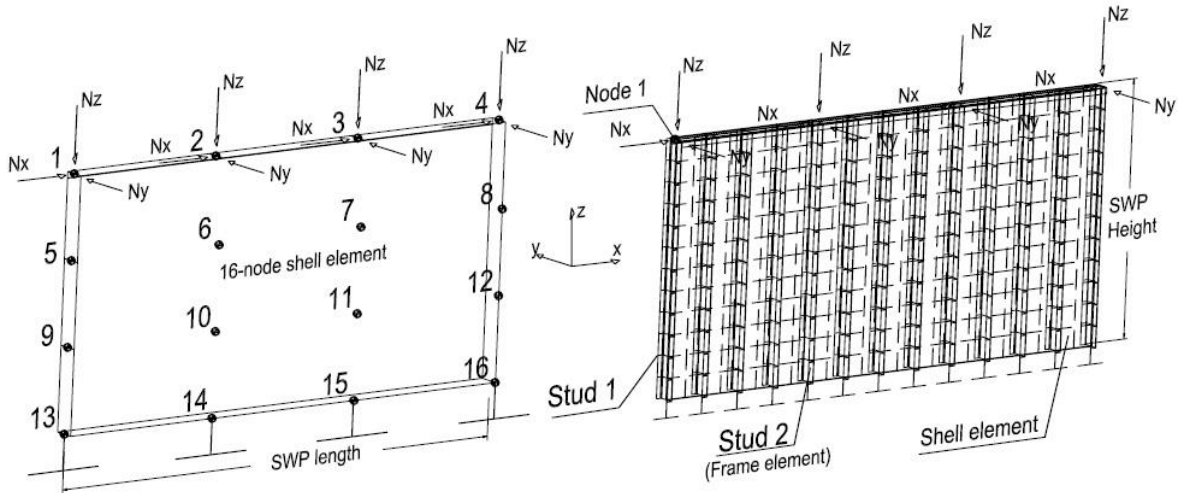


Figure 3.23. A Sixteen-Node Equivalent Shell Element, Martinez and Xu (2011).

where P_a is the applied load whereas P_R is the lateral strength of the shear wall panel obtained from experimental investigations or design tables. β is a stiffness degradation nonlinearity exponent which has to be calibrated according to the sheathing material and screw spacing.

Findings proposed that the stiffness degradation model matches reasonably well to the experimental data. After performing finite element analysis for an example, the lateral displacements are in good agreement whereas internal forces on the studs were overestimated. The accuracy and efficiency of the proposed method was found satisfactory, however it was not recommended for the evaluation of axial forces on studs.

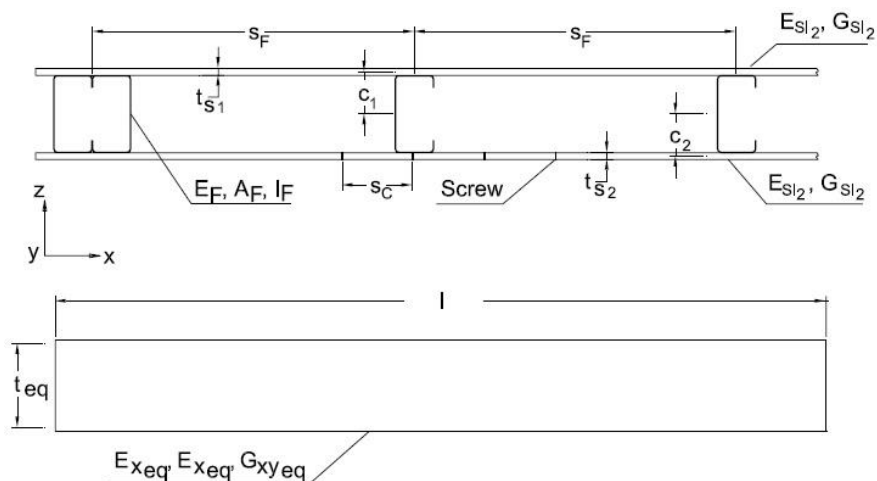


Figure 3.24. Orthotropic Properties of Equivalent Shell Element, Martinez and Xu (2011).

4. SOLUTION APPROACH

4.1. The Bouc-Wen-Baber-Noori Model

In this paper, Bouc-Wen-Baber-Noori (BWBN) model is used to represent the hysteretic behavior of the wall system. Section 4.1 is excerpted from the doctoral dissertation of Foliente (1993) as a summary of the BWBN model which was explained in detail with a new pinching function proposed by Foliente (1993).

4.1.1. Background

The model was first suggested by Bouc (1967) as a versatile, smoothly varying hysteresis model for a single-degree-of-freedom (SDOF) mechanical system under forced vibration. Wen (1976, 1980) generalized Bouc's hysteretic constitutive law and developed an approximate solution procedure for random vibration analysis based on the method of equivalent (or statistical) linearization. Baber and Wen (1981) extended the model to admit stiffness and/or strength degradation as a function of hysteretic energy dissipation. Baber and Noori (1986) further extended the Bouc model by incorporating pinching while maintaining it in a form compatible with Baber and Wen's equivalent linearization solution. The model, with Baber and Noori's single-element pinching model, was known as the Bouc-Wen-Baber-Noori (BWBN) model. With the features added by Baber and Wen (1981) and Baber and Noori (1986), the model became more accurate tool to approximate the hysteretic behavior of structural elements and systems. The model was taken its final form with the new pinching function proposed by Foliente (1993).

4.1.2. Equation of Motion and Constitutive Relations

Considering a single-degree-of-freedom hysteretic system, with a forcing function, $F(t)$, as demonstrated in Figure 4.1, the equation of motion of BWBN can be written as

$$m\ddot{u} + c\dot{u} + \alpha k u + (1-\alpha)kz = F(t) \quad (4.1)$$

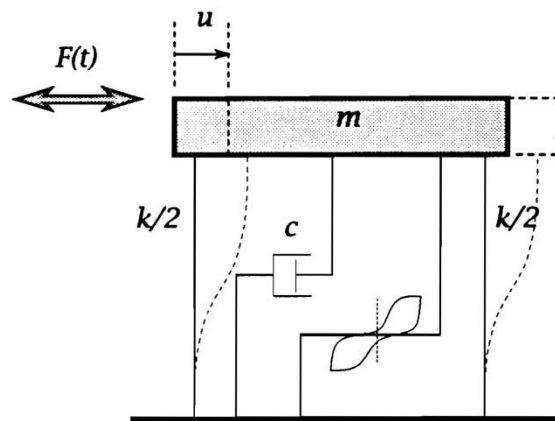
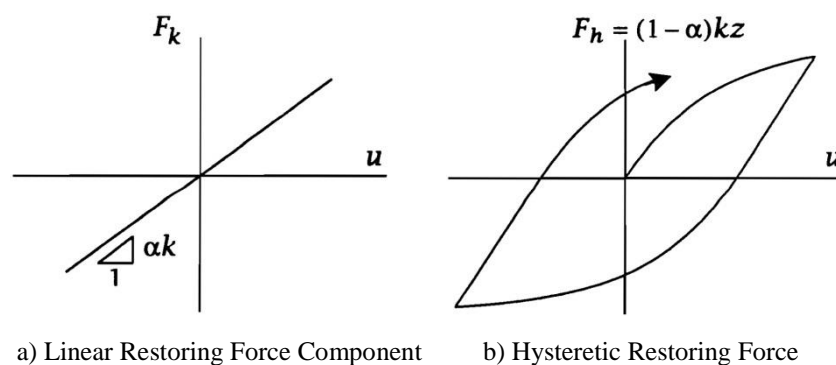


Figure 4.1. Schematic Model (Foliente, 1993).

where dots represent time derivatives. The restoring force acting on the mass, m , contains three discrete components: The inertial restoring force is given by $m\ddot{u}$, the damping restoring force is given by $c\dot{u}$ which is assumed to be a linear function of the velocity, and non-damping restoring force is given by $F_k = \alpha ku$ and $F_h = (1-\alpha)kz$ which are the linear restoring force component and the hysteretic (non-linear) restoring force component as illustrated in Figure 4.2a and Figure 4.2b, respectively. k is the stiffness coefficient and α is a weighting constant (rigidity ratio in the range $0 \leq \alpha \leq 1$) representing the relative participations of the linear and non-linear terms. Obviously, the restoring force is purely hysteretic if $\alpha = 0$ and purely elastic if $\alpha = 1$.



a) Linear Restoring Force Component b) Hysteretic Restoring Force

Figure 4.2. Non-Damping restoring Force (Foliente, 1993).

Dividing by m in both sides of Equation 4.1, the following standard form of the mass-normalized equation of motion is obtained:

$$\ddot{u} + 2\xi_0\omega_0\dot{u} + \alpha\omega_0^2u + (1-\alpha)\omega_0^2z = f(t) \quad (4.2)$$

where $f(t)$ is the mass-normalized forcing function (i.e. acceleration), ω_0 is the pre-yield natural frequency of the system ($\sqrt{k/m}$), ζ_0 is the linear damping ratio ($c / 2 \sqrt{k/m}$), and z is a function of the time history of u ; it is related to through the following first-order nonlinear differential equation:

$$\dot{z} = h(z) \left\{ \frac{A\dot{u} - v(\beta|\dot{u}||z|^{n-1}z + \gamma\dot{u}|z|^n)}{\eta} \right\} \quad (4.3)$$

where A is the parameter that regulates the tangent stiffness and ultimate hysteretic strength; β , γ , n are hysteresis shape parameters; v and η are strength and stiffness degradation functions, respectively; and $h(z)$ is the pinching function.

In BWBN model, degradation and pinching are represented in terms of the hysteretic energy dissipated. The dissipated hysteretic energy, $\varepsilon(t)$, is obtained with the continuous integration of the hysteretic force, F_h , over the total displacement, u , by Equation 4.4 and the rate of change of the hysteretic energy dissipation can be written as Equation 4.5.

$$\varepsilon(t) = \int_{u(0)}^{u(t)} F_h du = (1-\alpha)\omega_0^2 \int_{u(0)}^{u(t)} z du \frac{dt}{dt} = (1-\alpha)\omega_0^2 \int_0^t z(u,t) \dot{u} dt \quad (4.4)$$

$$\dot{\varepsilon} = (1-\alpha)\omega_0^2 z \dot{u} \quad (4.5)$$

4.1.3. BWBN Parameters

The BWBN model contains 13 unspecified parameters, which includes hysteresis shape parameters A , α , β , γ , and n ; strength and stiffness degradation parameters δ_v and δ_η ; and pinching parameters ζ_s , p , q , ψ_0 , δ_ψ , and λ .

A regulates the ultimate hysteretic strength, Z_u , and sets the initial tangent stiffness. As the value of A increases, both the ultimate hysteretic strength, Z_u , and the initial tangent stiffness, dz/du at $z=u=0$, increase. After some numerical manipulations, α is stated as the ratio of the final tangent stiffness to the initial stiffness.

Three hysteresis parameters β , γ and n and their interactions determine the basic hysteresis shape. Absolute values of β and γ inversely influence hysteretic stiffness and strength, as well as the smoothness of the hysteresis loops. For, $n=1$, the relationships between β and γ and their effects on hysteresis are shown in Figure 4.3.

When $\beta=0$, the equations for loading and unloading become same and the loading and unloading paths coalesce into a single path which is non-hysteretic even though the path may remain nonlinear (when $n>1$). When $\beta<0$, a negative dissipation energy, which cannot be explained physically, is obtained, therefore β should always be positive, regardless of the value of γ . With the restriction for β to have positive values, hysteresis shapes for possible combinations of β and γ are demonstrated in Figure 4.3.

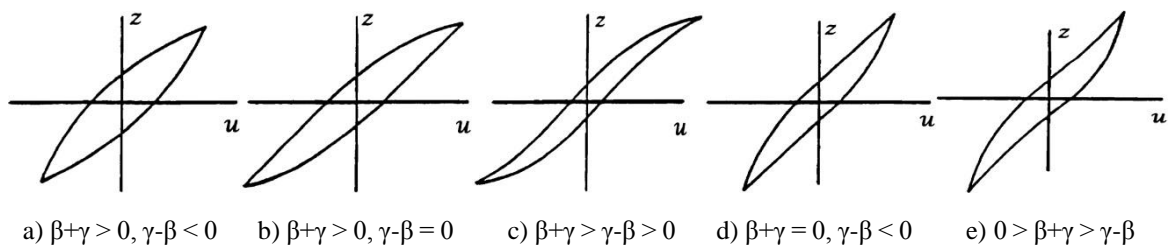


Figure 4.3. Possible Hysteresis Shapes (adapted from Foliente, 1993).

Softening and hardening behavior of the model depend on γ . A softening model is obtained when the slope of the hysteresis path decreases with increasing $|z|$ whereas a hardening model is obtained when the slope of the hysteresis path increases with increasing $|z|$. As illustrated in Figure 4.5, positive γ tends to cause softening and negative γ tends to cause hardening, but the limiting behavior will remain softening unless $|\gamma|>|\beta|$ and $\gamma<0$. Also if $\gamma=\beta$, a linear unloading path is obtained.

The effect of n on the skeleton curves of the hysteresis is demonstrated in Figure 4.4. The skeleton curves drawn for various values of n are shown for the case where $A=1$, $\beta=\gamma=0.5$. It is obvious that as $n \rightarrow \infty$, the hysteresis in $z-u$ plane produces an elasto-plastic model. This can be verified analytically with i.e. the softening model, $(\beta+\gamma)>0$.

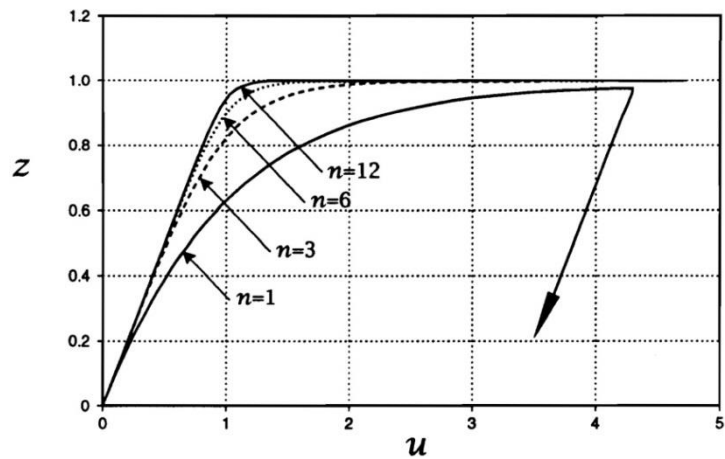


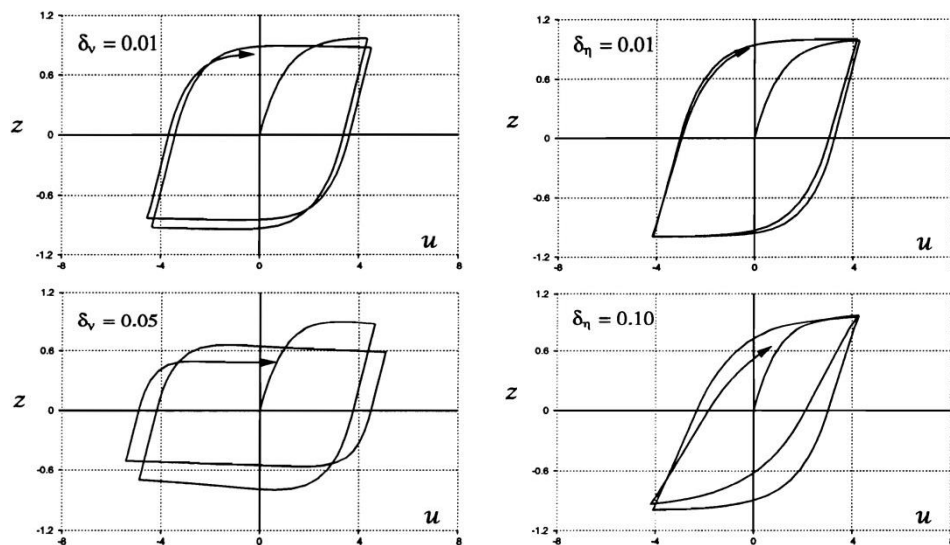
Figure 4.4. Skeleton curves with varying n (Foliente, 1993).

The strength and stiffness degradation is controlled by the parameters ν and η as functions of the dissipated hysteretic energy given by in Equation 4.4 and may be written as

$$\nu(\varepsilon) = 1.0 + \delta_\nu \varepsilon \quad (4.6)$$

$$\eta(\varepsilon) = 1.0 + \delta_\eta \varepsilon \quad (4.7)$$

where δ_ν and δ_η are the strength and stiffness degradation rates, respectively. A value of each $\delta = 0$ means no degradation. If ν increases (i.e. $\delta_\nu > 0$), strength alone degrades (Figure 4.5a). If η increases (i.e. $\delta_\eta > 0$), stiffness alone degrades (Figure 4.5b).



a) Strength Degradation (effect of varying ν) b) Stiffness Degradation (effect of varying η)

Figure 4.5. Parameters Control Degradation Rates (Foliente, 1993).

The new pinching function proposed by Foliente (1993) instead of the original one defined by Baber and Noori (1986), $h(z)$, with introducing a new parameter, q , which is the percentage of ultimate restoring force Z_u and is given, in a new form, by,

$$h(z) = 1 - \zeta_1 e^{[-(z \operatorname{sgn}(\dot{u}) - qZ_u)^2 / \zeta_2^2]} \quad (4.8)$$

where $\operatorname{sgn}(\dot{u})$ is sign or signum function of \dot{u} , and Z_u is the ultimate hysteretic displacement given by,

$$Z_u = \pm \left[\frac{A}{\nu(\beta + \gamma)} \right]^{1/n} \quad (4.9)$$

Two pinching functions $\zeta_1(\varepsilon)$ and $\zeta_2(\varepsilon)$ control the progress of the pinching and are written as,

$$\zeta_1(\varepsilon) = \zeta_s [1 - e^{-p\varepsilon}] \quad (4.10)$$

$$\zeta_2(\varepsilon) = (\psi_0 + \delta_\psi \varepsilon)(\lambda + \zeta_1) \quad (4.11)$$

ζ_1 controls the severity of pinching by regulating the magnitude of the initial drop in the slope, dz/du as a function of the dissipated energy ε , depending on the ζ_s and p values; where ζ_s is the total slip and p is the parameter that controls the rate of initial drop in slope. ζ_2 controls the rate of change of the slope dz/du , thus the rate of pinching as a function of the dissipated energy ε , depending on the ζ_1 , ψ_0 , δ_ψ , and λ values; where ψ_0 is the parameter that contributes to the amount of pinching, δ_ψ is the parameter specified for the desired rate of change of ζ_2 based on ε , and λ is a small parameter that controls the rate of change of ζ_2 as ζ_1 . Figure 4.6a shows that when ζ_1 is varied while ζ_2 is kept constant, dz/du drops at the start of the second and successive loading cycles. Pinching is induced by forcing minimum tangent stiffness when $z=0$. Then the stiffness increases relatively rapidly as z increases, slowing down as the original slope is approached. When ζ_2 is kept constant, the original slope is reached at the same level of z in all cycles. When ζ_2 is varied and ζ_1 is kept constant (Figure 4.6b), the level of drop at the start of the second and successive loading cycles remains the same but the original slope is reached at increasing levels of z . Thus, it may be stated that ζ_1 controls the severity of pinching while ζ_2 controls the rate of pinching. Figure 4.6c shows the pinching function effect when both ζ_1 and ζ_2 vary.

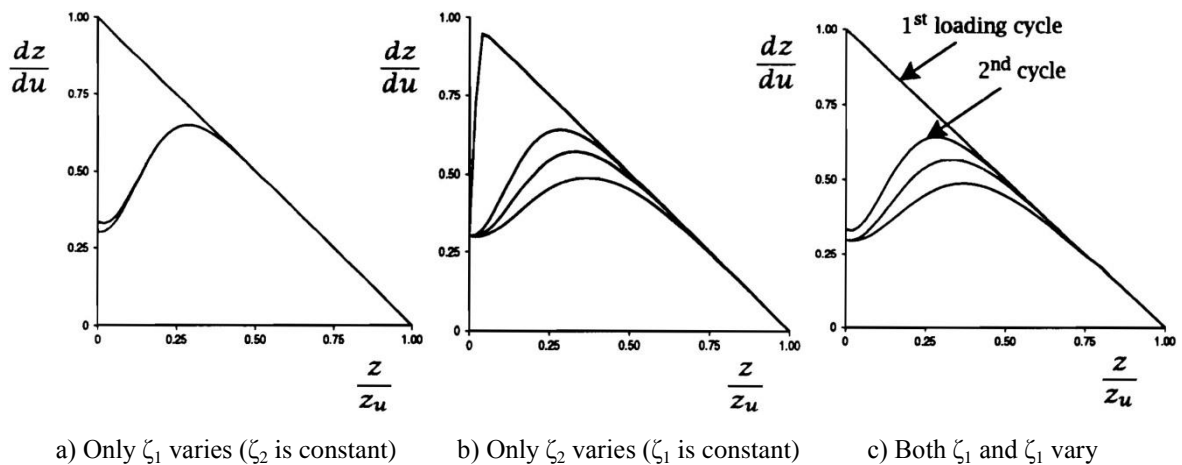


Figure 4.6. Baber and Noori's Pinching Function Effect (Foliente, 1993).

When $q=0$, the model reverts back to Baber and Noori's original function. The modification to the pinching function results in the enhanced model versatility with the generalized pinching capability. The modified BWBN model is, in fact, applicable to structures made of different types of materials, such as steel, wood and reinforced concrete that exhibit pinching similar to that observed in sheathed shear walls (Foliente, 1993).

4.1.4. Summary of BWBN Model

The BWBN hysteresis model incorporates all the experimentally observed characteristics of cold-formed steel-framed sheathed shear walls that were identified in the Chapter 3. Since the mechanical model consists of three parallel elements: a linear viscous damping, a linear spring and a hysteretic element; the model can simulate a nonlinear, inelastic load-displacement relationship with stiffness and strength degradation and pinching behavior. The hereditary nature of the constitutive relations satisfies the requirement that the response depends not only on instantaneous displacement but also on its past history. The overall response of the model is controlled by 13 unspecified parameters with various values in different intervals and their combinations yield to different hysteretic behavior, thus different load-displacement backbone curves. Table 4.1 summarizes these parameters. Generalized in-plane lateral load performance of wall panel systems identified in Chapter 3 can be simulated by these parameters after investigating the effect of each parameter as the configuration of the wall panel system (aspect ratios, stud spacing fastener spacing, sheathing type, sheathing thickness etc.) is varied.

Table 4.1. Summary of BWBN Hysteresis Model Parameters.

| Parameter | Explanation / Features | Related Figures |
|---|--|-----------------|
| System Properties and Hysteresis Parameters | | |
| A | Regulates the ultimate hysteretic strength, Zu , and initial tangent stiffness at $z=u=0$. | |
| α | Rigidity ratio (weighing parameter represents the relative participations of the linear and nonlinear terms); ratio of the final tangent stiffness to initial tangent stiffness when $A=1$; α varies between 0 and 1; if $\alpha = 0$, model becomes purely hysteretic whereas if $\alpha = 1$, model becomes purely elastic. | Figure 4.2 |
| β | Hysteresis shape parameter. Since dissipated energy must be positive, β is always positive. | Figure 4.3 |
| γ | Hysteresis shape parameter. A softening model is obtained when the slope of the hysteresis path decreases with increasing $ z $, a hardening model is obtained when the slope of the hysteresis path increases with increasing $ z $. Positive values of γ tend to softening whereas negative values of γ tend to hardening. | |
| n | Controls hysteretic curve smoothness. As $n \rightarrow \infty$, the hysteresis in the $z-u$ plane produces an elasto-plastic model. | Figure 4.4 |
| Degradation Parameters | | |
| δ_v | Parameter that controls strength degradation. | Figure 4.5 |
| δ_n | Parameter that controls stiffness degradation. | Figure 4.5 |
| Pinching Parameters | | |
| ζ_1 | Parameter that controls the magnitude of initial drop in slope, dz/du ; ($\zeta_1 < 1.0$), controls the severity of pinching; depends on the values of ζ_s and p . | Figure 4.6 |
| ζ_2 | Parameter that controls the rate of change of the slope dz/du , controls the rate of pinching; depends on the values of ζ_1 , Ψ_0 , ζ_1 and λ . | Figure 4.6 |
| Ψ_0 | Parameter that contributes the amount of pinching. | |
| δ_Ψ | Parameter specified for the desired rate of change of ζ_2 based on ϵ . | |
| p | Constant that controls the rate of initial drop in slope | |
| q | Percentage of ultimate restoring force Zu where pinching (or slipping) occurs. | |
| ζ_s | Measure of total slip (e.g., $\zeta_s = 0.98$ means a high pinching system and $\zeta_s = 0.70$ means a low pinching system.) | |
| λ | Small parameter that controls the rate of change of ζ_2 as ζ_1 | |

4.2. Solution Algorithm

The main objective of the solution approach explained in this section is to simulate the force-displacement curve obtained from the successive hysteretic cycles of Bouc-Wen-Baber-Noori (BWBN) model with an n degree polynomial. Therefore; using the $n+1$ coefficients of the polynomial (known function), each displacement value can be achieved with corresponding force level. Prior to this curve replication process, first appropriate BWBN parameters, thus the cyclic curves should be obtained depending mainly on the analysis type; it may be either dynamic or quasi-static.

Based on the analysis type; function of the loading protocol, equation of motion and constitutive relations with hysteretic shape parameters of BWBN model are implemented to a MATLAB (2008) code. Since most of the experimental studies explained in Chapter 3 are quasi-static and displacement controlled; quasi-static hysteresis model is regarded as a more efficient tool instead of the dynamic one for the verification of the model and the numerical examples. In accordance, with the quasi-static model, a stiff set of first-order nonlinear ordinary differential equations are integrated with a member of family of second order Runge-Kutta methods. Thus, global and hysteretic force-displacement curves are obtained.

For the calibration of the model with the experimental data, both model and experimental backbone curves are considered as polynomials. The curve passing through the peaks of hysteretic cycles of the model is represented by a polynomial having degree, n providing minimized error between peak points and the polynomial. Further, certain points of the experimental curve are converted to another polynomial, having the same degree, providing minimized error between the model and the experimental polynomials. Final error function to be minimized is based on the mean and standard deviations of these two separate error functions.

When the final error is adequately reduced, all appropriate hysteretic shape parameters, thus the model force-displacement curve, are obtained for the defined wall configuration. The solution approach procedure used in the MATLAB code is summarized in the following flowchart.

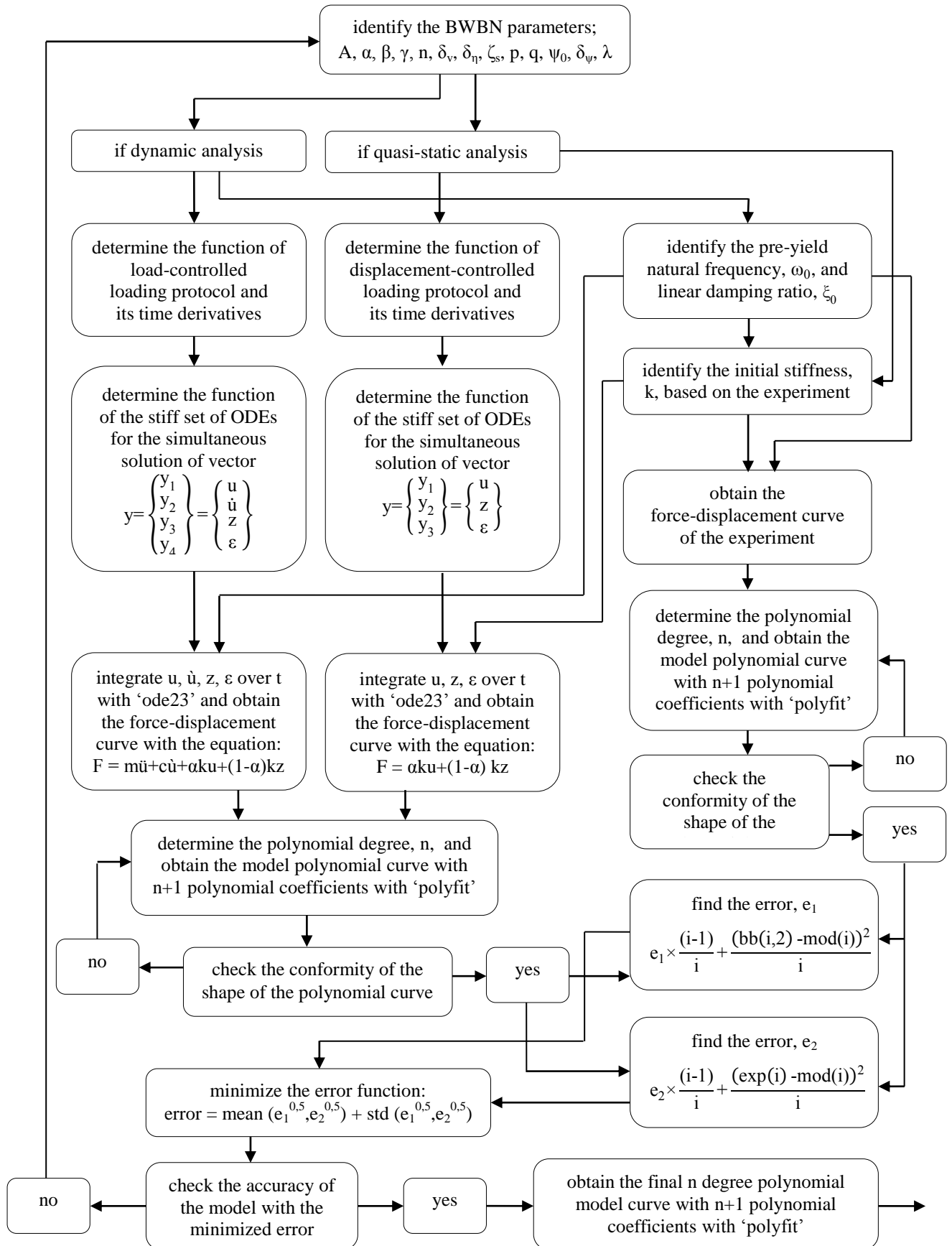


Figure 4.7. MATLAB Algorithm to Obtain the Model Force-Displacement Curve.

Herein after, three wall configurations, Type I, Type II and Type III as explained in Section 3.1.3, from experimental study carried out by Fülöp and Dubina (2004a), are used for model verification following the flowchart demonstrated on the Figure 4.7. Details of the solution approach are explained in the following sections.

4.2.1 Quasi-Static BWBN Model

The BWBN model presented in Section 4.1 is rate dependent and mostly preferred in the nonlinear time history analysis. However, most of the experimental studies explained in Chapter 3 are quasi-static and displacement controlled. So, in order to calibrate the BWBN model according to the experimental results, the dynamic BWBN model is adapted to a quasi-static BWBN model with following the similar way used by Nithyadharan and Kalyanaraman (2013) as follows.

The dynamic BWBN model is described as below to represent the equation of motion in the state vector form, consider a vector y defined as

$$y = \begin{Bmatrix} y_1 \\ y_2 \\ y_3 \\ y_4 \end{Bmatrix} = \begin{Bmatrix} u \\ \dot{u} \\ z \\ \varepsilon \end{Bmatrix} \quad (4.12)$$

Then, Equation 4.2, Equation 4.3 and Equation 4.4 may be rearranged into a set of four first-order nonlinear ODEs as below,

$$\dot{y}_1 = y_2 \quad (4.13)$$

$$\dot{y}_2 = -\alpha\omega_0^2 y_1 - 2\xi_0\omega_0 y_2 - (1-\alpha)\omega_0^2 y_3 + f(t) \quad (4.14)$$

$$\dot{y}_3 = h(z) \left\{ \frac{A y_2^{-\nu} \left(\beta |y_2| |y_3|^{n-1} y_3 + \gamma y_2 |y_3|^n \right)}{\eta} \right\} \quad (4.15)$$

$$\dot{y}_4 = (1-\alpha)\omega_0^2 y_2 y_3 \quad (4.16)$$

This arrangement results in a stiff set of equations where $f(t)$ is a forcing function such as loading protocol, as series of sinusoidal function typically used in load controlled

tests or an arbitrary acceleration input such as earthquake ground acceleration used for nonlinear time history analysis. Other parameters are explained in Section 4.1.

On the other hand, quasi-static and displacement controlled experiments described in Chapter 3 are carried out at a slow rate, in which the force contribution from the mass ($m\ddot{u}$) and damping ($c\dot{u}$) are not significant. Thus, in order to model the quasi-static and displacement controlled experimental results; the mass normalized dynamic equation of motion in Equation 4.14 is removed from the set of BWBN dynamic model equations. Accordingly, for the quasi-static model, BWBN model with three first order stiff-set of ODE's in Equation 4.18, Equation 4.19 and Equation 4.20 are to be solved instead. Furthermore, for the calculation of the dissipated energy; initial stiffness of the system, k , as shown in Equation 4.20 is used instead of the natural frequency, ω_0^2 (i.e. k/m), used in dynamic BWBN model.

The quasi-static BWBN model in state vector format becomes,

$$y = \begin{Bmatrix} y_1 \\ y_2 \\ y_3 \end{Bmatrix} = \begin{Bmatrix} u \\ z \\ \varepsilon \end{Bmatrix} \quad (4.17)$$

with three first-order nonlinear stiff-set of ODEs as below,

$$\dot{y}_1 = V \quad (4.18)$$

$$\dot{y}_2 = h(z) \left\{ \frac{AV - (\beta|V||y_2|^{n-1}y_2 + \gamma V|y_2|^n)}{\eta} \right\} \quad (4.19)$$

$$\dot{y}_3 = (1-\alpha)ky_2V \quad (4.20)$$

When the force contribution from the mass ($m\ddot{u}$) and damping ($c\dot{u}$) are disregarded, the restoring force in Equation 4.1 becomes,

$$F = \alpha ku + (1-\alpha)kz \quad (4.21)$$

The loading protocol used in the experiment is defined as function of time, t and corresponding displacement, u and $V = \dot{u}$ is the time derivative of input displacement

loading protocol and integrated over time to obtain the corresponding \dot{y}_1 value. The plot of the loading protocol according to the experimental research is demonstrated in Figure 4.8.

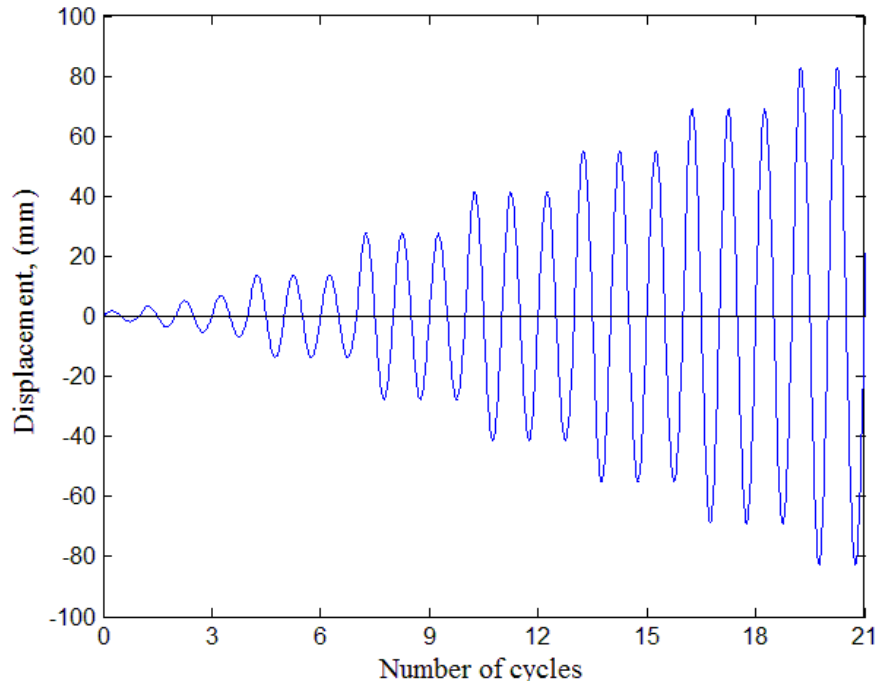


Figure 4.8. Loading Protocol - Input Displacement.

Fülöp and Dubina (2004a) followed ECCS-No: 45 (1986) to determine the displacement amplitudes for the quasi-static loading cyclic tests. Accordingly, at the beginning of the cyclic test, the amplitude of the step was changing in every cycle but after yield every cycle was repeated three times. Thus, cyclic tests with the increase of displacement, which has the following successive cycle characteristics; one cycle in each $\frac{1}{4} \Delta_{el} - \frac{1}{4} \Delta_{el}$ interval, $\frac{1}{2} \Delta_{el} - \frac{1}{2} \Delta_{el}$ interval, $\frac{3}{4} \Delta_{el} - \frac{3}{4} \Delta_{el}$ interval, $\Delta_{el} - \Delta_{el}$ interval; and three cycles in each $2 \Delta_{el} - 2 \Delta_{el}$ interval, $4 \Delta_{el} - 4 \Delta_{el}$ interval, $(2+2n) \Delta_{el} - (2+2n) \Delta_{el}$ interval ($n=1,2,3,\dots$) and so on were performed until failure or a significant decrease of load bearing capacity. Furthermore, there were one monotonic and two cyclic (3 cycles/min and 6 cycles/min) experiments were carried out for each type of wall specimen. However, different loading velocities did not yield a significant difference (Fülöp and Dubina, 2004a).

Further, since the displacement function is known from the displacement controlled tests; thus, derivative of the displacement function, V , or the velocity function, is also

known. Therefore, the stiff set of ODEs representing the quasi-static cyclic test can be numerically solved with the integration of ODEs in Equation 4.18, Equation 4.19 and Equation 4.20 with the utilization of integration method defined in the next section.

4.2.2 Integration of the Stiff Set of ODEs

In numerical analysis, the Runge-Kutta methods are an important family of implicit and explicit iterative methods for the approximation of solutions of ordinary differential equations (Boyce and DiPrima, 2000). The Bogacki–Shampine method³ (Bogacki and Shampine, 1989) is a Runge-Kutta method of order three with four stages with the First Same as Last (FSAL) property and has an embedded second-order method which can be used to implement adaptive step size. The method is implemented in the “ode23” function in MATLAB, 2008 with an algorithm as below. Let

$$y'=f(t,y) \quad (4.22)$$

and y_n denotes the numerical solution at time t_n and h_n is the step size, defined by,

$$h_n=t_{n+1}-t_n \quad (4.23)$$

Then, one step of the Bogacki–Shampine method is given by

$$k_1=f(t_n,y_n) \quad (4.24)$$

$$k_2=f\left(t_n+\frac{1}{2}h_n,y_n+\frac{1}{2}hk_1\right) \quad (4.25)$$

$$k_3=f\left(t_n+\frac{3}{4}h_n,y_n+\frac{3}{4}hk_2\right) \quad (4.26)$$

$$y_{n+1}=y_n+\frac{2}{9}hk_1+\frac{1}{3}hk_2+\frac{4}{9}hk_3 \quad (4.27)$$

$$k_4=f(t_n+h_n,y_{n+1}) \quad (4.28)$$

$$z_{n+1}=y_n+\frac{7}{24}hk_1+\frac{1}{4}hk_2+\frac{1}{3}hk_3+\frac{1}{4}hk_4 \quad (4.29)$$

³ The Bogacki–Shampine method, proposed by Przemyslaw Bogacki and Lawrence F. Shampine in 1989, is a method for the numerical solution of ordinary differential equations

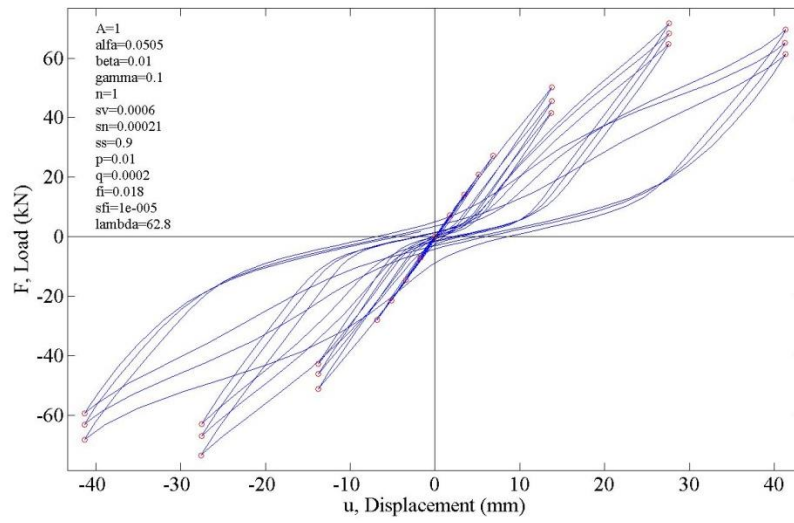
Here, z_{n+1} is a second order approximation to the exact solution whereas y_{n+1} is a third order approximation, so the difference between y_{n+1} and z_{n+1} is used to adapt the step size, h_n . The FSAL property is that the stage value k_4 in one step equals k_1 in the next step; thus, only three function evaluations are needed per each step.

Three first-order nonlinear ordinary differential equations of quasi-static BWBN model given in Equation 4.18, Equation 4.19 and Equation 4.20 are integrated over the defined timespan utilizing the ode23 function with zero initial boundary conditions. Then, for each displacement value in consequence of the loading protocol, corresponding load value, f , is calculated based on Equation 4.21. Therefore, the load-displacement curves composed of successive hysteretic cycles related to three wall types are obtained as demonstrated in Figure 4.9.

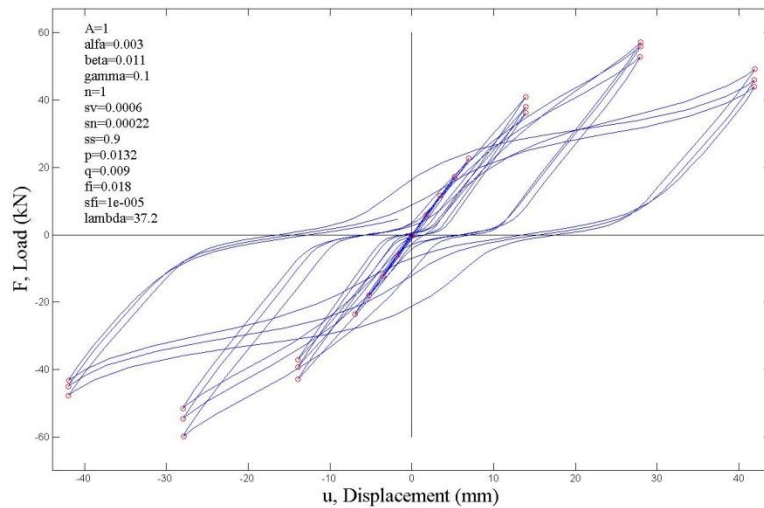
Note that for the illustration purpose, it is preferred to illustrate final form of the figures, so these curves are achieved after following the algorithm in Figure 4.7 for the calibration. Therefore, the final BWBN parameters of the calibrated curves are demonstrated in Table 4.2.

Table 4.2. Final BWBN Parameters of the Calibrated Curves Related.

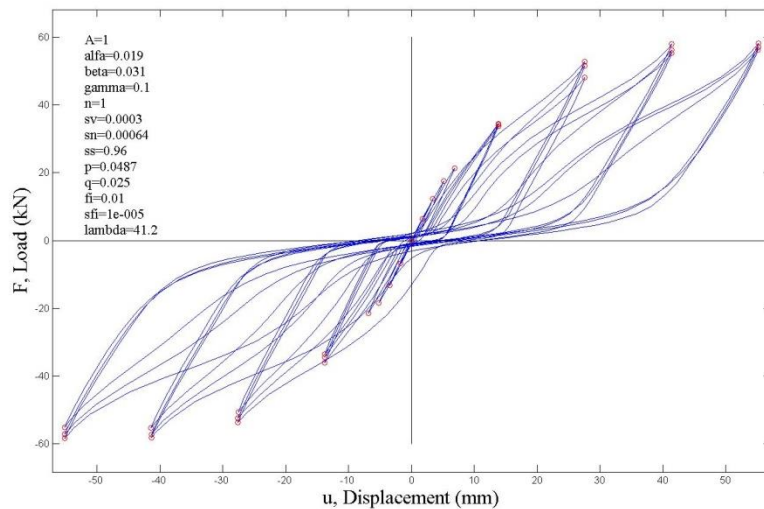
| BWBN parameters | Wall Type | | |
|-----------------|-----------|---------|---------|
| | I | II | III |
| A | 1 | 1 | 1 |
| α | 0.505 | 0.003 | 0.019 |
| β | 0.01 | 0.011 | 0.031 |
| γ | 0.1 | 0.1 | 0.1 |
| n | 1 | 1 | 1 |
| δ_v | 0.0006 | 0.0006 | 0.0003 |
| δ_n | 0.00021 | 0.00022 | 0.00064 |
| δ_s | 0.9 | 0.9 | 0.96 |
| p | 0.01 | 0.0132 | 0.0487 |
| q | 0.0002 | 0.0009 | 0.025 |
| ψ_0 | 0.018 | 0.018 | 0.01 |
| δ_ψ | 0.00001 | 0.00001 | 0.00001 |
| λ | 62.8 | 37.2 | 41.2 |



a) Successive Hysteresis Cycles for Wall Type I



b) Successive Hysteresis Cycles for Wall Type II



c) Successive Hysteresis Cycles for Wall Type III

Figure 4.9. The Successive Hysteretic Cycles.

4.2.3 Model and Experimental Polynomial Curves

The backbone curve passing through the peak and dip points of successive cycles is formed with the identification of the location of local extremas with the help of “findpeaks” function. The function identifies the point as a local peak if it is larger than both of its neighbor points (MATLAB, 2008). The location of each peak and dip point is used then as an input for the polynomial curve fitting function, “polyfit”,

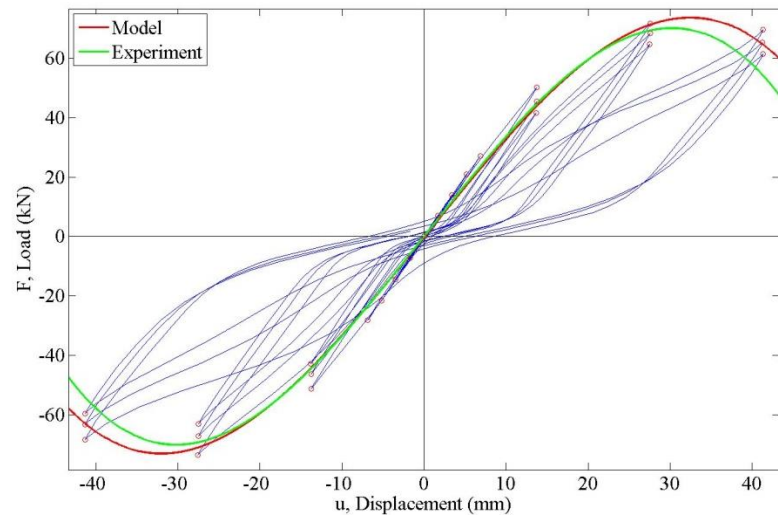
$$p=\text{polyfit}(x,y,n) \quad (4.30)$$

which finds the coefficients of a polynomial $p(x)$ of degree n that approximately fits the data, $p(x(i))$ to $y(i)$, in a least square sense (MATLAB, 2008). The result p is a row vector of length $n+1$ containing the polynomial coefficients in descending powers as below

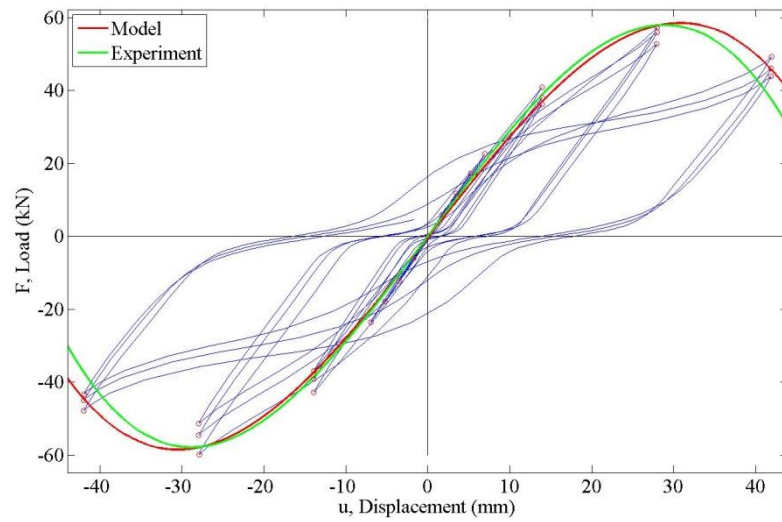
$$p(x)=p_1x^n+p_2x^{n-1}+\dots+p_nx+p_{n+1} \quad (4.31)$$

During the calibration of the BWBN model with the experimental results for each wall type, it is investigated that when the degree of the polynomial is set to 4, the shape of the curve fits to the experimental one more accurately. So, the degree of the polynomial is set to 4 for all cases, thus, the polyfit function calculates 5 coefficients of each polynomial.

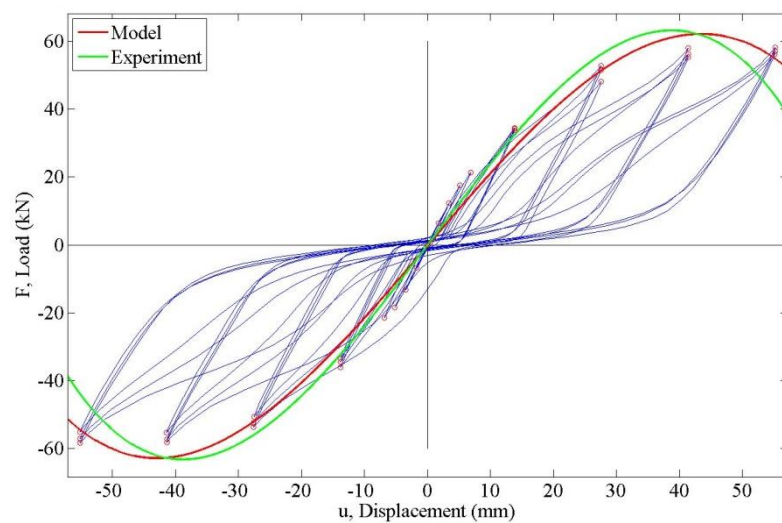
Afterwards, the coefficients of the polynomial are calculated based on the polynomial that passes nearest through peak points of the cycles providing the least square of the distance between each point and the polynomial. The 5 coefficients of the both experimental and model’s 4th degree polynomials of each wall types are tabulated in Table 4.3. Then the “polyval” function (MATLAB, 2008) evaluates the f value of the polynomial at each x point by using the polynomial coefficients obtained with the “polyfit” function. Thus the backbone curves are obtained with the calculated polynomials for each x values as plotted in Figure 4.10.



a) Polynomial Backbone Curves for Wall Type I



b) Polynomial Backbone Curves for Wall Type II



c) Polynomial Backbone Curves for Wall Type III

Figure 4.10. Experimental and Model Polynomial Backbone Curves.

4.2.4 Error Minimization

There are two error functions used for the calibration process. The first one accounts for the difference between the peak points of hysteresis and the model polynomial backbone curve with the following expression,

$$e_1 = e_1 \times \frac{(i-1)}{i} + \frac{(bb(i,2) - \text{mod}(i))^2}{i} \quad i=1,2,\dots \quad (4.32)$$

where $bb(i,2)$ is the f values of each peak and dip points of successive cycles whereas $\text{mod}(i)$ is the model polynomial value of step i . The other error function accounts for the difference between the experimental and model polynomial backbone curves with following expression,

$$e_2 = e_2 \times \frac{(i-1)}{i} + \frac{(\text{exp}(i) - \text{mod}(i))^2}{i} \quad i=1,2,\dots \quad (4.33)$$

where $\text{exp}(i)$ is the experimental polynomial value of step i whereas $\text{mod}(i)$ is the model polynomial value of step i . The final error function to be minimized is calculated with mean and standard deviation of square roots of e_1 and e_2 for corresponding step i as follows

$$\text{error} = \text{mean}(e_1^{0.5}, e_2^{0.5}) + \text{std}(e_1^{0.5}, e_2^{0.5}) \quad (4.34)$$

When the error is minimized sufficiently, the coefficients for model and experimental polynomials are obtained as in the following table where the letter M refers for model whereas E refers for the experiment)

Table 4.3. The 5 Coefficients of the Model and Experimental 4th Degree Polynomials.

| Wall Type | Coefficients | | | | |
|-----------|----------------|----------------|----------------|----------------|----------------|
| | p ₁ | p ₂ | p ₃ | p ₄ | p ₅ |
| I M | 1.06E-07 | -1.10E-03 | 4.90E-04 | 3.41E+00 | -3.47E-01 |
| I E | 1.32E-20 | -1.27E-03 | -2.97E-17 | 3.48E+00 | 1.03E-14 |
| II M | 1.54E-07 | -1.02E-03 | 2.28E-04 | 2.86E+00 | -3.96E-01 |
| II E | -6.42E-21 | -1.20E-03 | 2.42E-17 | 3.01E+00 | -9.12E-15 |
| III M | 1.74E-07 | -3.87E-04 | -3.72E-04 | 2.17E+00 | -2.54E-01 |
| III E | 6.01E-22 | -5.41E-04 | -2.50E-18 | 2.44E+00 | -2.82E-16 |

5. FINITE ELEMENT MODEL

In order to evaluate the lateral behavioral properties of the wall system, the calibrated Bouc-Wen-Baber-Noori model backbone curves are used for evaluation of the lateral behavior of the wall system with finite elements method (FEM) herein after. SAP2000 (2010), a finite element analysis and design software, is used for the equivalent bracing model after some geometrical and mathematical operations performed with MS Excel following the algorithm in Figure 5.1. Details of the finite element model are explained in the following sections.

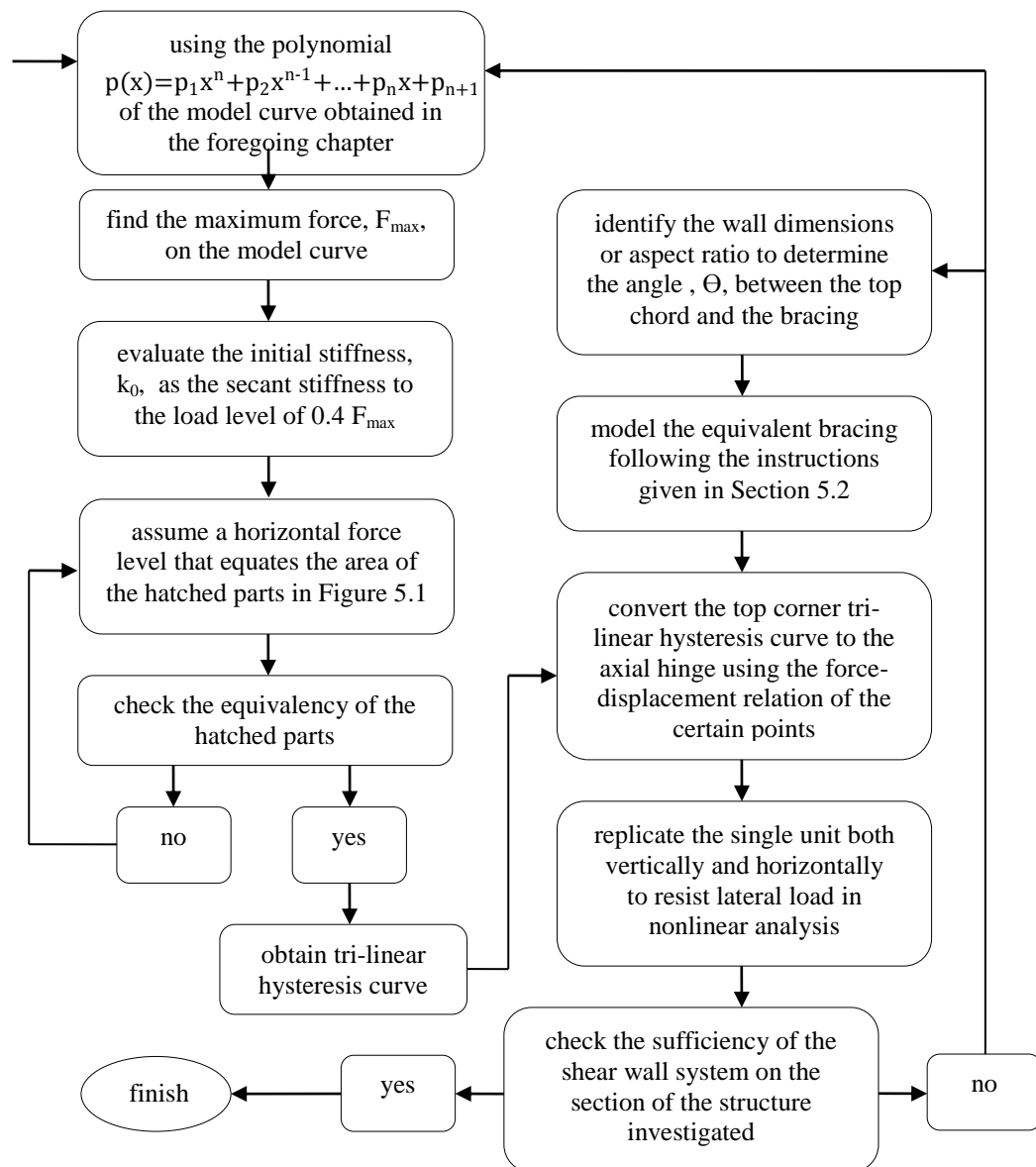


Figure 5.1. MS Excel and SAP2000 Equivalent Bracing Flowchart.

5.1. Interpretation of the Model Backbone Curve

The force-displacement curve obtained from the Bouc-Wen-Baber-Noori model, defined in the previous section, or directly from the full scale shear wall test is converted into tri-linear idealized elasto-plastic model including the certain points as illustrated in Figure 5.2. This interpretation is carried out by utilizing the method developed by Kawai *et al.* (1999).

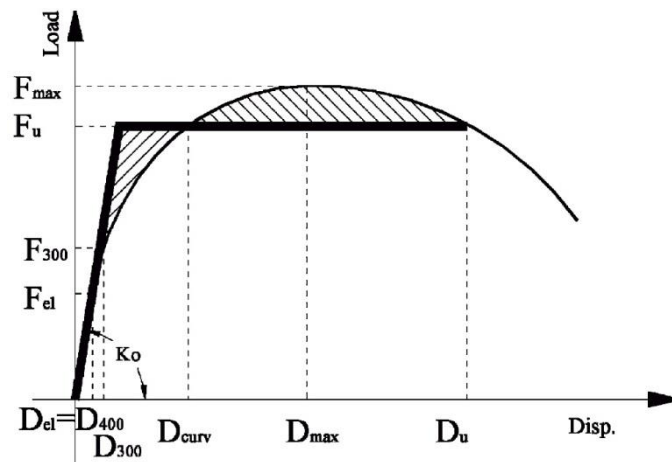
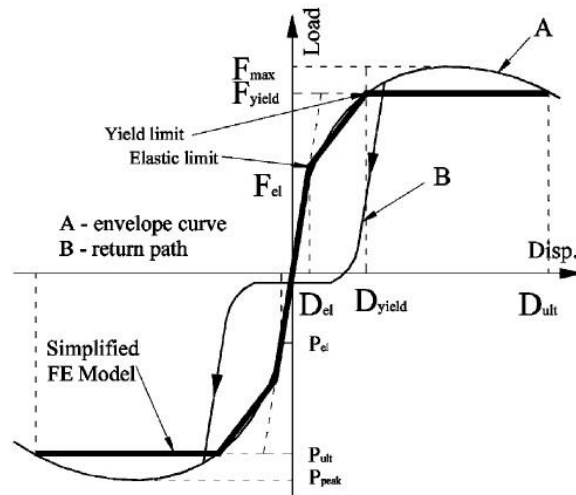


Figure 5.2. Method Developed by Kawai *et al.* (1999) to Determine the Equivalent Elasto-Plastic Model (Fülöp and Dubina, 2004a).

The initial rigidity (stiffness), K_0 , is defined as the starting portion of the behavior backbone curve and determined by the secant between the origin point and the point on the curve corresponding to the drift angle of $1/400$, D_{400} . The yield limit, F_u , is chosen in a way that the hatched parts in Figure 5.1 have the same area. D_{max} is the displacement where the force level is the maximum, F_{max} , on the curve whereas ultimate displacement, D_u , can be identified as the point where force level on the curve falls under the yield limit. The elastic force, F_{el} , and the corresponding displacement, D_{el} , are referred as minimum of the force at story drift angle $1/300$, F_{300} and $2/3 F_{max}$ and corresponding displacement, respectively. Then, the ductility, μ , is obtained by the ratio of the D_{max} to D_{el} . The Figure 5.3 summarizes these force and displacement values.

There is also another method for the evaluation of the equivalent elasto-plastic model. In accordance, initial stiffness may be determined as the secant stiffness to the load level of $0.4F_{max}$. Then, conventional elastic limit is identified as the intersection point of

the elastic line, K_0 , and the line of $0.1K_0$ rigidity, tangent to the backbone curve. Based on the conventional elastic limit, other points are evaluated by the intersections on the curve. Details of the method can be found in the by ECCS-No: 45 (1986).

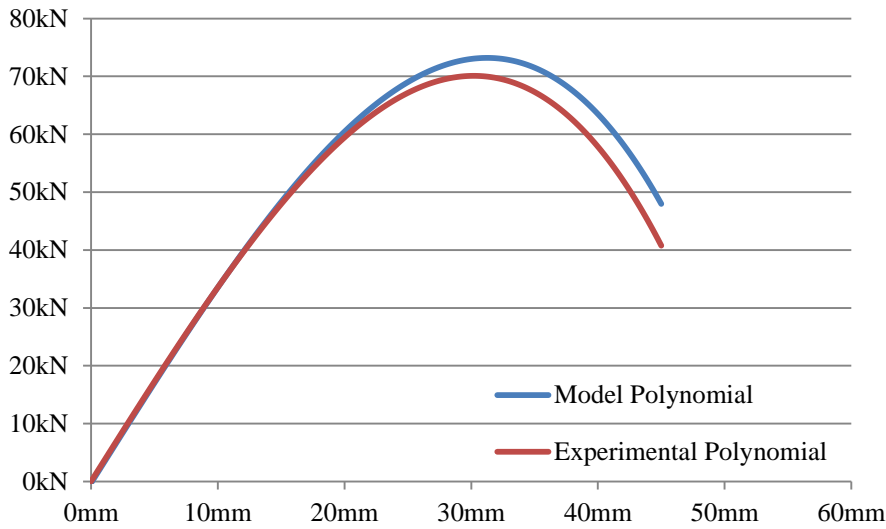


a) Tri-Linear Hysteretic Model

Figure 5.3. Tri-Linear Idealized Hysteretic Model (Fülöp and Dubina (2004b)).

Fülöp and Dubina (2004a,b) also stated that the abovementioned two methods yield to similar results. Initial rigidity values are almost the same, although two methods start to differ for the evaluation of the ultimate limit beyond the elastic behavior. In this section, the combination of these two methods is used: First, the conventional elastic limit is calculated as the secant stiffness to the load level of $0,4F_{\max}$ and then F_u is calculated based the equality of the hatched areas in Figure 5.2.

In accordance with the coefficients in Table 4.3, for each wall type both model and experimental force-displacement backbone polynomials are plotted as in Figure 5.4. It is observed that the calibrated model polynomials simulate the experimental polynomial reasonably accurate. Therefore, equating the hatched areas can be performed.



Wall Type I

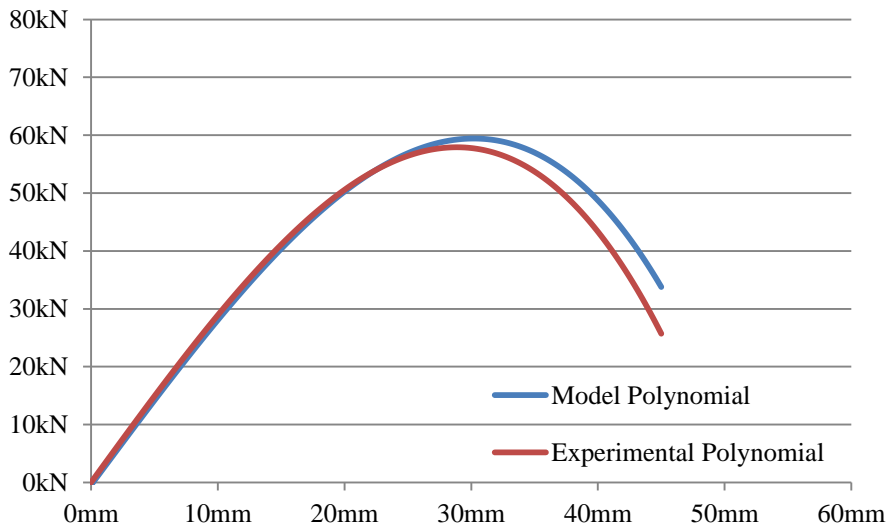
Model Poly. Coeff.

$p_1 = -9.55E-07$
 $p_2 = -1.19E-03$
 $p_3 = -2.19E-03$
 $p_4 = 3.48E+00$
 $p_5 = -2.82E-02$

Exper. Poly. Coeff.

$p_1 = 1.32E-20$
 $p_2 = -1.27E-03$
 $p_3 = -2.97E-17$
 $p_4 = 3.48E+00$
 $p_5 = 1.03E-14$

a) Model and Experimental Polynomial Curves for Wall Type I



Wall Type II

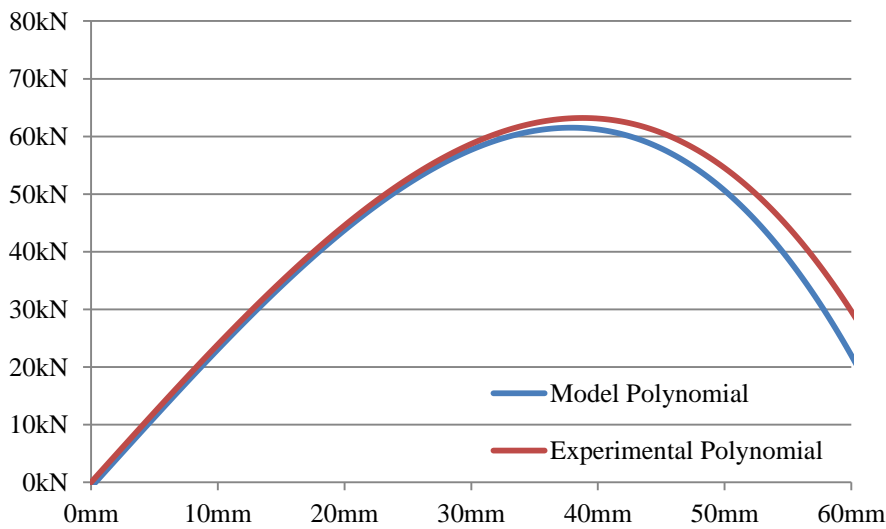
Model Poly. Coeff.

$p_1 = -5.12E-07$
 $p_2 = -1.09E-03$
 $p_3 = -1.51E-03$
 $p_4 = 2.94E+00$
 $p_5 = -4.58E-01$

Exper. Poly. Coeff.

$p_1 = -6.42E-21$
 $p_2 = -1.20E-03$
 $p_3 = 2.42E-17$
 $p_4 = 3.01E+00$
 $p_5 = -9.12E-15$

b) Model and Experimental Polynomial Curves for Wall Type II



Wall Type III

Model Poly. Coeff.

$p_1 = -3.80E-07$
 $p_2 = -5.71E-04$
 $p_3 = 1.44E-03$
 $p_4 = 2.43E+00$
 $p_5 = -8.47E-01$

Exper. Poly. Coeff.

$p_1 = 6.01E-22$
 $p_2 = -5.41E-04$
 $p_3 = -2.50E-18$
 $p_4 = 2.44E+00$
 $p_5 = -2.82E-16$

c) Model and Experimental Polynomial Curves for Wall Type III

Figure 5.4. Model and Experimental Force-Displacement Backbone Polynomial Curves.

Since the coefficients of the polynomials are known, for each displacement value, related load value can be obtainable. So, with the help of an MS Excel spreadsheet, load values are calculated for small displacement increments. After identification of maximum load on the curve, the elastic limit (F_{el} , D_{el}) is defined as load value for $0,4F_{max}$ and corresponding displacement whereas initial rigidity is noted as the load change per unit displacement increment at that point. Another advantage of dealing with polynomials is the ease of computation of the area under the curve with basic integral operations. In accordance, a force level is assumed for the yield line, then from Figure 5.2,

$$\begin{aligned} & \int_{D_{curv}}^{D_{ult}} p_1 x^n + p_2 x^{n-1} + \dots + p_n x + p_{n+1} dx - (D_{ult} - D_{curv}) x F_u = \quad (5.1) \\ & = D_{curv} x F_u - \int_0^{D_{curv}} p_1 x^n + p_2 x^{n-1} + \dots + p_n x + p_{n+1} dx - F_u^2 / 2k_0 \end{aligned}$$

to satisfy the above equation, the correct level of the yield line is achieved with some iterations. Following the identification of the elastic and yield points, other parameters are also obtained as demonstrated in Table 5.2.

Although, it seems that the model and experimental polynomial backbone curves match considerably well from Figure 5.4; Table 5.2 illustrates the behavioral difference between the polynomials and physical experiment itself.

First of all, it is found that there is an inaccuracy between the experimental polynomial curve and the exact experimental data. It is concluded that the 4th degree polynomial does not simulate the experiment well although it is the most suitable degree among other trials, when the overall shape of the curve is considered. The reason behind this inaccuracy is there is only limited data can be used to form the experimental polynomial. Model polynomial fits to the experimental polynomial very well in terms of the initial stiffness, ultimate force, etc. as it is demonstrated in Figure 5.4, however it computes initial stiffness much less than the exact value which yields to wrong values for other parameters listed in Table 5.2.

Table 5.2. The Comparison of the Calibrated Values Obtained from the Full-Scale Test and BWBN Model and Experimental Polynomials.

| Limit Points | Wall Type | | | | | | | | | | | | | | | | | |
|---------------------------------------|---------------|--------------|----------------|-------------------|-------------------|-------------------|---------------|--------------|----------------|-------------------|-------------------|-------------------|---------------|--------------|----------------|-------------------|-------------------|-------------------|
| | Wall Type I | | | | | | Wall Type II | | | | | | Wall Type III | | | | | |
| | A Model Poly. | B Exp. Poly. | C Exp. (Orig.) | A vs. B Diff. (%) | A vs. C Diff. (%) | B vs. C Diff. (%) | A Model Poly. | B Exp. Poly. | C Exp. (Orig.) | A vs. B Diff. (%) | A vs. C Diff. (%) | B vs. C Diff. (%) | A Model Poly. | B Exp. Poly. | C Exp. (Orig.) | A vs. B Diff. (%) | A vs. C Diff. (%) | B vs. C Diff. (%) |
| F_{el} (kN) | 29.279 | 28.038 | 28.942 | 4.43 | 1.16 | -3.12 | 23.772 | 23.168 | 24,086 | 2.61 | -1.31 | -3.81 | 24.605 | 25.279 | 26.566 | -2.67 | -7.38 | -4.84 |
| D_{el} (mm) | 8.600 | 8.600 | 6.890 | 0.00 | 24.82 | 24.82 | 8.400 | 8.100 | 6.990 | 3.70 | 20.17 | 15.88 | 10.600 | 10.300 | 6.900 | 2.91 | 53.62 | 49.28 |
| k_0 (kN/mm) | 3.405 | 3.260 | 4.201 | 4.43 | -18.95 | -22.39 | 2.830 | 2.860 | 3.446 | -1.06 | -17.87 | -16.99 | 2.321 | 2.454 | 3.850 | -5.42 | -39.71 | -36.26 |
| F_{yield} (kN) | 58.914 | 55.147 | 48.944 | 6.83 | 20.37 | 12.67 | 47.312 | 45.774 | 33.560 | 3.36 | 40.98 | 36.39 | 52.258 | 53.120 | 39.819 | -1.62 | 31.24 | 33.40 |
| D_{yield} (mm) | 19.200 | 17.800 | 17.490 | 7.87 | 9.78 | 1.77 | 18.100 | 17.050 | 14.950 | 6.16 | 21.07 | 14.05 | 25.000 | 25.000 | 15.580 | 0.00 | 60.46 | 60.46 |
| F_{max} (kN) | 73.198 | 70.096 | 69.844 | 4.43 | 4.80 | 0.36 | 59.429 | 57.920 | 62.584 | 2.61 | -5.04 | -7.45 | 61.513 | 63.197 | 57.430 | -2.67 | 7.11 | 10.04 |
| D_{max} (mm) | 31.300 | 30.200 | 25.320 | 3.64 | 23.62 | 19.27 | 30.200 | 28.900 | 30.540 | 4.50 | -1.11 | -5.37 | 37.900 | 38.800 | 38.240 | -2.32 | -0.89 | 1.46 |
| D_{ult} (mm) | 41.700 | 40.850 | 42.850 | 2.08 | -2.68 | -4.67 | 40.400 | 38.900 | 42.610 | 3.86 | -5.19 | -8.71 | 48.800 | 50.550 | 57.290 | -3.46 | -14.82 | -11.76 |
| geometric mean diff. for force values | | | | 5.11 | 4.85 | 2.43 | | | | 2.84 | 6.46 | 10.11 | | | | 2.26 | 11.79 | 11.76 |
| geometric mean diff. for disp. values | | | | 0.00 | 11.14 | 7.93 | | | | 4.46 | 7.04 | 10.11 | | | | 0.00 | 14.38 | 15.05 |

For all wall types investigated, experimental polynomial estimates the maximum force level, F_{max} , achieved during the experiments reasonably well (with differences less than 10 percent). The corresponding displacement at the maximum load level, D_{max} , also well replicated except Wall Type I. For Wall Type I, experimental and model polynomials match well, however they both yield to higher displacement levels of about 20%.

Since both polynomials are found to be suitable tools to obtain F_{max} , they are also good predictors for the elastic limit load level, F_{el} , since it is assumed to be the 40% of the ultimate force. This assumption is also verified for the numerical analysis. On the other hand, this situation is not valid for elastic displacement, D_{el} , which is calculated more than the exact value due to the difference in initial stiffness (it differs between 20% - 40%) values for all cases. The slope of initial portion of the curve is very similar for both polynomials, but they cannot represent the actual initial stiffness. This probably may be due to the lack of enough points to define the transition from the elastic point level (F_{el} , D_{el}) to the yield point level (F_y , D_y). The polynomial therefore cannot represent the first two lines of the tri-linear curve, instead they tend towards to have almost a single line that having an uniform slope which seems to be the average of actual stiffness values related to the first line ($0,0 - F_{el}$, D_{el}) and second line (F_{el} , $D_{el} - F_y$, D_y). When the two lines up to the yield point are broken to reduce the initial stiffness, yield force, F_y , and corresponding displacement level, D_y , are found to be much more than exact values after equating the areas above and below the equivalent-energy-elastic-plastic-curve.

For the overall performance of the polynomials are investigated, it can be readily stated that the polynomials are still good predictors for the overall behavior of the wall system and the model and experimental polynomials match reasonably well. However, main problem is to represent the original experiment with the appropriate polynomial. This can be achieved easily with flowchart explained in the beginning of the chapter, if the full data of the experiment is obtained. Thus, the problem for the computation for less initial stiffness and excess of the yield line level will be removed. The all results are demonstrated in Table 5.2 and Figure 5.5 for the comparison.

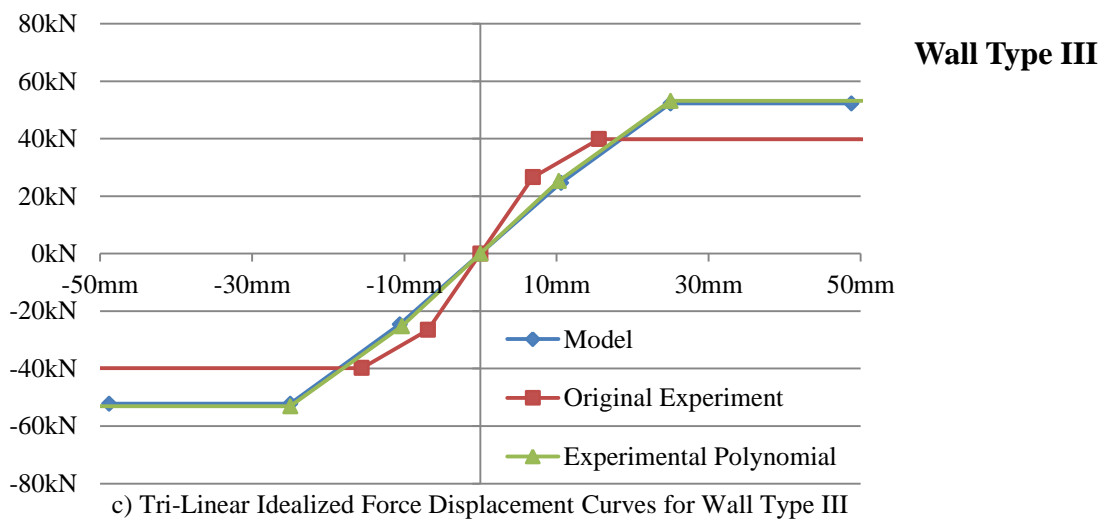
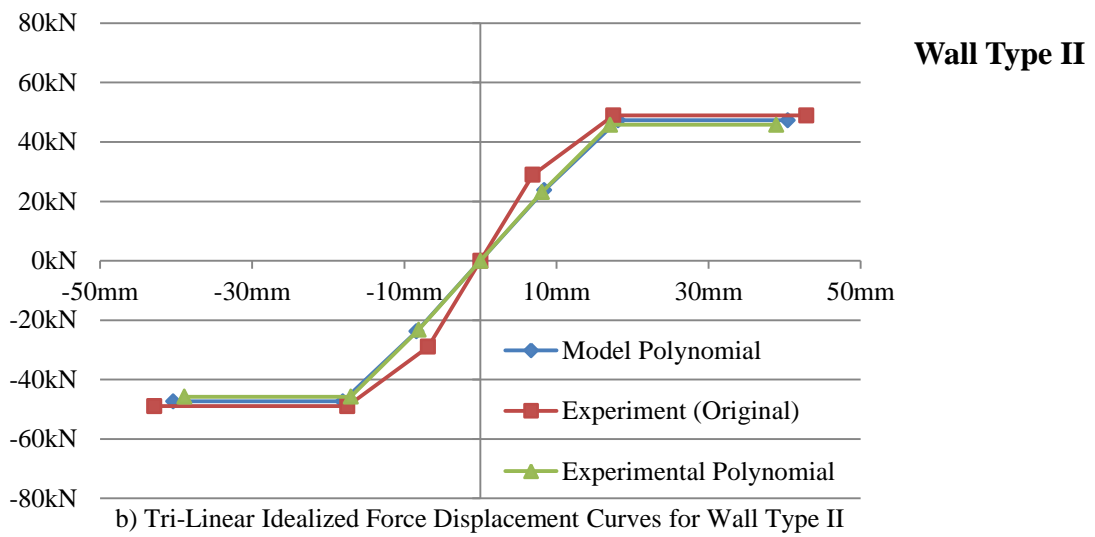
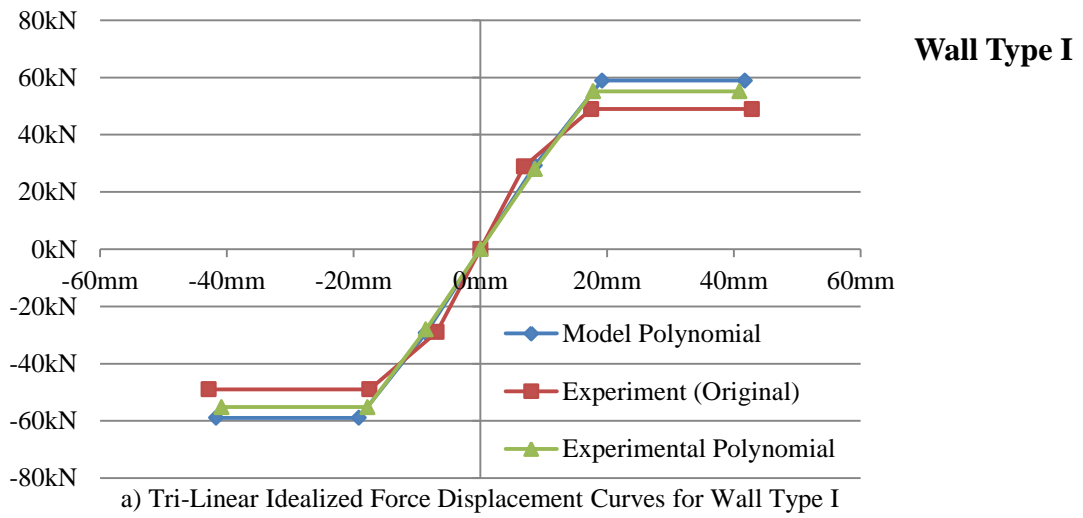


Figure 5.5. Tri-Linear Idealized Force-Displacement Curves.

5.2. Finite Element Modeling - Equivalent Bracing Model

In current engineering practice, to obtain the overall behavior of the cold-formed steel structure instead of elemental behavior, the conventional finite element analysis is commonly carried out. To conduct such an analysis, all framing members are modeled as beam-column elements and structural sheathings simulated by meshes of shell elements which can be time consuming process. Furthermore, the nonlinear behavior mostly governed by the fasteners, so an additional effort has to be made to model the fastener behavior such as with utilizing nonlinear spring elements which makes reviewing and analyzing the results becomes cumbersome and tedious due to the large number of elements involved in the model. For that reason, a simplified equivalent bracing model is used to lessen the burden associated with the use of finite element analysis for such types of buildings.

The hysteretic model should represent the actual behavior of the wall panel system under in-plane lateral loads. So, the idealized tri-linear model defined in Section 5.1 is implemented to a single-degree-of-freedom (SDOF) equivalent braced bar model in SAP2000 (2010) as demonstrated in Figure 5.6.

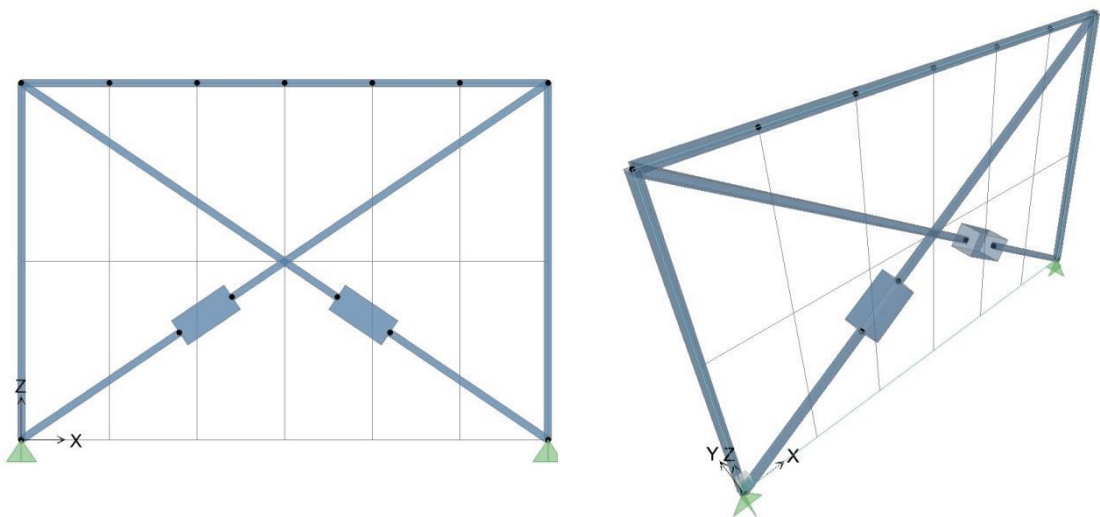


Figure 5.6. Proposed SDOF Single Unit Equivalent Braced Bar Model.

Each wall panel system is modeled with identical three frame members and two diagonal members. The main assumption for the bar model is the contribution of each individual bar member to the lateral strength of the wall system is negligible since the overall behavior of the wall system is represented by the equivalent bracings. Accordingly, the top chord of the frame is constrained by a diaphragm at the end nodes to make the bar carry no load thus experience no change in its length. All column ends are pinned to the frame to prevent their contribution to the load bearing capacity whereas the bottom chord is not included in the model since the bottom nodes are already fixed.

The response of the wall simulated with X braces. The braces are identical and their ends are released, so any moment occurs at the nodes. To satisfy the condition that only one of them carries the load depending on the direction (+ or – in global X direction), they are modeled as tension only members. Thereby, any buckling problems related to these slender members also prevented. Then the nonlinear behavior is assigned to the braces by utilizing axial hinges on members having one tenth of the brace length and four times cross-sectional area of brace itself. Thus, these stub members will not experience any change in their form when they are subjected to tensile force. The idealized tri-linear curves formed in Section 5.1 are used for the displacement control parameters defined for the hinge property following the procedure explained below.

Since, the idealized tri-linear curve is the force-displacement curve of the upper-right corner of the wall panel system; the curve should be converted into force-displacement curve of the brace member benefiting from the relation between the tip deflection and the angle between the brace and frame member at each force level on the original curve with an iterative manner. The Table 5.3 demonstrates the converted force displacement curve for each type of wall type used for the definition of the axial hinges. H and L are the original height and length of the wall specimen, respectively. F_{corner} is the load subjected to the upper-left corner of the wall and ΔL_i is the corresponding displacement value at the upper-right corner. L'_i is the new coordinate of the upper-right corner at i th step whereas D_i is the calculated value of the length of the diagonal at i th step with the assumption of height of the wall is not changed. Finally, depending on the change in the angle between the top chord and the diagonal, Θ_i , force and corresponding elongation on the braces are recorded and force-displacement curve is obtained.

Table 5.3. The Converted Axial Force-Displacement Curve Values for the Brace Members.

| H mm | L mm | F _{corner} kN | ΔL_i mm | L' _i mm | D _i mm | Θ_i | cos Θ_i | F _{bracing} kN | ΔD_i mm |
|---------------|---------|---------------------------|--------------------|-----------------------|----------------------|------------|----------------|----------------------------|--------------------|
| Wall Type I | | | | | | | | | |
| 2440 | 3600 | 0.000 | 0.00 | 3600.00 | 4348.98 | 34.13 | 0.82778 | 0.000 | 0.00 |
| 2440 | 3600 | 29.279 | 8.60 | 3608.60 | 4356.10 | 34.07 | 0.82840 | 35.344 | 7.12 |
| 2440 | 3600 | 58.914 | 19.20 | 3619.20 | 4364.88 | 33.99 | 0.82916 | 71.052 | 15.91 |
| 2440 | 3600 | 58.914 | 41.70 | 3641.70 | 4383.56 | 33.82 | 0.83076 | 70.915 | 34.58 |
| Wall Type II | | | | | | | | | |
| 2440 | 3600 | 0.000 | 0.00 | 3600.00 | 4348.98 | 34.13 | 0.82778 | 0.000 | 0.00 |
| 2440 | 3600 | 23.771 | 8.40 | 3608.40 | 4355.93 | 34.07 | 0.82839 | 28.696 | 6.96 |
| 2440 | 3600 | 47.312 | 18.10 | 3618.10 | 4363.97 | 34.00 | 0.82908 | 57.065 | 14.99 |
| 2440 | 3600 | 47.312 | 40.40 | 3640.40 | 4382.48 | 33.83 | 0.83067 | 56.956 | 33.50 |
| Wall Type III | | | | | | | | | |
| 2440 | 3600 | 0.000 | 0.00 | 3600.00 | 4348.98 | 34.13 | 0.82778 | 0.000 | 0.00 |
| 2440 | 3600 | 24.605 | 10.60 | 3610.60 | 4357.76 | 34.05 | 0.82855 | 29.697 | 8.78 |
| 2440 | 3600 | 52.258 | 25.00 | 3625.00 | 4369.69 | 33.94 | 0.82958 | 62.994 | 20.72 |
| 2440 | 3600 | 52.258 | 48.80 | 3648.80 | 4389.46 | 33.77 | 0.83126 | 62.866 | 40.48 |

5.3. Case Study

To investigate the seismic performance of a multi-story building, a three story building that is composed of different wall types (defined in previous chapters) is chosen as a case study. The structure (Figure 5.7) is formed as a panelized construction and dimensions are based on the original dimensions of the wall panels tested by Fülöp and Dubina (2004a). Thus, axis distance is fixed to 3.6 m whereas the story height is designed as 2.44 m. The shear walls are located at the corners providing that the layout of the structure to be point-symmetrical to neglect the any possible torsional effects.

It should be noted that the individual equivalent braced wall panels can be used in the multi-story structures with the following assumptions:

- (i) Each wall panel is assumed to be fully sheathed (no openings) and is perfectly anchored to the lower floor (or foundation).
- (ii) Studs and tracks are rigid and hinged to each other whereas the floors are assumed to behave as rigid diaphragms.

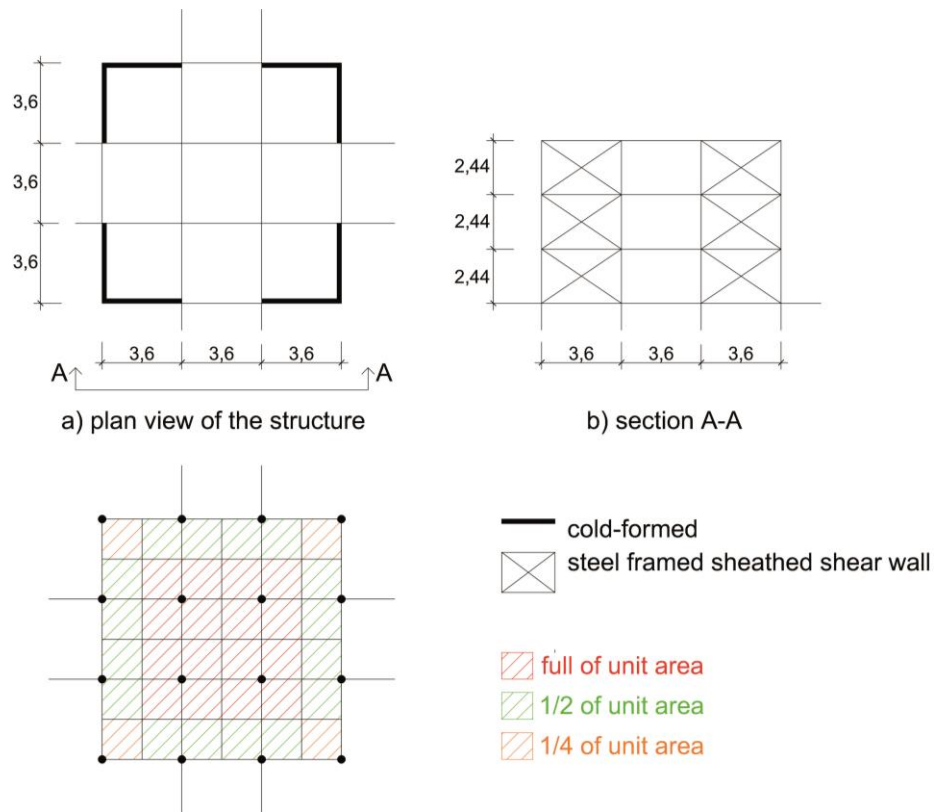


Figure 5.7. Case Study: Three-Story Building.

The unit weights of the materials (Table 5.4) used in the structure is chosen based on the study of Fiorino *et al.* (2012) and for the simplicity it is intended to fix them to the intermediate values in their intervals and applied same for all wall types. Live load is determined as 2.00 kN/m^2 whereas snow load which is participated in the seismic weight is determined as 0.75 kN/m^2 . Vertical loads distributed over the area based on the influence area of all intersections as demonstrated in Figure 5.7. Vertical point loads applied on the wall section (Figure 5.7b) is shown in Table 5.5 and Table 5.6.

For the nonlinear analysis of the structure, seismic forces subjected to the building is calculated with equivalent earthquake load method defined in TDY-07 (2007) as

$$V_t = \frac{WA(T_1)}{R_a(T_1)} \geq 0.10A_0IW \quad (5.2)$$

$$W = \sum_{i=1}^N w_i \quad (5.3)$$

$$w_i = g_i + nq_i \quad (5.4)$$

Table 5.4. Unit Weights (adapted from Fiorino *et al.*, 2012).

| Part | Explanation | Unit weight range defined by Fiorino <i>et al.</i> (2012) (kN/m ²) | Selected Value (kN/m ²) |
|----------------|----------------------|--|-------------------------------------|
| Floor and Roof | Steel Members | 0.08 - 0.25 | 0.80 for slabs and 0.85 for roof |
| | OSB Panels | 0.10 - 0.15 | |
| | GWB Panels | 0.00 - 0.10 | |
| | Insulation | 0.02 - 0.30 | |
| | Floor Finishing | 0.10 - 0.40 | |
| | False Ceiling | 0.10 - 0.30 | |
| Total | | 0.40 - 1.50 | |
| Walls | Steel Members | 0.03 - 0.08 | 0.60 for walls |
| | External Board - OSB | 0.05 - 0.20 | |
| | Insulation | 0.02 - 0.30 | |
| | External Finishing | 0.10 - 0.30 | |
| | Internal Finishing | 0.00 - 0.20 | |
| Total | | 0.30 - 1.10 | |

Table 5.5. Distribution of Vertical Loads-I.

| Story | Floors | | | Walls | | Loads | | |
|-------|---------------------------|---------------------------|------------------------|---------------------------|------------------------|-----------|-----------|-----------|
| | Slab (kN/m ²) | Roof (kN/m ²) | Area (m ²) | Wall (kN/m ²) | Area (m ²) | Dead (kN) | Live (kN) | Snow (kN) |
| 1 | 0.80 | 0.00 | 116.64 | 0.60 | 105.41 | 156.56 | 233.28 | 0.00 |
| 2 | 0.80 | 0.00 | 116.64 | 0.60 | 105.41 | 156.56 | 233.28 | 0.00 |
| 3 | 0.00 | 0.85 | 116.64 | 0.60 | 105.41 | 162.39 | 0.00 | 87.48 |
| Total | | | | | | 475.50 | 466.56 | 87.48 |

Table 5.6. Distribution of Vertical Loads-II.

| Dead (kN) | | Live (kN) | | Snow (kN) | |
|-----------|-------|-----------|-------|-----------|-------|
| outer | inner | outer | inner | outer | inner |
| 4.35 | 8.70 | 6.48 | 12.96 | 0 | 0 |
| 4.35 | 8.70 | 6.48 | 12.96 | 0 | 0 |
| 4.51 | 9.02 | 0 | 0 | 2.43 | 4.86 |

where V_t is the total base shear, W is the total weight of the structure, w_i is the weight of i th story, g_i is the total dead load on the i th story, q_i is the total live load on the i th story, n is the live load participation factor, I is the building importance factor, A_0 is the effective ground acceleration coefficient, R_a is the response modification factor, T_1 is the first modal period of the structure, and A is the spectral acceleration is calculated as (TDY-07, 2007)

$$A(T)=A_0IS(T) \quad (5.5)$$

where $S(T)$ (Figure 5.8) is the spectrum factor which is determined depending on the local soil conditions (spectrum characteristic periods T_A & T_B) and natural period of the structure, T .

$$S(T)=1+1.5\left(\frac{T}{T_A}\right) \quad 0 \leq T < T_A \quad (5.6)$$

$$S(T)=2.5 \quad T_A < T \leq T_B \quad (5.7)$$

$$S(T)=2.5 \left(\frac{T_B}{T}\right)^{0.8} \quad T_A < T \leq T_B \quad (5.8)$$

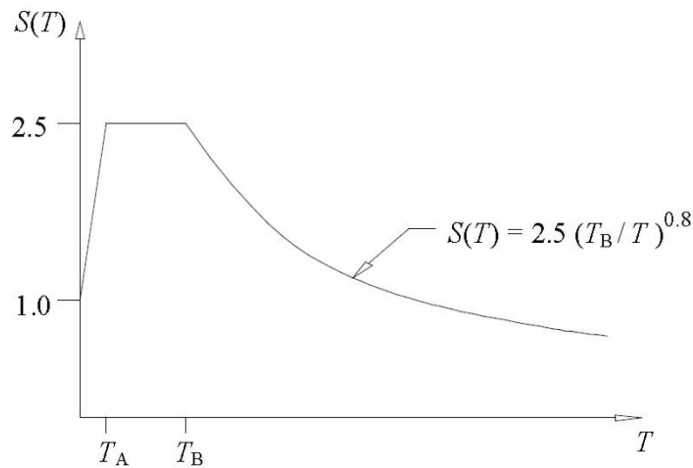


Figure 5.8. Spectrum Factor (TDY-07, 2007).

It is assumed that the soil conditions and the natural period of the structure satisfy Equation 5.7 that makes $S(T)$ equal to 2.5. The building importance factor is chosen as 1 and the structure is located on the 1st degree earthquake region with A_0 equals to 0.4. R is selected as 6.5 according to ASCE 7-05 (2006)

The earthquake forces subjected to the each floor level is calculated based on the method defined by TDY-07 (2007) as below and demonstrated in Table 5.6.

$$V_t = \Delta F_N + \sum_i^N F_i \quad (5.9)$$

$$\Delta F_N = 0.0075 N V_t \quad (5.10)$$

$$F_i = (V_t - \Delta F_n) \frac{w_i H_i}{\sum_i^N w_j H_j} \quad (5.11)$$

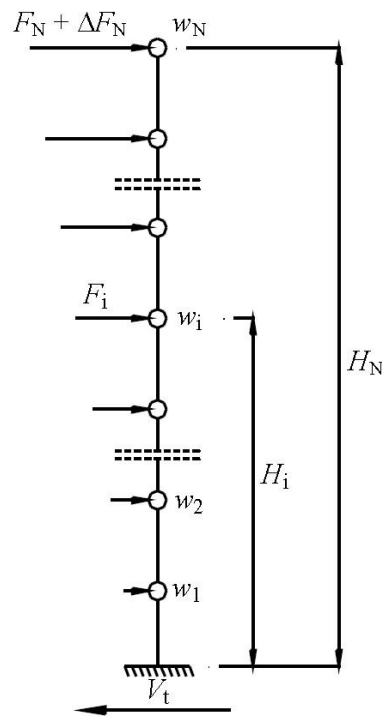


Figure 5.9. Earthquake Forces Subjected to the Each Floor Level (TDY-07, 2007).

Table 5.7. Earthquake Forces Subjected to each Floor Level

| Story | Loads | | | V_t (kN) | ΔF_N (kN) | w_i (kN) | h_i (m) | $w_i \times h_i$ | $w_i \cdot h_i / \sum w_i \cdot h_i$ | $(V_t - \Delta F_N) \times$ $(w_i \cdot h_i / \sum w_i \cdot h_i)$ | + ΔF_N (kN) | 1/2 of load subjected to each section |
|-------|--------------|---------------------|---------------------|---------------|----------------------|---------------|----------------------|------------------|--------------------------------------|---|---------------------------|---|
| | Dead (kN) | 0.3 Live (kN) | 0.3 Snow (kN) | | | | | | | | | |
| 1 | 156.56 | 69.98 | 0.00 | 98.70 | 2.2207 | 226.54 | 2.44 | 552.76 | 0.1819 | 17.55 | 17.55 | 8.77 |
| 2 | 156.56 | 69.98 | 0.00 | | | 226.54 | 4.88 | 1105.52 | 0.3638 | 35.09 | 35.09 | 17.55 |
| 3 | 162.39 | 0.00 | 26.24 | | | 188.63 | 7.32 | 1380.79 | 0.4543 | 43.83 | 46.05 | 23.03 |
| Total | | | | | | 641,71 | $\sum w_i \cdot h_i$ | 3039.07 | | | | |

Table 5.8. Relative Joint Displacements Check According to TDY-07 (2007).

| Wall Type | Force Mod. Factor, R | Story Height, h_i | Joint Disp. in +X dir. (mm) | | | Rel. Disp. btw 3rd and 2nd story (mm) | | | Rel. Disp. btw 2nd and 1st story (mm) | | | Rel. Disp. btw 1st str. and ground (mm) | | |
|-----------|----------------------|---------------------|--------------------------------|--------|--------|---|-------------------------------|---------|---|-------------------------------|---------|---|-------------------------------|---------|
| | | | Jt 85 | Jt 58 | Jt 31 | Δ_{3-2} | $\Delta_{3-2} \times R / h_i$ | < 0.02? | Δ_{2-1} | $\Delta_{2-1} \times R / h_i$ | < 0.02? | Δ_{1-0} | $\Delta_{1-0} \times R / h_i$ | < 0.02? |
| I | 6.5 | 2440 | 17.888 | 14.082 | 7.667 | 3.806 | 0.010 | ok | 6.415 | 0.017 | ok | 7.667 | 0.020 | ok |
| II | 6.5 | 2440 | 21.280 | 16.800 | 9.196 | 4.481 | 0.012 | ok | 7.603 | 0.020 | ok | 9.196 | 0.024 | no! |
| III | 6.5 | 2440 | 25.563 | 20.209 | 11.066 | 5.354 | 0.014 | ok | 9.144 | 0.024 | no! | 11.066 | 0.029 | no! |

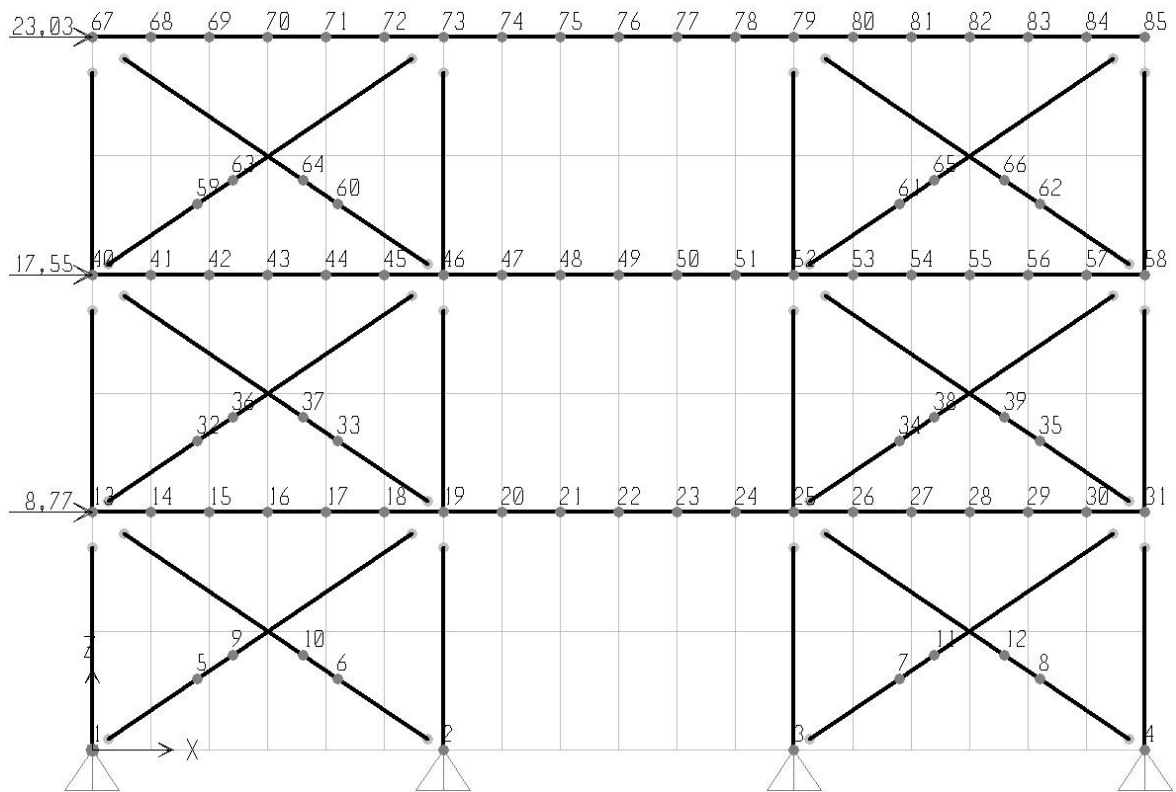
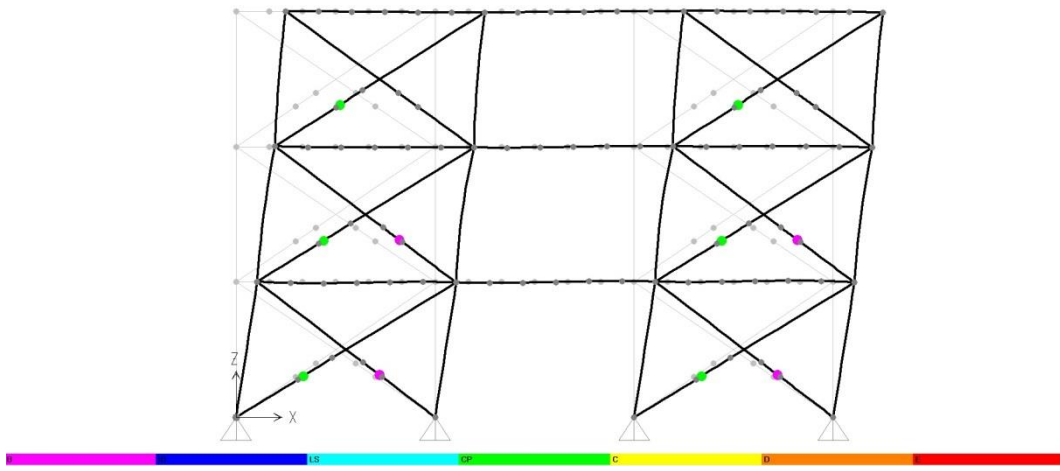


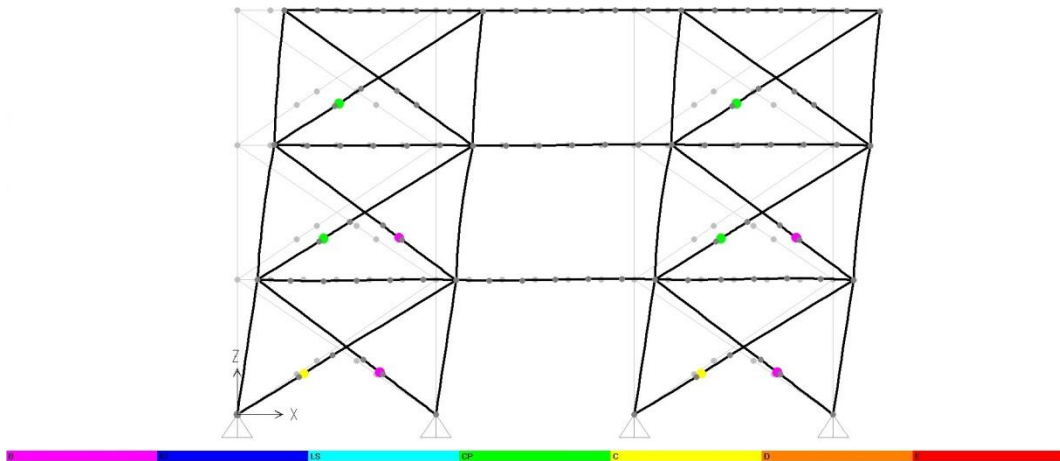
Figure 5.10. Earthquake Forces Subjected to the Structure.

Figure 5.10 demonstrates the earthquake forces subjected to the structure and the Table 5.7 summarizes the nodal displacements of joints labeled 85, 58 and 31. The table shows that if Wall Type I is used as the shear walls, the structure satisfies the relative drift check on margin whereas Wall Type II and III failed for this drift check. This situation can be also observed as a result of nonlinear analysis with SAP2000 (2010) on Figure 5.11, where CP (green) is for the collapse prevention, LS (blue) is for life safety and IO (dark blue) is for immediate occupancy. It is obvious that the equivalent bracings of first floors of WT II and WT III exceeds the acceptance criteria and become to yield (yellow).

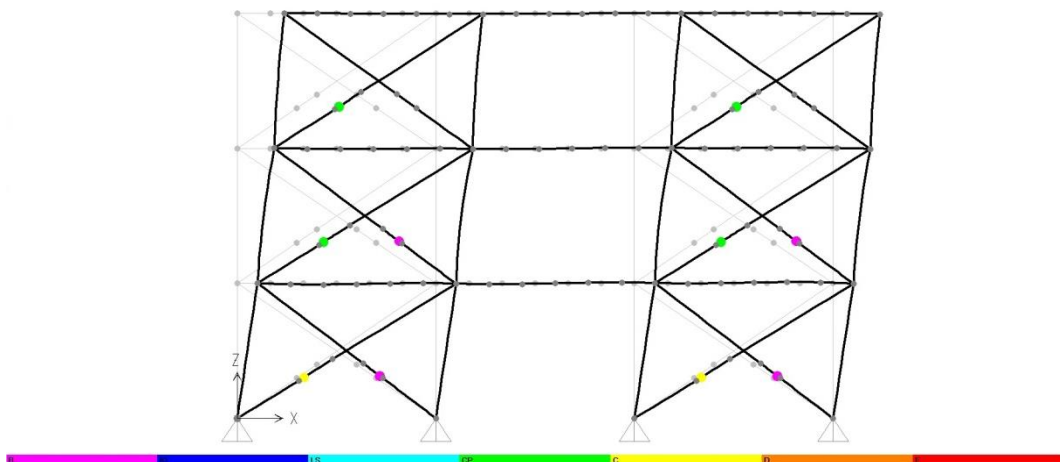
This case study shows that using equivalent bracing system in multi-story structures gives rational and consistent results. Furthermore, it provides great ease of use, once the certain points of force-displacement curves of the wall panels are assigned to the axial hinges, the lateral displacements can be obtained for even much more complex structures with great simplicity. However, this approach should be applied to more cases to check its accuracy.



a) Wall Type I



b) Wall Type II



c) Wall Type III

Figure 5.11. Nonlinear Acceptance Criteria.

6. CONCLUSION

In order to model the complex nature of the lateral performance of cold-formed steel-framed shear walls, first, current in use design codes are investigated based on the sheathing braced design. It is observed that North American codes, specifications, and manuals are more comprehensive than the other ones for the overall design of the shear wall as an assembly. Thus, based on several North American codes, a general algorithm for the design of the shear wall is formed. However, even the most recent code still cannot provide general rules for the sheathing braced design but permit the design in accordance with an appropriate theory, tests, or rational engineering analysis.

There are numerous experimental studies have been carried out by several research groups, some important ones are explained with dramatic outcomes. It is observed that the experimental studies address effects of different variables such as loading protocol and conditions, wall dimensions and aspect ratio, stud geometry and spacing, sheathing type and orientation, presence of blocking members, fastener types and schedule, anchor types and spacing, presence of hold-down devices, non-structural elements, etc. at different ages. Each study explained, or not, plays a significant role in the development and accumulation of the knowledge. On the other hand, it is observed that findings of these test results, consequently the tabulated design values, cannot be applied or extrapolated to wall assemblies in different configurations or construction details, so the application of the design tables are limited by the variation of the wall configuration tested so far.

Accordingly, numerical model studies for the prediction of the wall behavior are investigated. Among several options, a smooth hysteretic mechanical based model, Bouc-Wen-Baber-Noori (BWBN) model, is chosen for the numerical studies. It is proposed that the experimental data curve can be converted to into a 4th degree polynomial. This aim can be partly achieved due to the lack of sufficient test data provided about the selected experiment. However, the 13 parameters of BWBN model can easily be calibrated according to the experimental polynomial (it is a bit different from the actual one) and simulate it reasonably well.

It is understood that if enough number of data points on the experimental force-displacement curves are known about the experimental studies in the literature, then influence of each of the BWBN model parameters on the behavior and their variation ranges can be understood well. Thus, the model can be regarded as an alternative tool with its calibrated and generalized parameters for the simulation of the behavior. Consequently, the cost and time wasting of research can be reduced by minimizing the number of large scale shear wall tests to be carried out for every new configuration where this construction technique is new to use such as Turkey.

With the help of the BWBN model hysteretic backbone curve, the system is converted into finite elements (FE) based equivalent bracing system for the final user with the less burden associated with the use of FE analysis for the overall design of the structure. The results showed that the equivalent bracing matches well the model after the BWBN model is interpreted with the energy equivalent elastic plastic (EEEP) model. Further, with some assumptions on the inter-story relations, the model is shown to be applied on multi-story structures with different wall configurations.

Finally, the algorithm for the modeling of cold-formed steel structures with sheathed shear wall panels in seismic regions explained in this thesis can be regarded as an introductory approach and needs to be developed.

APPENDIX A: SUMMARY OF EXPERIMENTAL STUDIES

| Study | Loading | Wall Geometry | | | Sheathing and/or Bracing | |
|--|--|---|---|---------------------------------|---|-------------------------------------|
| Author / Year / Number of Tests | 1 Loading Type / Loading Protocol/ Number of Tests | 2A Dimensions, H x L | 2B Aspect Ratio, H/L | 2C Sheathing Area Rat., r | 3A Type/Thickness | 3B Configuration/ Orientation |
| | Frame Members | | | Fastener Schedule/Anchorage | | |
| | 4A Steel Grade | 4B Member Type/ Member Size/ Steel Grade | 4C Interior Stud/Exterior Stud/End Condition/Stud Spacing/Track/Horizontal Blocking | 5A Fastener Type | 5B Frame-to-Frame/ Sheathing-to-Frame/ Spacing at the perimeter/ Spacing at the field | 5C Type of Anchor. |

NOTES: (?) means present but unknown, (-) means not present; 1 - M: Monotonic; C: Cyclic / Loading protocols used throughout the experiment / Number in brackets indicates the number of wall specimen; 2A - All dimensions in mm; 2B - Number in brackets indicates the number of wall specimen; 2C - Sheathing area ratio, $r = 1/[1 + A_o/(h \sum L_i)]$ with A_o : area of the openings and L_i : length of the full height wall segment and (-) means no opening; 3A - GSB: Gypsum sheathing board; GWB: Gypsum wallboard; FBW: Fiber board wall; OSB: Oriented strand board; PLY: Plywood; SCS: Steel corrugated sheet; SSS: Steel sheet sheathing; SS: Steel Strap; CSB: Calcium Silicate Board; $_x_$: width x thickness of the strap; all dimensions in mm; number in brackets indicates the number of wall specimen; 3B - H: Horizontal placement; V: Vertical placement; 4A - Steel Grade for both studs, tracks and blocking members if available; 4B - C: lipped channel section; $_x_x_x_$: web depth x flange size x lip size x thickness or $_x_x_$: web depth x flange size x thickness in mm; U: un-lipped channel section; $_x_x_$: web depth x flange size x thickness; spacing of studs on center in mm; SS: single stud at the ends of the wall; DS: double studs (back-to-back) at the ends of the wall ; DSJ: double stud (back-to-back) at the joint of two adjacent sheathing; 4C - Number in brackets indicates the number of wall specimen; 5A - BHSC: bugle-head screws; FHSC: flat head screws; LPHSC: low profile head screws; MTHSC: modified truss head screws; WHSC: wafer head screws; PHSC: pan head screws; HHSC: hex head screws; $_x_$: nominal diameter x length in mm; NA: Nails diameter; PI: Pins diameter; 5B - Number in brackets indicates the number of wall specimen; 5C - BCA: bolted clip angles; PCA: clip angles fixed with powder actuated fasteners; HD: hold-down; SHD: strip-hold down

Table A.1. Summary of Experimental Studies.

| | | | | | | |
|-----------------------------|------------------------------|--|--|---|---|--|
| Mc Creless & Tarpay 1978 | M/ASTM E564-76 (16) | 3660x3660 3660x4880 3660x7320 3050x3660 3050x4880 3050x7320 2440x2440 2440x3660 2440x4880 2440x7320 | 1.00 (2) 0.75 (1) 0.50 (1) 0.83 (1) 0.63 (1) 0.42 (1) 1.00 (1) 0.67 (1) 0.50 (1) 0.33 (1) | 1.00 (16) | A. GWB/12.7 | A+A/? (16) |
| | G1.? | C1. 89x25x13x0.84/G1 U1. 92x38x0.84/G1 HB. ?? | C1/C1/DS/610/U1 (15) C1/C1/DS/610/U1 - HB (1) | FF1. LPHSC 4.8x13 SH1. BHSC 3.5x25 | FF1/SH1/305/305 (16) | BCA |
| Tarpay & Girard 1982 | M/ASTM E564-76 (11) | 2440x2440 2440x3660 | 1.00 (10) 0.67 (1) | 1.00 (11) | A. GWB/12.7 B. GSB/12.7 C. PLY/12.7 | A+A/H (9) A+B/H (1) A+C/H (1) |
| | G1. ASTM A36 | C1. 89x25x13x0.84/G1 U1. 92x38x0.84/G1 | C1/C1/DS/610/U1 (10) C1/C1/DS/406/U1 (1) | FF1. LPHSC 4.8x13 SH1. BHSC 3.5x25 | FF1/SH1/305/305 (11) | BCA (8) PCA (1) NO (2) |
| Tissel 1993 | M/ASTM E72-80 (8) | 2440x2440 | 1.00 (8) | 1.00 (8) | A. OSB/11.1 B. OSB/15.1 C. PLY/9.5 D. PLY/15.9 | A/V (2) B/V (2) C/V (4) D/V (1) |
| | G1.? | C1. 64x41x1.88/G1 C2. 92x41x1.50/G1 C3. 92x41x1.19/G1 U1. 64x41x1.88/G1 U2. 92x41x1.50/G1 U3. 92x42x1.19/G1 | C1/C1/SS/610/U1 (3) C2/C2/SS/610/U2 (2) C3/C3/SS/610/U3 (3) | FF1. SC ? SH1. SC 4.2 SH2. SC 4.8 SH3. PI 3.7x32 | FF1/SH1/76/305 (1) FF1/SH1/102/305 (1) FF1/SH1/152/305 (1) FF1/SH2/102/305 (3) FF1/SH3/102/305 (1) FF1/SH3/152/305 (1) | HD |
| Serrette 1994 | M/ASTM E72-80 (12) | 2440x2440 | 1.00 (12) | 1.00 (12) | A. GWB/12.7 B. OSB/11.1 C. PLY/12.7 D. XB/FL50.8x0.88 | A+A/V (1) A+A+D/V (1) B/V (4) C/H (2) C/V (3) D (1) |
| | G1. ASTM A653 SQ Grade 33 | C1. 152x41x0.84/G1 U1. 152x32x0.84/G1 HB. ?? | C1/C1/DS/610/U1 (10) C1/C1/DS/610/U1-HB (2) | ? | ? | ? |

Table A.1. Summary of Experimental Studies (*cont'd.*).

| | | | | | | |
|---------------------------------|---------------------------|---|--|---|--|--|
| Serrette & Ogunfunmi 1996 | M/ASTM E72-80 (13) | 2440x2440 | 1.00 (13) | 1.00 (13) | A - GWB/12.7 B - GSB/12.7 C - XB/FL50.8x0.88 | A+B/V (5) A+B+C/V (4) A+B+C+C/V (1) C (3) |
| | G1. ASTM A446 Grade A | C1. 152x32x0.88/G1 U1. 152x0.88/G1 | C1/C1/DS/610/U1 (13) | FF1. WHSC 4.2x13 SH1. WHSC 14x4.2x13 (C) SH2. BHSC 3,5x25 | FF1/SH1 (3) FF1/SH2/152/305 (5) FF1/SH2(C)-SH1(A+B)/152/305 (5) | BCA |
| Serrette – Monotonic 1996a,b | M (24) | 2440x2440 2440x1220 | 1.00 (10) 2.00 (14) | 1.00 (24) | A. GWB/12.7 B. OSB/11.1 C. PLY/11.9 | A+A/H (4) A+B/V (6) B/H (4) B/V (8) C/V (2) |
| | G1. ASTM A653 SQ Grade 33 | C1. 89x41x10x0.84/G1 U1. 89x32x0.84/G1 HB. FL38x0.84/G1 | C1/C1/DS/610/U1 (20) C1/C1/DS/610/U1-HB (4) | FF1. WHSC 4.2x13 SH1. FHSC 4.2x25 SH2. BHSC 3.5x32 | FF1/SH1/51/305 (3) FF1/SH1/76/305 (2) FF1/SH1/102/305 (3) FF1/SH1/152/305 (9) FF1/SH2/178/178 (5) FF1/SH2/102/102 (2) | HD |
| Serrette – Cyclic 1996a,b | C (16) | 2440x1220 | 2.00 (16) | 1.00 (16) | A. OSB/11.1 B. PLY/11.9 | A/V (8) B/V (8) |
| | G1. ASTM A653 SQ Grade 33 | C1. 89x41x10x0.84/G1 U1. 89x32x0.84/G1 | C1/C1/DS/610/U1 (16) | FF1. WHSC 4.2x13 SH1. FHSC 4.2x25 | FF1/SH1/51/305 (4) FF1/SH1/76/305 (4) FF1/SH1/102/305 (4) FF1/SH1/152/305 (4) | HD |

Table A.1. Summary of Experimental Studies (*cont'd.*).

| | | | | | | |
|-------------------------------|------------------------------|---|---|--|---|---|
| Serrette 1997a | M/ASTM E72-80 (18) | 2440x2440 | 1.00 (18) | 1.00 (18) | A. GWB/12.7 B. OSB/11.1 C. PLY/11.9 D. FBW/12.7 | A+A/H (1) A+A/V (3) A+C/V (1) B/H (1) B/V (2) C/H (2) C/V (3) D/V (3) D+D/V (2) |
| | G1. ASTM A446 Grade A | C1. 152x41x10x0.84/G1 U1. 152x25x0.84/G1 HB. FL51x0.84/G1 SB. 152x25x0.84/G1 | C1/C1/DS/610/U1 (15) C1/C1/DS/610/U1-HB-SB (3) | FF1. WHSC 4.2x13 SH1. BHSC 3.5x25 SH2. BHSC 3.5x32 SH3. BHSC 4.2x32 SH4. PI 3.7 | FF1/SH1/152/305 (7) FF1/SH2/152/305 (3) FF1/SH3/152/305/(2) FF1/SH4/152/305/(5) FF1/SH1(C)-SH4(A) /152-178/305-178 (1) | HD |
| Serrette - Monotonic 1997b | M (16) | 2440x1220 2440x610 | 2.00 (6) 4.00 (10) | 1.00 (16) | A. OSB/11.1 B. SSS/0.46 C. SSS/0.69 D. XB/FL114x0.84 E. XB/FL191x0.84 | A/V (6) B/V (4) C/V (2) D (2) E (2) |
| | G1. ASTM A653 SQ Grade 33 | C1. 89x43x13x0.84/G1 C2. 89x43x13x1.09/G1 U1. 89x32x0.84/G1 U2. 89x32x1.09/G1 | C1/C1/DS/610/U1 (14) C2/C2/DS/610/U2 (2) | FF1. MTHSC 4.2x13 SH1. MTHSC 20x4.2x13 (E) SH2. MTHSC 30x4.2x13 (F) SH3. FHSC 4.2x25 SH4. MTHSC 4.2x13 | FF1/SH1 (2) FF1/SH2 (2) FF1/SH3/51/305 (2) FF1/SH3/102/305 (2) FF1/SH3/152/305 (2) FF1/SH4/102/305 (2) FF1/SH4/152/305 (4) | HD |
| Serrette - Cyclic 1997b | C/SPD (28) | 2440x1220 2440x610 | 2.00 (18) 4.00 (10) | 1.00 (28) | A. OSB/11.1 B. PLY/11.9 C. SSS/0.46 D. SSS/0.69 E. XB/FL114x0.84 F. XB/FL191x0.84 | B/V (8) A/V (10) C/V (2) D/V (4) E (2) F (2) |
| | G1. ASTM A653 SQ Grade 33 | C1. 89x43x13x0.84/G1 C2. 89x43x13x1.09/G1 C3. 89x43x13x1.37/G1 U1. 89x32x0.84/G1 U2. 89x32x1.09/G1 U3. 89x32x1.37/G1 | C1/C1/DS/610/U1 (16) C1/C2/DS/610/U1 (8) C2/C2/DS/610/U2 (2) C3/C3/DS/610/U3 (2) | FF1. MTHSC 4.2x13 SH1. MTHSC 20x4.2x13 (E) SH2. MTHSC 30x4.2x13 (F) SH3. FHSC 4.2x25 SH4. MTHSC 4.2x13 | FF1/SH1 (2) FF1/SH2 (2) FF1/SH3/51/305 (6) FF1/SH3/76/305 (4) FF1/SH3/102/305 (2) FF1/SH3/152/305 (6) FF1/SH4/51/305 (2) FF1/SH4/102/305 (2) FF1/SH4/152/305 (2) | HD |

Table A.1. Summary of Experimental Studies (*cont'd.*).

| | | | | | | |
|--------------------------------|--|--|--------------------------|---|--|----------------------------------|
| NAHB 1997 | M/ASTM E564-95 (4) | 2440x12190 | 0.20 (4) | 1.00 (1) 0.76 (2) 0.48 (1) | A. GWB/12.7 B. OSB/11.1 | A+B/V (4) |
| | G1.Fy = 360 Mpa | C1. 89x38x0.84/G1 U1. 89x38x0.84/G1 | C1/C1/?/610/U1 (4) | FF1. SC 4.2 SH1. SC 4.2 (A) SH2. SC 3.5 (B) | FF1/SH1-SH2/152-178 /305-254 (4) | HD (3) NO HD (1) |
| Selenikovich 1999 | M (6) C/SPD acc. to SEAOSC-97(10) | 2440x12190 | 0.20 (16) | 1.00 (4) 0.76 (3) 0.56 (3) 0.48 (3) 0.30 (3) | A. GWB/12.7 B. OSB/11.1 | A+B/V (1) B/V (15) |
| | G1.? | C1. 89x38x0.84/G1 U1. 89x32x0.84/G1 | C1/C1/DS+DSO/610/U1 (16) | FF1. LPHSC 4.2x13 SH1. BHSC 4.2x49 (A) SH2. BHSC 4.2x49 (B) | FF1/SH1-SH2/178-152 /254-305 (16) | HD |
| COLA-UCI 2001 | C/TCCMAR acc. to. SEAOSC-97 (18) | 2440x2440 | 1.00 (18) | 1.00 (18) | A. OSB/11.1 B. PLY/11.9 | A/V (9) B/V (9) |
| | G1. ASTM A653 SQ Grade 33 | C1. 89x41x10x1.01/G1 U1. 89x38x1.01/G1 | C1/C1/DS/610/U1 (18) | FF1. MTHSC 4.2x13 SH1. BHSC 4.2x25 | FF1/SH1/51/305 (6) FF1/SH1/102/305 (6) FF1/SH1/152/305 (6) | HD |
| Branston <i>et.al.</i> 2003 | M (6) C (6) | 2440x2440 2440x1220 | 1.00 (6) 2.00 (6) | 1.00 (12) | A. OSB/11.1 B. PLY/11.9 | A/V (6) B/V (6) |
| | G1. ASTM A653 SQ Grade 33 | C1. 89x41x10x0.84/G1 U1. 89x38x0.84/G1 | C1/C1/DS/610/U1 (12) | FF1. WHSC 4.2x13 SH1. FHSC 4.2x25 | FF1/SH1/102/305 (6) FF1/SH1/152/305 (6) | HD |
| Branston 2004 | M/Method acc. to. Serette, 1996a (21) C/CUREE acc. to. Krawinkler et. al, 2000 (22) | 2440x1220 | 2.00 (43) | 1.00 (43) | A. OSB/11.1 B. PLY (SOFT)/12.5 C. PLY (FIR)/12.5 | A/V (18) B/V (12) C/V (13) |
| | G1. ASTM A653 Grade 230 | C1. 92x41x13x1.12/G1 U1. 92x30x1.12/G1 | C1/C1/DS/610/U1 (43) | FF1. WHSC 4.2x13 SH1. BHSC 4.2x38 | FF1/SH1/76/305 (19) FF1/SH1/102/305 (6) FF1/SH1/152/305 (18) | HD |

Table A.1. Summary of Experimental Studies (*cont'd.*).

| | | | | | | |
|----------------------------|--|---|--|--|--|-------------------------------|
| Chen 2004 | M/Method acc. to. Serette, 1996a (24) C/CUREE acc. to. Krawinkler et. al, 2000 (22) | 2440x2440 2440x610 | 1.00 (22) 4.00 (24) | 1.00 (46) | A. OSB/11.1 B. PLY (SOFT)/12.5 | A/V (12) B/V (34) |
| | G1. ASTM A653 Grade 230 | C1. 92x41x13x1.12/G1 U1. 92x30x1.12/G1 | C1/C1/DS+DSM/610/U1 (43) | FF1. WHSC 4.2x13 SH1. BHSC 4.2x38 | FF1/SH1/76/305 (7) FF1/SH1/102/305 (21) FF1/SH1/152/305 (18) | HD |
| Boudreault 2005 | M (10) C/CUREE acc. to. Krawinkler et. al, 2000 (6) C/SPD acc. to. Serette, 2002 (4) | 2440x1220 | 2.00 (20) | 1.00 (20) | A. PLY (SOFT)/12.5 B. PLY (FIR)/12.5 | A/V (13) B/V (7) |
| | G1. ASTM A653 Grade 230 | C1. 92x41x13x1.12/G1 U1. 92x32x1.12/G1 | C1/C1/DS/610/U1 (20) | FF1. WHSC 4.2x13 SH1. BHSC 4.2x38 | FF1/SH1/102/305 (20) | HD |
| Blais 2006 | M/Method acc. to. Serette, 1996a (9) C/CUREE acc. to. Krawinkler et. al, 2000 (9) | 2440x1220 | 2.00 (18) | 1.00 (18) | A. OSB/9 | A/V (18) |
| | G1. ASTM A653 Grade 230 | C1. 92x41x13x1.09/G1 U1. 92x32x1.09/G1 | C1/C1/DS/610/U1 (18) | FF1. WHSC 4.2x13 SH1. BHSC 4.2x38 | FF1/SH1/76/305 (6) FF1/SH1/102/305 (6) FF1/SH1/152/305 (6) | HD |
| Al-Kharat & Rogers 2007 | M/2.5 mm/min (9) C/CUREE acc. to. Krawinkler et. al, 2000 (7) | 2440x2440 | 1.00 (16) | 1.00 (16) | A. XB (G1)/FL58.4x1.22 B. XB (G1)/FL101x1.52 C. XB (G1)/FL152x1.91 | A+A (6) B+B (6) C+C (4) |
| | G1. ASTM A653 Grade 230 G1. ASTM A653 Grade 345 | C1. 92x41x13x1.22/G1 C2. 152x41x13x1.22/G1 C3. 152x41x13x1.52/G2 C4. 152x41x13x1.91/G2 U1. 92x32x1.22/G1 U2. 152x32x1.52/G2 U3. 152x32x1.91/G2 HB. 38x13x1.22/G1 | C1/C1/DS/406/U1-HB (6) C2/C3/DS/406/U2-HB (6) C2/C4/DS/406/U3-HB (4) | FF1. WHSC 4.2x? SH1. WHSC 10x4.2x? SH2. 3mm fillet weld (strap-to-gusset-to-stud/track) | FF1/SH1 (6) FF1/SH2 (10) | HD |

Table A.1. Summary of Experimental Studies (*cont'd.*).

| | | | | | | |
|----------------------------|---|--|--|--|---|----------------------------------|
| Yu 2007 | M/ASTM E564-06 (30) C/CUREE acc. to ICC-ES AC130-04 (30) | 2440x1220 2440x610 | 2.00 (36) 4.00 (24) | 1.00 (60) | A. SSS (G1)/0.838 B. SSS (G1)/0.762 C. SSS (G1)/0.686 | A/V (24) B/V (24) C/V (12) |
| | G1. ASTM A1003 Grade 33 | C1. 89x41x1.09/G1 C2. 89x41x0.84/G1 U1. 89x38x1.09/G1 U2. 89x38x0.84/G1 | C1/C1/DS/610/U1 (48) C2/C2/DS/610/U2 (12) | FF1. MTHSC 4.2x13 SH1. MTHSC 4.2x13 | FF1/SH1/51/305 (20) FF1/SH1/102/305 (20) FF1/SH1/152/305 (20) | 1 x HD (M) 2 x HD (C) |
| Comeau 2008 | M/2.5 mm/min (20) C/CUREE acc. to. Krawinkler et. al, 2000 (10) | 2440x2440 2440x1220 2440x610 | 1.00 (18) 2.00 (6) 4.00 (6) | 1.00 (30) | A. XB (G1)/FL63.5x1.09 B. XB (G2)/FL69.9x1.37 C. XB (G2)/FL101.6x1.73 | A+A (9) B+B (9) C+C (12) |
| | G1. ASTM A1003 Grade 33 G2. ASTM A1003 Grade 50 | C1. 92x41x13x1.09/G1 C2. 152x41x13x1.09/G1 C3. 152x41x13x1.37/G2 C4. 152x41x13x1.73/ G2 U1. 92x32x1.09/G1 U2. 92x32x1.37/G2 U3. 152x32x1.37/G2 U4. 152x32x1.73/G2 U5. 152x32x2.46/G2 | C1/C1/DS/406/U1-SB (3) C1/C1/DS/406/U2-SB (6) C2/C3/DS/406/U3-SB (3) C2/C3/DS/305/U3-SB (3) C2/C3/DS/406/U4-SB (3) C2/C4/DS/406/U4-SB (6) C2/C4/DS/305/U4-SB (3) C2/C4/DS/406/U5-SB (3) | FF1. MTHSC 4.2x13 SH1. MTHSC 4.2x13 (strap-to-interior studs) (in one direction sharp only) SH2. 3mm fillet weld (strap-to-gusset-to- stud/track) | FF1/SH1-SH2 (30) | HD |
| Yu & Chen - Task 1 2009 | M/ASTM E564-06 (7) C/SPD acc. to. Serette, 1997 (1) C/CUREE acc. to method C ASTM 2126-07 (6) | 2440x1220 2440x610 | 2.00 (4) 4.00 (10) | 1.00 (14) | A. SSS (G1)/0.686 B. SSS (G1)/0.457 | A/V (10) B/V (4) |
| | G1 ASTM A1003 Grade 33 | C1. 89x41x0.84 U1. 89x38x0.84 | C1/C1/DS/610/U1 (14) | FF1. MTHSC 4.2x13 SH1. MTHSC 4.2x13 | FF1/SH1/51/305 (6) FF1/SH1/152/305 (8) | 1 x HD (M) 2 x HD (C) |

Table A.1. Summary of Experimental Studies (*cont'd.*).

| | | | | | | | |
|----------------------------|---|--|--|---|-----------|---|--|
| Yu & Chen - Task 2 2009 | M/ASTM E564-06 (6) C/ ISO acc. to. ASTM E2126-07 (17) | 2440x1830 2440x1220 2440x610 | 1.33 (19) 2.00 (2) 4.00 (2) | | 1.00 (23) | A. SSS (G1)/0.838 B. SSS (G1)/0.762 C. SSS (G1)/0.686 | A/V (16) B/V (5) C/V (2) |
| | G1. ASTM A1003 Grade 33 G2. ASTM A1003 Grade 50 | C1. 89x41x1.09/G1 C2. 89x41x1.37/G2 C3. 152x41x1.09/G1 U1. 89x38x1.09/G1 U2. 89x38x1.37/G2 U3. 152x32x1.09/G1 | C1/C1/DS/610/U1 (14) C2/C2/DS/610/U2 (3) C3/C3/DS/610/U3 (6) | FF1. MTHSC 4.2x13 SH1. MTHSC 4.2x13 SH2. MTHSC 4.8x19 | | FF1/SH1/51/305 (5) FF1/SH2/51/305 (18) | 1 x HD (M) 2 x HD (C) |
| Morello 2009 | M/7.5 mm/min Method acc. to. Serette, 1997 (4) C/CUREE acc. to. Krawinkler et. al, 2000 (4) | 2440x1220 | 2.00 (8) | | 1.00 (8) | A. GWB (C CORE)/12.7 B. GWB (REGULAR)/12.7 | A/V (6) B/V (2) |
| | G1. ASTM A653 Grade 230 | C1. 92x41x13x1.09/G1 U1. 92x32x1.09/G1 | C1/C1/DS/610/U1 (8) | FF1. WHSC 4.2x13 SH1. BHSC 3.5x25 | | FF1/SH1/100/300 (2) FF1/SH2/150/300 (4) FF1/SH2/200/300 (2) | HD |
| Velchev 2009 | M/2.5 mm/min Method acc. to. Al-Kharat & Rogers, 2007 (18) C/CUREE acc. to. Krawinkler et. al, 2000 (12) | 2440x2440 | 1.00 (30) | | 1.00 (30) | A. XB (G1)/FL95-64x1.09 B. XB (G1)/FL127x1.09 C. XB (G2)/FL108-70x1.37 D. XB (G2)/FL152- 102x1.91 | A+A (10) B+B (1) C+C (7) D+D (12) |
| | G1. ASTM A1003 Grade 33 G2. ASTM A1003 Grade 50 | C1. 92x41x13x1.09/G1 C2. 152x41x13x1.09/G1 C3. 152x41x13x1.37/G2 C4. 152x41x13x1.73/ G2 U1. 92x32x1.09/G1 U2. 152x32x1.37/G2 U3. 152x32x1.73/G2 HB. 38x13x1.09/G1 | C1/C1/DS/406/U1-HB (10) C2/C3/DS/406/U2-HB (8) C2/C4/DS/406/U3-HB (12) | FF1. WHSC 4.2x13 SH1. WHSC 4.8x19 | | FF1/SH1 (30) | HD |

Table A.1. Summary of Experimental Studies (*cont'd.*).

| | | | | | | |
|--------------------------|---|--|---|--------------------------------------|--|---|
| Moghimi & Ronagh 2009 | C/Method B acc. to. ASTM E2126-05 (20) | 2400x2400 | 1.00 (20) | 1.00 (20) | A. GWB/10 B. XB (G2)/FL 30x0.84 (solid) C. XB (G3) /FL 30x0.84 (perforated) | A/H (1) A+XB/H (2) XB (14) XB+XB (3) |
| | G1. G550 acc. to. AS 1397:2011 G2. G300 acc. to. AS 1397:2011 G3. G200 acc. to. AS 1397:2011 | C1. 90x35x6x0.75/G1 U1. 90x35x6x0.75/G1 HB. 90x35x6x0.75/G1 BR. 90x35x6x0.75/G1 | C1/C1/SS/600/U1-HB (6) C1/C1/SS/600/U1-HB-BR (3) C1/C1/DS/600/U1-HB (6) C1/C1/DS/600/U1-HB-BR (2) C1/C1/SS-DS/600/U1-HB (1) | FF1. RV ? SH1. SC 4x4.8x? | FF1/SH1 | HD |
| Balh 2010 | M/ 2.5 mm/min Method acc. to. Serette, 1997 (35) C/CUREE acc. to. Krawinkler et. al, 2000 (19) | 2440x2440 2440x1830 2440x1220 2440x610 | 1.00 (4) 1.33 (3) 2.00 (37) 4.00 (10) | 1.00 (54) | A. SSS (G1)/0.762 B. SSS (G1)/0.457 | A/V (37) B/V (17) |
| | G1. ASTM A653 Grade 33 | C1. 92x41x13x0.84 C2. 92x41x13x1.09 U1. 92x32x0.84 U2. 92x32x1.09 | C1/C1/DS/610/U1 (11) C2/C2/DS/610/U2 (43) | FF1. WHSC 4.2x13 SH1. PHSC 4.2x19 | FF1/SH1/51/305 (19) FF1/SH1/76/305 (1) FF1/SH1/102/305 (18) FF1/SH1/152/305 (14) FF1/SH1/various/305 (2) | HD |

APPENDIX B: MATLAB CODES FOR BWBN MODEL

MATLAB Code for Loading Protocol - Input Velocity

```
%loading protocol-input velocity

function y=loadprotocol(c,del)

c=c/(2*pi);

%del represents the conventional elastic limit displacement
%c represents the number of cycles

if(c>=0 && c<=4)
    y=0.25*ceil(c)*del*cos(c*2*pi);
elseif(c>4 && c<=22)
    y=2*ceil((c-4)/3)*del*cos(c*2*pi);
end
```

MATLAB Code for Quasi-Static Bouc-Wen-Baber-Noori Equations

```
%quasi-static Bouc-Wen-Baber-Noori equations
%determination of global and hysteretic displacement values, u
and z; and absorbed hysteretic energy, eps

function yp = QSBWBN(c,y)

%initial stiffness
k=4.1973;

%BWBN model parameters
%hysteresis parameters
A=1;
alfa=0.0505;
beta=0.01;
gamma=0.1;
n=1;
%degradation parameters
sv=0.0006;
sn=0.00021;
%pinching parameters
ss=0.9;
p=0.01;
```

```

q=0.0002;
fi=0.018;
sfi=0.00001;
lambda=62.8;

%strength and stiffness degradation functions, respectively
ve=1+sv*y(3);
ne=1+sn*y(3);

%pinching functions control the progress of pinching
s1=ss*(1-(exp(-p*y(3))));
s2=(fi+sfi*y(3))*(lambda+s1);

%ultimate hysteretic displacement
zult=(A/((1+sv*y(3))*(beta+gamma)))^(1/n);

%y(1)=u
%y(2)=z
%y(3)=eps

yp=zeros(3,1);

%first-order nonlinear stiff-set of ODEs
yp(1)=loadprotocol(c,6.89);
yp(2)=(1-s1*exp(-(y(2)*sign(yp(1))-
q*zult)^2)/((s2)^2))* (A*yp(1)-
ve*(beta*abs(yp(1))*(abs(y(2))^n-
1)*y(2)+gamma*yp(1)*(abs(y(2))^n)))/ne);
yp(3)=(1-alfa)*k*y(2)*yp(1);

```

MATLAB Code for the Model Polynomial Curve with the Minimized Error

```

%solution of the quasi-static Bouc-Wen-Baber-Noori equations
%determination of model and experimental polynomial curves
and error between the ploynomials

%experimental data
load experimentalvalues.txt;

%timespan of the experiment
tspan=[0 81.64];

%initial conditions
y0=[0;0;0];

%initial stiffness
k=4.1973;

```

```

%BWBN model parameters
%hysteresis parameters
A=1;
alfa=0.0505;
beta=0.01;
gamma=0.1;
n=1;
%degredation parameters
sv=0.0006;
sn=0.00021;
%pinching parameters
ss=0.9;
p=0.01;
q=0.0002;
fi=0.018;
sfi=0.00001;
lambda=62.8;

%integration of quasi-static BWBN
[t,y]=ode23('QSBWBN',tspan,y0);

%the equation of motion of quasi-static BWBN
for i=1:1:length(y)
    f(i)=alfa*k*y(i,1)+((1-alfa)*k*y(i,2));
end

%plot of load vs displacement curve
plot(y(:,1),f(:))
xlim = get(gca,'xlim');
ylim = get(gca,'ylim');
hold on

%labels on x and y axis
xlabel('u, Displacement (mm)', 'FontName', 'Times New
Roman', 'FontSize', 12);
ylabel('F, Load (kN)', 'FontName', 'Times New
Roman', 'FontSize', 12);

%x=0 and y=0 axis on the plot
plot([xlim(1) xlim(2)], [0 0], 'k')
hold on
plot([0 0], [ylim(1) ylim(2)], 'k')
hold on

%legend for the BWBN model parameters
txstr(1)=[ 'A=', num2str(A) ];
txstr(2)=[ 'alfa=', num2str(alfa) ];
txstr(3)=[ 'beta=', num2str(beta) ];
txstr(4)=[ 'gamma=', num2str(gamma) ];
txstr(5)=[ 'n=', num2str(n) ];

```

```

txstr(6)={'sv=',num2str(sv)};
txstr(7)={'sn=',num2str(sn)};
txstr(8)={'ss=',num2str(ss)};
txstr(9)={'p=',num2str(p)};
txstr(10)={'q=',num2str(q)};
txstr(11)={'fi=',num2str(fi)};
txstr(12)={'sfi=',num2str(sfi)};
txstr(13)={'lambda=',num2str(lambda)};

text(-
40,37,txstr,'HorizontalAlignment','Left','EdgeColor','w','FontName','Times New Roman','FontSize',10)

%determination of local extremas
%bb represents peak and dip points should exist on the
backbone curve
[peaks location_p]=findpeaks(f);
[dips location_d]=findpeaks(f.*-1);
bb=[0 0; y(location_p,1) transpose(peaks); y(location_d,1)
transpose(dips.*-1)];

%determination of model and experimental polynomial curve
coefficients
%p_mod represents model curve coefficients
%p_exp represents experimental curve coefficients
p_mod=polyfit(bb(:,1),bb(:,2),4);
p_exp=polyfit(experimentalvalues(:,1),experimentalvalues(:,2)
,4);

%determination of model and experimental f values obtained
from polynomial
%function
%mod_f represents model f values in the displacement range
%exp_f represents experimental f values in the displacement
range
mod_f=polyval(p_mod, (xlim(1):0.01:xlim(2)));
exp_f=polyval(p_exp, (xlim(1):0.01:xlim(2)));

%plot of model and experimantal backbone curves
mod_plot=plot((xlim(1):0.01:xlim(2)),mod_f,
'Color','r','LineWidth',2);
hold on
exp_plot=plot((xlim(1):0.01:xlim(2)),exp_f,
'Color','g','LineWidth',2);
hold on

%legend for the backbone curves
legend([mod_plot,exp_plot],'Model','Experiment','Location','Southeast');
set(gca,'FontName','Times New Roman','FontSize',10);

```


REFERENCES

AISI Lateral, 2004, *Standard for Cold-Formed Steel Framing - Lateral Design*, 2004 Edition, American Iron and Steel Institute (AISI), Washington, DC.

AISI Research Report RP07-3, 2007, *Steel Sheet Sheathing Options for Cold-Formed Steel-framed Shear Wall Assemblies Providing Shear Resistance*, American Iron and Steel Institute (AISI), Washington, DC.

AISI Research Report RP09-2, 2009, *Steel Sheet Sheathing Options for Cold-Formed Steel-framed Shear Wall Assemblies Providing Shear Resistance - Phase 2*, American Iron and Steel Institute (AISI), Washington, DC.

AISI S100-07, 2007, *North American Specification for the Design of Cold-Formed Steel Structural Members*, 2007 Edition, American Iron and Steel Institute (AISI), Washington, DC.

AISI S200-07, 2007, *Standard for Cold-Formed Steel Framing - General Provision*, 2007 Edition, American Iron and Steel Institute (AISI), Washington, DC.

AISI S211-07, 2007, *North American Standard for Cold-Formed Steel Framing - Wall Stud Design*, 2007 Edition, American Iron and Steel Institute (AISI), Washington, DC.

AISI S213-07-S1-09, 2009, *North American Standard for Cold-Formed Steel Framing - Lateral Design*, 2007 Edition with Supplement 1, American Iron and Steel Institute (AISI), Washington, DC.

AISI 1996 Specification, 1996, *Specification for the Design of Cold-Formed Steel Structural Members*, 1996 Edition, American Iron and Steel Institute (AISI), Washington, DC.

Allen, D., 2006, *History of Cold Formed Steel*, Structure Magazine, November (2006), pp. 28-32.

APA, 1999, *Wood Design Concepts Form No: X305 - Introduction Lateral Design*, the Engineered Wood Association, Tacoma - Washington.

APA, 2011, *Performance Rated Panels - Product Guide Form No: F405M*, the Engineered Wood Association, Tacoma – Washington.

Aoki, H. and K., Ikeda, 2006, “Hysteresis Model of Low-Rise Steel-Frame Building and Its Seismic Performance”, *Steel Structures*, Vol. 6, pp. 327-336.

ASCE 7-05, 2006, *Minimum Design Loads for Buildings and Other Structures*, 2006 Edition, American Society of Civil Engineers (ASCE), Virginia.

ASTM C1513, 2004, *Standard Specification for Steel Tapping Screws for Cold-Formed Steel Framing Connections*, American Society for Testing and Materials (ASTM), Pennsylvania.

Baber, T.T. and Noori, M.N., 1986, “Modeling General Hysteresis Behavior and Random Vibration Application”, *Journal of Vibration, Acoustics, Stress and Reliability in Design*, ASME, Vol. 108, pp. 411-420.

Baber, T.T. and Wen, Y.K., 1981, “Random Vibration of Hysteretic Degrading Systems”, *Journal of the Engineering Mechanics Division*, ASCE, Vol. 107, pp.1069-1089.

Bogacki, P. and Shampine, L. F., 1989, "A 3(2) pair of Runge-Kutta formulas," *Applied Mathematics Letters*, Vol. 2, pp. 321–325.

Bouc, R., 1967, “Forced Vibration of Mechanical Systems with Hysteresis”, *Proceeding of the Fourth Conference on Nonlinear Oscillation*, Prague, Czechoslovakia.

Boudreault, F.A., 2005, *Seismic Analysis of Steel Frame/Wood Panel Shear Walls*, Master's Thesis, Department of Civil Engineering and Applied Mechanics, McGill University, Montreal, QC, Canada.

Boyce, W.E. and C., DiPrima, 2000, *Elementary Differential Equations and Boundary Value Problems*, Seventh Edition, John Wiley & Sons, Inc., New York.

Branston, A.E., 2004, *Development of a Design Methodology for Steel Frame/Wood Panel Shear Walls*, Master's Thesis, Department of Civil Engineering and Applied Mechanics, McGill University, Montreal, QC, Canada.

Brockenbrough, R.L. and Merritt F.S., 1999, *Structural Steel Designer Handbook*, Third Edition, McGraw-Hill, New York.

CFSEI TN F102, 2011, *Technical Note F102-11 - Screw Fastener Selection for Cold-Formed Steel Frame Construction*, Cold-Formed Steel Engineers Institute (CFESI), Washington DC.

Chen, C.Y., 2004, *Testing and Performance of Steel Frame / Wood Panel Shear Walls*, Master's Thesis, Department of Civil Engineering and Applied Mechanics, McGill University, Montreal, QC, Canada.

TDY-07, 2007, *Turkish Earthquake Resistant Design Code*, 2007 Edition, Türk Standartları Enstitüsü (TSE), Ankara.

Dolan, J.D., S., Vagh, W.S. and Easterling, 2000, *Effect of Anchorage and Sheathing Configuration on the Cyclic Response of Long Steel-Frame Shear Walls*. Report No: TE-2000-002, Virginia Polytechnic Institute and State University, Blacksburg, Virginia.

Drain 3DX, 1994, *Version 1.10 - Base Program Description and User Guide*, Department of Civil Engineering, University of California at Berkeley, California.

Dubina, D., 2008, "Behavior and Performance of Cold-Formed Steel-Framed Houses under Seismic Action", *Journal of Constructional Steel Research*, Vol. 64, pp. 896-913.

ECCS-No: 45, 1986, *No: 45 - Recommended Testing Procedure for Assessing the Behavior of Structural Steel Elements under Cyclic Loads*, European Convention for Constructional Steelwork, Brussels.

Ellis, J., 2008, "the New CFSEI Shear Wall Design Guide", *NCSEA Conference*, Cleveland, 23.11.2008, Structural Engineers Association of Ohio (SEAOO).

Ellis, J., 2012, "Designing Cold-Formed Steel-Framed Lateral Force Resisting Systems", *Structure Magazine*, August (2012), pp. 12-15.

EN.1993.1.3, 2006, *Eurocode 3 - Design of Steel Structures - Part 1-3: General Rules - Supplementary Rules for Cold-formed Members and Sheeting*, European Committee for Standardization (CEN), Brussels.

Erdemir, 2013, *Erdemir Ürün Katalağı*, 2013 Edition, Erdemir Demir Çelik A.Ş, Ankara.

Faherty, K.F. and T.G., Williamson, 1999, *Wood Engineering and Construction Handbook*, Third Edition, McGraw-Hill, New York.

Fiorino, L., 2003, *Seismic Behavior of Sheathed Cold-Formed Steel Stud Shear Walls: An Experimental Investigation*, Ph.D. Thesis, the University of Naples Federico II, Italy.

Fiorino, L., G., Della Corte, and R., Landolfo, 2007, "Experimental Tests on Typical Screw Connections for Cold-Formed Steel Housing", *Engineering Structures*, Vol. 29, pp. 1761-1773.

Fiorino, L., O., Iuorio, R., Landolfo, 2012, "Seismic Analysis of Sheathing-Braced Cold-Formed Steel Structures" *Engineering Structures*, Vol. 34, pp. 538-547.

Foliente, G.C., 1993, *Stochastic Dynamic Response of Wood Structural Systems*, Ph.D. Thesis, Virginia Polytechnic Institute and State University, Blacksburg, Virginia.

Fülöp, L.A. and D., Dubina, 2004a, “Performance of Wall-Stud Cold-Formed Shear Panels under Monotonic and Cyclic Loading - Part I: Experimental Research”, *Thin-Walled Structures*, Vol. 42, pp.321-338.

Fülöp, L.A. and D., Dubina, 2004b, “Performance of Wall-Stud Cold-Formed Shear Panels under Monotonic and Cyclic Loading - Part II: Numerical Modeling and Performance Analysis”, *Thin-Walled Structures*, Vol. 42, pp.339-349.

Gypsum Association, 2013, *Gypsum Board Construction*, <http://www.gypsum.org>.

Kawai, Y., R., Kanno, N., Uno and Y., Sakumoto, 1999, “Seismic Resistance and Design of Steel-Framed Houses”, *Nippon Steel Technical Report*, No: 79.

Klippstein, K.H., and T.S., Tarpy, 1992, *Research Report CF92-2: Shear Resistance of Walls with Steel Studs*, Committee on Specifications for the Design of Cold-Formed Steel Structural Members, American Iron and Steel Institute (AISI), Washington DC.

LaBoube, A.R. and J.W., Larson, 2006, “Removing the Guesswork” *Structure Magazine*, August (2006), pp. 16-18.

Ibarra, L.F., R.A., Medina and H., Krawinkler, 2005, “Hysteretic Models that Incorporate Strength and Stiffness Deterioration”, *Earthquake Engineering and Structural Dynamics*, Vol. 34, pp. 1489-1511.

IBC2000, 2000, International Building Code, 2000 Edition, International Code Council (ICC), Illinois.

IBC2003, 2003, International Building Code, 2003 Edition, International Code Council (ICC), Illinois.

IBC2006, 2006, International Building Code, 2006 Edition, International Code Council (ICC), Illinois.

IBC2012, 2012, International Building Code, 2012 Edition, International Code Council (ICC), Illinois.

MATLAB, 2008, *MATLAB (Version 7.7 - R2008b) - The Language of Technical Computing*, MathWorks, Massachusetts.

Martinez, M.J. and L., Xu, 2011, "Simplified Nonlinear Finite Element Analysis of Buildings with CFS Shear Panels", *Journal of Constructional Steel Research*, Vol. 67, pp.565-575.

McCreless, S. and T.S., Tarpy, 1978, "Experimental Investigation of Steel Stud Shear Wall Diaphragms", *In Proceedings of the 4th International Specialty Conference on Cold-Formed Steel Structures*, St. Louis, Missouri, USA, pp. 647-672.

Mostaghel, N., 1999, "Analytical Description of Pinching Degrading Hysteretic Systems", *Journal of Engineering Mechanics*, American Society of Civil Engineers (ASCE), Vol. 125, pp.216-224.

NAHB Research Center, 1997, *Monotonic Tests of Cold-Formed Steel Shear Walls with Openings*, National Association of Home Builders (NAHB), Upper Marlboro, Maryland, USA.

NBCC, 1995, *National Building Code of Canada*, 1995 Edition, Institute for Research in Construction (IRC) - National Research Council of Canada (NRCC), Ottawa, Canada.

Nithyadharan, M. and V. Kalyanaraman, 2013, "Modeling Hysteretic Behavior of Cold-Formed Steel Wall Panels", *Engineering Structures*, Vol. 46, pp.643-652.

Paevere, P.J., 2002, *Full Scale Testing, Modeling and Analysis of Light-Frame Structures under Lateral Loading*, Ph.D. Thesis, Department of Civil and Environmental Engineering, the University of Melbourne, Australia.

Prescriptive Method, 1997, *Prescriptive Method for Residential Cold-Formed Steel Framing*, Second Edition, The National Association of Home Builders (NAHB) Research Center, Inc., Upper Marlboro.

Rahnama M, and H., Krawinkler, 1993, *Effects of Soft Soil and Hysteresis Model on Seismic Demands - John A. Blume Earthquake Engineering Center, Report No. 108*, Department of Civil and Environmental Engineering, Stanford University.

Salenikovich, A.J., J.D., Dolan and W.S., Easterling, 1999, *Monotonic and Cyclic Tests of Long Shear Walls with Openings Report No: TE-1999-001*, Virginia Polytechnic Institute and State University, Blacksburg, Virginia.

SAP 2000, 2010, *SAP 2000 (Version 14) - Integrated Software for Structural Analysis and Design*, Computers & Structures Inc., Berkeley.

SCI P301, 2009, *Building Design using Cold Formed Steel Sections: Light Steel Framing in Residential Construction*, the Steel Construction Institute (SCI), Berkshire.

Serrette, R. and K., Chau, 2003, *Estimating the Response of Cold-Formed Steel Frame Shear Walls - Research Report: RP03-7*, Revision 2006, American Iron and Steel Institute (AISI), Washington, DC.

Serrette, R., J., Encalada, G., Hall, B., Nguyen, Matchen, H., and A., Williams, 1997, *Additional Shear Wall Values for Light Weight Steel Framing - Report No. LGSRG-1-97*, Light Gauge Steel Research Group (LGSRG), Department of Civil Engineering - Santa Clara University, Santa Clara, California, USA.

Serrette, R., H., Nguyen, and G., Hall, 1996. *Shear Wall Values for Light Weight Steel Framing - Report No: LGSRG-3-96*, Light Gauge Steel Research Group (LGSRG), Department of Civil Engineering - Santa Clara University, Santa Clara, California, USA.

Serrette, R., K.A., Morgan, and M.A., Sorhouet, 2002, *Performance of Cold-Formed Steel-Framed Shear Walls: Alternative Configurations - Final Report: LGSRG-06-02 Submitted to NAHB Research Center*, Light Gauge Steel Research Group (LGSRG), Department of Civil Engineering - Santa Clara University, Santa Clara, California, USA.

Serrette, R. and K., Ogunfunmi, 1996, "Shear Resistance of Gypsum-Sheathed Light Gauge Steel Stud Walls", *Journal of Structural Engineering*, April (1996), pp.383-389.

SFS, 2006, *Pitched Roofing and Cladding Fastening Systems for the Construction Industry*, SFS Intec LTD., Leeds, UK.

Simpson Strong-Tie, 2010, *C-CFS 10: Cold-Formed Steel Connectors for Residential and Mid-Rise Construction*, Simpson Strong-Tie Company Inc., USA.

Simpson Strong-Tie, 2011, *C-FS 11: Fastening Systems*, Simpson Strong-Tie Company Inc., USA.

Sivaselvan, M.V. and A.M., Reinhorn, 2000, "Hysteretic Models for Deterioration Inelastic Structures", *Journal of Engineering Mechanics*, American Society of Civil Engineers (ASCE), Vol. 126-6, pp.633-640.

Stahl D560, 2002, *Dokumentation 560 - Hauser in Stahl-Leichtbauweise*, 2002 Edition, Stahl-Informations-Zentrum, Düsseldorf.

Stahl - Merkblatt 480, *Wohnungsbau mit Stahl - Profilhandbuch*, Stahl-Informations-Zentrum, Düsseldorf.

Sugiyama, H., 1981, "The Evaluation of Shear Strength of Plywood Sheathed Walls with Openings", *Wood Industry*, Issue 36-7.

Sugiyama, H. and T., Matsumoto, 1994, "Empirical Equations for the Estimation of Racking Strength of Plywood-Sheathed Shear Walls with Openings", *Summaries of Technical Papers of Annual Meetings, Transactions of the Architectural Institute of Japan*, September (1994).

Tarpy, T.S., 1980, "Shear Resistance of Steel-Stud Wall Panels", *In Proceedings of the 5th International Specialty Conference on Cold-formed Steel Structures*, St. Louis, Missouri, USA, pp. 331-348.

Tarpy, T.S., and J.D., Girard, 1982, "Shear Resistance of Steel-Stud Wall Panels", *In Proceedings of the 6th International Specialty Conference on Cold-formed Steel Structures*, St. Louis, Missouri, USA, pp. 449-465.

Tarpy, T.S., and S.F., Hauenstein, 1978, *Effect of Construction Details on Shear Resistance of Steel-Stud Wall Panels, Project No.1201-412, Sponsored by American Iron and Steel Institute (AISI)*, Vanderbilt University, Nashville, Tennessee, USA.

Tissell, J. R., 1993, *Structural Panel Shear Walls - Research Report No. 154*, American Plywood Association (APA), Tacoma, Washington.

TS EN 10346, 2010, *Continuously Hot-dip Coated Strip and Sheet of Structural Steels - Technical Delivery Conditions*, 2010 Edition, Türk Standartları Enstitüsü (TSE), Ankara.

TS 11372, 1994, *Lightweight Steel Structures - Composed of Cold Formed Steel Members - Design Rules*, 1994 Edition, Türk Standartları Enstitüsü, İstanbul.

UBC1997, 1997, *Uniform Building Code*, 1997 Edition, International Conference of Building Officials (ICBO), Illinois.

Uygar, C, 2006, *Seismic Design of Cold Formed Steel Structures in Residential Applications*, Master's Thesis, Middle East Technical University, 2006.

Uzgider, E. and T.S., Arda, 1989, *Soğukta Şekil Verilmiş İnce Cidarlı Çelik Elemanlar*, İTÜ İnşaat Fakültesi Matbaası, İstanbul.

Wen, Y.K., 1976, “Method for Random Vibration of Hysteretic Systems”, *Journal of the Engineering Mechanics*, ASCE, Vol. 102, pp. 249-263.

Wen, Y.K., 1980, “Equivalent Linearization for Hysteretic Systems under Random Excitation”, *Journal of Applied Mechanics Division*, ASME, Vol. 47, pp. 150-154.

Wolford, D.S. and W.W., Yu, 2000, *Building Design and Construction Handbook*, Sixth Edition, McGraw-Hill, New York.

Yasamura, M. and H., Sugiyama, 1984, “Shear Properties of Plywood-Sheathed Wall Panels with Openings”, *Transactions of the Architectural Institute of Japan*, No.338 April (1984).

Yu, C., 2007, *Steel Sheet Sheathing Options for Cold-Formed Steel-framed Shear Wall Assemblies Providing Shear Resistance Report No. UNT-G76234*, American Iron and Steel Institute (AISI), Washington, DC.

Yu, C. and Y., Chen, 2009, *Steel Sheet Sheathing Options for Cold-Formed Steel-framed for Shear Wall Assemblies Providing Shear Resistance - Phase 2: Report No. UNT-G76234*, American Iron and Steel Institute (AISI), Washington, DC.

Yu, W.W. and LaBoube, R.A., 2010, *Cold Formed Steel Design*, Fourth Edition, John Wiley & Sons Inc., New York.

Zeynalian, M., H.R., Ronagh and P., Dux, 2012, “Analytical Description of Pinching, Degrading, and Sliding in a Bilinear Hysteretic System”, *Journal of Engineering Mechanics*, American Society of Civil Engineers (ASCE), Vol. 138-11, pp.1381-1387.

Zhao, Y., 2002, *Cyclic Performance of Cold-Formed Steel Stud Shear Walls*, Master's Thesis, Department of Civil Engineering and Applied Mechanics, McGill University, Montreal, QC, Canada.